NASA TM X-1194

INVESTIGATION OF HYDROTEST FAILURE OF THIOKOL CHEMICAL CORPORATION 260-INCH-DIAMETER SL-1 MOTOR CASE

By John E. Srawley and Jack B. Esgar

Lewis Research Center
Cleveland, Ohio

in Collaboration with the
260-SL-1 Hydrotest Failure Investigating Committee

NATIONAL AERONAUTICS AND SPACE ADMINISTRATION

For sale by the Clearinghouse for Federal Scientific and Technical Information
Springfield, Virginia 22151 – Price $3.00

260-SL-1 HYDROTEST FAILURE INVESTIGATING COMMITTEE

Jack B. Esgar, Chairman	NASA Lewis Research Center
Edward F. Becht	Cameron Iron Works Incorporated
Jose R. Canal	Cameron Iron Works Incorporated
Preston S. Craig	Thiokol Chemical Corporation
R. M. Donaldson	Newport News Shipbuilding and Dry Dock Company
Frank D. Duffey	Newport News Shipbuilding and Dry Dock Company
Clyde A. Furgason	Ladish Company
Stephen D. Hart	U. S. Naval Research Laboratory
Joseph A. Kies	U. S. Naval Research Laboratory
James J. Kramer	NASA Lewis Research Center
William T. Lankford, Jr.	United States Steel Corporation
L. F. Matthies	Thiokol Chemical Corporation
William F. Payne	USAF Rocket Propulsion Laboratory
James J. Pelouch, Jr.	NASA Lewis Research Center
L. E. Spencer	Newport News Shipbuilding and Dry Dock Company
John E. Srawley	NASA Lewis Research Center
Stewart Turner	USAF Rocket Propulsion Laboratory
Robert A. Wasel	NASA Headquarters
Charles Witherell	International Nickel Company, Inc.

Invited Consultants

Ward D. Abbott	Excelco Developments, Inc.
Thomas H. Burns	Thiokol Chemical Corporation
Charles F. Tiffany	The Boeing Company
Max L. Williams, Jr.	California Institute of Technology

CONTENTS

INVESTIGATION OF HYDROTEST FAILURE OF THIOKOL CHEMICAL CORPORATION 260-INCH-DIAMETER SL-1 MOTOR CASE

by John E. Srawley and Jack B. Esgar in Collaboration with the 260-SL-1 Hydrotest Failure Investigating Committee

Lewis Research Center

SUMMARY

The Thiokol Chemical Corporation 260-inch-diameter SL-1 motor case failed during hydrotest at a pressure of 542 pounds per square inch, which was about 56 percent of proof pressure. The motor case was constructed of 250 grade maraging steel plate joined mostly by submerged arc automatic welding. An investigation of the failure was conducted by a Committee composed of members from Industry and Government. Investigation showed that the failure originated from a defect that was not detected by nondestructive testing techniques prior to aging. Nondestructive testing was not conducted between aging and hydrotest. The defect causing the failure was in the heat-affected zone of a longitudinal submerged arc weld on the cylindrical section of the motor case. The area where the defect was located had been repaired by a manual gas-tungsten-arc (TIG) weld. The defect, which was submerged within the vessel wall and oriented longitudinally, was approximately 1.4 inches long and had a width of about 0.10 inch. Four other undetected defects of significant size were discovered after the motor case failure. All of these defects were also located beneath manual TIG weld repairs. One of these defects, which was in the same longitudinal weld as the defect causing the motor case failure, was involved in the fracture as a secondary origin. The other defects were discovered during reinspection of all welds by nondestructive testing techniques after hydroburst.

Although the detailed mechanism of the formation of these defects has not been established, it is reasonably certain that their formation was a consequence of the TIG weld repairs to the original welds.

The fracture toughness of the submerged arc welds was inadequate to tolerate crack-like defects as large as those that occurred in the motor case. It had been believed that much smaller defects could be detected with high reliability by the nondestructive inspection procedures that were used. The fracture toughness would have been sufficient if no defects had been present larger than what had been considered to be the detectable size.

As part of the failure investigation, a limited test program was conducted to determine the sensitivity of radiographic and ultrasonic procedures for detecting tight fatigue cracks in flat plate specimens. It was found that these nondestructive testing methods were much less sensitive and reliable than expected. It is concluded that much more research is required on nondestructive testing techniques for detection of small defects in thick pressure vessel walls before materials and weld procedures having the toughness found in the Thiokol motor case can be successfully utilized.

INTRODUCTION

In the course of a program to demonstrate the feasibility of 260-inch-diameter solid-rocket motors by Thiokol Chemical Corporation, a short-length case failed during hydrotest. An investigation of the failure was conducted by a Committee composed of technical representatives from Government and Industry. The findings of this Committee are reported herein.

The large solid-propellant rocket-motor program was initiated in 1963. Thiokol Chemical Corporation and the Aerojet-General Corporation were selected by the U. S. Air Force to demonstrate the feasibility of 260-inch-diameter solid-propellant rocket motors. NASA took over funding of the program on July 1, 1964 and assumed technical management March 1, 1965. Both Thiokol and Aerojet-General were under contract to build and test two motor cases of full diameter but only one-half the length required for the reference motor, which will produce 6 million pounds of thrust for 2 minutes. The two short-length motors scheduled to be built and tested by Thiokol were designated 260-SL-1 and 260-SL-2, and they were designed to produce 3 million pounds of thrust for 2 minutes.

During hydrotest of the Thiokol 260-SL-1 motor case on April 11, 1965, the case failed at an internal pressure of 542 pounds per square inch, which was about 56 percent of proof pressure. A failure investigating committee was formed to determine the cause of the failure and remedial actions that will prevent similar failures in other rocket motor cases. The first meeting of this Committee was held on April 26 and 27, 1965, after the failed motor case had been removed from the hydrotest tower, laid out in a protected area for inspection, and a preliminary inspection and mapping of the fracture paths had been performed by Mr. J. A. Kies from the U. S. Naval Research Laboratory and Mr. J. E. Srawley from the NASA Lewis Research Center. Although the investigation was not complete at that time, the origin and probable cause of the failure were determined. A preliminary report for NASA use was issued on May 7, 1965 listing the preliminary findings of the Committee. The investigation then continued with emphasis on a detailed metallographic study of the failure pieces in the region of the fracture origins and reinspection of most of the welds in the failed motor case to determine if previously undetected defects could be found. The metallographic investigation was conducted by the United States Steel Corporation, Applied Research Laboratories. Their report on the metallographic investigation, authored by A. J. Baker, A. J. Birkle, P. S. Trozzo, and R. P. Wei, is included as appendix A. Reinspection of motor case welds was conducted by the Newport News Shipbuilding and Dry Dock Company and the U. S. Naval Research Laboratory.

In addition to the regular committee members, several consultants with related experience in large, solid motor case problems were invited to inspect the case failure and provide comments to the Committee. The final findings of the Committee on the causes and factors relating to the motor case failure are presented in this report.

MOTOR CASE CONSTRUCTION

Design and Fabrication

The Thiokol cases were designed by the Space Booster Division of Thiokol Chemical Corporation and manufactured by the Newport News Shipbuilding and Dry Dock Company. The material specified in the USAF request for proposal was maraging steel (18 Ni-Co-Mo-Ti). Thiokol selected the 250 grade air-melted maraging steel. The term 250 grade refers to a nominal yield strength of 250 000 pounds per square inch (psi) for the material. The case design was based on a plate yield strength of 230 000 psi and a weld efficiency of 90 percent for a design strength in the welds of 207 000 psi. Using a factor of safety of 1.3 for the welds resulted in a nominal plate thickness of 0.730 inch in the cylindrical section and 0.477 inch in the hemispherical domes. In the weld area, a mismatch of 10 percent of the thickness was allowed, but it was not to exceed 0.060 inch. The eccentricity of membrane forces from this mismatch in a longitudinal weld results in an elastic stress magnification factor of 1.25.

The case fabrication procedure consisted of the buildup of three subassemblies, as shown in figure 1. The aft subassembly consisted of the aft closure, aft Y-ring, aft skirt, and one cylindrical section. The closure, skirt, and cylinder were welded to the Y-ring. The center subassembly consisted of two cylindrical sections. The forward subassembly consisted of the forward dome, forward Y-ring, forward skirt, and one cylindrical section.

All welds in the cylinder and the domes were accomplished by using the submerged arc process (hereinafter called subarc). The Y-rings were built up from four circumferential segments. The four longitudinal welds used to join the Y-ring segments were accomplished by using the vertical submerged arc process. This process was used because of the thickness of the part $\left(1\frac{7}{8}\text{ in.}\right)$ at the time of welding. The forward and aft skirts were welded to the respective Y-rings by using the multipass gas-tungsten-arc (TIG) process because the geometrical configuration permitted the weld to be deposited only along the outside circumference.

The three subassemblies of the motor case were aged separately at 835° F for 4 hours. The subassemblies were then joined to form the case by girth welds by using the two-pass subarc welding procedure. These welds were then locally aged with the same heat-treatment schedule as used for the subassemblies.

Several weld repairs were made during motor case construction. The weld repairs were all made by manual TIG welding, and they were made before aging. The welding records for the motor case showed the total weld length to be approximately 975 feet. Weld repairs were contained in 200 feet of this total length. In some cases, the weld repairs had to be re-repaired. The total length of weld repairs made during the construction was approximately 330 feet.

Nondestructive Testing

Nondestructive testing and inspection were generally carried out during the fabrication by four methods: (1) visual, (2) liquid penetrant (PT), (3) ultrasonic (UT), and (4) radiographic (RT). A very limited amount of magnetic particle (MT) inspection was also used for one weld joint. A brief description of the equipment and procedures used is given in this section. After the motor case failure, plate specimens containing fatigue cracks were prepared for evaluation of the sensitivity of the nondestructive testing methods (NDT), as discussed in the section Nondestructive Testing Sensitivity Evaluation.

Liquid penetrant (PT). - The Type II (nonfluorescent) penetrant materials, produced by the Magnaflux Corporation, for inspection are as follows:

Spot Check - Cleaner - SKC-NF

Spot Check - Penetrant - SKL-HF

Spot Check - Developer - SKD-NF

The procedure used called for cleaning the surface with SKC-NF, drying with clean cloths, then wetting the surface for at least 15 minutes with penetrant. Not more than 20 minutes after penetrant application (unless the penetrant was kept wet) the excess was wiped off and the penetrant film was removed with SKC-NF dampened cloths or absorbent paper. Developer was applied within 10 minutes by spraying or brushing if necessary. Inspection was to be made not sooner than 7 nor later than 30 minutes after the developer had dried.

The inspection rejection criteria varied somewhat during the time fabrication was in process. Generally, rounded indications up to 0.070 inch in diameter were acceptable in plate, and rounded indications 0.045 inch in diameter were accepted in the welds and adjacent areas 6 inches on either side of the welds. Linear indications, regardless of size or orientation and linearly disposed rounded indications were cause for rejection in all cases.

When defects were found by any of the NDT methods, the area was excavated by grinding for weld repair. These excavations were PT inspected prior to welding.

Radiography (RT). - Each weld was radiographically inspected over 100 percent of its length. The radiographic technique was based on military specification MIL-STD-453 with some modifications. The radiographic quality level was 2-2T, which indicates that a penetrameter whose thickness T is no greater than 2 percent of the welded joint thickness shall be visible in the radiograph. It also indicates that a hole drilled through the penetrameter with a diameter equal to twice the thickness of the penetrameter shall be visible.

All production exposures were made with X-ray equipment of the Triplett and Barton portable 275 or 300 maximum KVP - 10 maximum milliampere type. Some of the early exposures were made by using a 57-inch target to film distance,

but most exposures were made at a 36-inch distance to reduce fog and exposure times. Standard Kodak Type M film was used with 0.005-inch lead front screens and 0.010-inch lead back screens, except for thick sections such as the Y-ring welds, where Type AA film was used. Film was used in cassettes until about January 22, 1965. After that time Kodak "Ready Pack" was used because it saved interpretation time and virtually eliminated artifacts. Cassettes were used for about 65 percent of the total exposures taken during fabrication. The acceptance criteria for welds was as outlined in Standard I of MIL-R-11468 ORD dated September 24, 1951.

Ultrasonic (UT). - Two UT inspection procedures were developed; one for plates and forgings, and one for welds. The plate inspection procedure covered inspection for thickness, compressional wave (through thickness) for laminar oriented defects, and shear wave in longitudinal and transverse directions for nonlaminar defects. The weld inspection procedure called for compressional wave (through thickness) and shear wave in transverse and longitudinal directions.

Calibrations and rejectable flaw sizes for inspection of plates were changed several times during motor case fabrication. The final criteria for rejection are discussed in the following paragraphs.

Plate and forging inspection procedure: The equipment used was Branson Sonoray models 5, 50, or 51 for soundness testing, and model 14 Vidigage for thickness testing. The transducer frequency used for nearly all the testing was 2.25 or 4.0 megacycles. On occasions, however, other frequencies and/or dual transducers were used to improve sensitivity. Rejectable defect signals were determined from calibration plates with machined notches or flat-bottomed holes for use as standards. The following standards were set up:

Thickness:

Equipment calibrated from plates with thickness predetermined by micrometers. Calibration was checked before, during, and after tests on each plate.

Compressional wave:

For plates, signal size was calibrated for a 1/8-inch-diameter flat-bottom hole halfway through the plate thickness. When the signal amplitude exceeded that obtained from a 1/8-inch-diameter flat-bottomed calibration hole, the flaw was further examined to determine its area. The plate was rejected if the discontinuity equalled or exceeded 0.11 square inch.

For forgings and potential heat-affected zones (HAZ), calibrations were made by using 5/64-inch-diameter flat-bottomed holes at various depths to obtain a distance-amplitude line on the oscilloscope screen. Signals that exceeded this distance-amplitude line were a basis for rejection.

Shear wave:

Signal size was calibrated for a machined notch 1/32-inch deep and 1/4-inch long (or equivalent area). Signals exceeding that for the calibration notch, for equivalent distances to the defect and the calibration notch, were a basis for rejection.

Weld inspection procedure: The equipment used was Branson Sonoray models 5, 50, and 51. The transducer frequency was 2.25 megacycles for all the shear wave testing and was 4.0 megacycles (dual transducer) for compressional wave testing. On occasions it was necessary to utilize other frequencies to improve sensitivity. The standards for the rejectable defect sizes were as follows:

Compressional wave:

Calibrations were made for 5/64-inch-diameter flat-bottomed holes at various depths to obtain a distance-amplitude line on the screen. Signals exceeding this line were a basis for rejection and repair.

Shear wave:

For longitudinal defects (relative to weld direction) the rejection calibration standard was a machined circular segment notch 1/32-inch deep and 1/4-inch long.

For transverse defects (relative to weld direction) the rejection calibration standard was a machined circular segment notch 1/64-inch deep and 1/4-inch long.

Magnetic particle (MT). - Inspection by the MT technique was not used as a routine procedure for the 260-inch-diameter motor cases. As discussed in the section Reinspection of Weld Areas After Hydrotest Failure, MT was not considered to be a generally reliable NDT technique for welded maraging steel. It was utilized only in a limited way for special cases where the other techniques were not applicable. For example, a special technique was employed on the circumferential weld in the center of the assembled motor case to provide a survey of intermittent centerline surface cracking first indicated by PT. In this instance, PT was not fully reliable because cracking was partly subsurface, and the shallow, tight nature of the cracks prevented UT and RT from being successful. The magnetic field for the MT inspection was provided by strong permanent magnets with their poles contacting the opposite sides of the weld joint.

Repair Procedures

All the nondestructive testing (except for acceptance tests of parent material prior to fabrication) was conducted after welding, but before aging. If defects were found by any of the three methods (RT, PT, or UT) the defective material was removed by grinding, and the weld was repaired by the TIG method. The repaired area was reinspected by all three methods, and the process was continued until there was no further evidence of defects. During excavation of

the defect prior to repair welding PT was used to determine the amount of excavation required.

Past experience by Newport News Shipbuilding and Dry Dock Company had indicated that aging of the welds should not introduce new defects. As a result, a joint decision was made by Newport News Shipbuilding and Dry Dock Company and Thiokol Chemical Corporation on January 13, 1965 that nondestructive testing would not be repeated after aging of the welds. This decision received U. S. Air Force concurrence.

HYDROTEST PROCEDURE

The completed rocket motor case was readied for hydrotest by bolting on a nozzle adapter manufactured by the Rohr Corporation and a hydrotest nozzle cone manufactured by Newport News Shipbuilding and Dry Dock Company. These components are indicated in figure 1. The case was supported in a hydrotest tower by bolting the forward skirt to the forward lifting ring, which, in turn, was bolted to the base pedestal of the hydrotest tower (fig. 2). A piston attached to the hydrotest tower sealed the case as a pressure vessel and provided thrust loads on the forward skirt. Case growth during pressurization was accommodated by movement of the case in the longitudinal direction relative to the piston.

Twenty-four accelerometers were located on the case in the locations shown in figure 3 to detect stress waves generated during hydrotest. Procedures for interpreting the output of such accelerometers are being studied and are not completely developed at this time. Appendix B describes the use of accelerometers for determining stress-wave origins. The output of the accelerometers was to be fully analyzed after the test.

Strain gages were located on both the inside and outside surfaces of the case. Certain areas of the case were expected to experience relatively high stress because of plate-thin spots and out-of-contour areas near welds. These areas were strain gaged. The out-of-contour areas were of particular concern because of the difficulty in stress analyzing these areas. The strain gages in these critical areas were monitored during the test. The test was to be aborted if stress levels significantly exceeded analytic predictions.

The case was filled with water on Saturday, April 10, 1965. The water was inhibited by the addition of 0.73 pound of sodium dichromate in each 1000 gallons of water. In addition, caustic soda was introduced in sufficient amounts to achieve pH neutrality. The water was heated by addition of steam during filling to give a temperature of approximately 62° F. The inhibited and heated water was introduced into the case through the forward closure (bottom of case during hydrotest). Fluid was bled from the case top, through a bleed line in the fixed piston, initially and after each depressurization in order to ensure that the case was entirely filled with liquid.

The maximum hydrotest pressure planned was 960 psi, 10 percent above the maximum expected operating pressure of the motor. The actual pressure-time history for the case is shown in figure 4. The 300-psi pressurization on

April 10 permitted instrumentation and pressurization system checkout. The 350-psi pressurization on April 11 verified the status of the instrumentation. During the final pressurization there were 5-minute holds at 300 to 500 psi in order to record strain gage readings.

During hydrotest, the accelerometer system mounted on the motor case indicated eight stress waves, including the wave that occurred at failure. The predicted origins and the pressures at stress wave initiation are also shown in figure 3. The first stress wave occurred at a pressure of 242 psi. Previous experience in using a stress-wave detection system on hydrotest of motor cases has shown similar stress wave initiations in areas not related to final failure. Three of the stress wave origins were in the region of the lower skirt where the motor case was bolted to the hydrotest thrust stand. It is probable that some of these stress waves resulted from movement at the bolt holes.

As the pressure was increased to 542 psi another stress wave was detected. At the same time a loud report was heard from the direction of the hydrotest tower. Visual inspection revealed the case to have failed catastrophically. Prior to failure, two stress waves had originated in the general area of the fracture initiation location. At the present stage of development of the stress-wave detection system, however, it is not possible to determine the positions of these origins while the test is underway. The data are recorded during the hydrotest and played back later to determine stress wave arrival sequences at each accelerometer. These data are then fed into a computer to determine the origin locations by triangulation.

FAILURE INVESTIGATION

On failure at a gage pressure of 542 psi, the motor case had shattered into several large pieces and many smaller ones that fell into a precarious, interlocked pile within the test tower. Several days were required to remove the pieces to a large shop where they were laid out on the floor for detailed examination. Figure 5 is a photograph taken during this operation that shows the test tower site. A large piece consisting of the aft head and part of the cylindrical section is resting in the framework of the tower, and another large piece of the cylindrical section that had been removed from the tower is shown in the foreground. In spite of the lengthy exposure in the open air, the fracture surfaces were not visibly rusted; nor were they mechanically damaged in handling to any important extent. It was necessary to cut two of the larger pieces with a torch to facilitate removal, but these cuts did not impair the subsequent examination. Figure 6 shows the pieces laid out on the shop floor with the aft head in the center foreground and the other pieces arranged as nearly as possible in proper relation to one another.

While the pieces were being transferred to the shop, work was started on mapping the fracture paths throughout the entire vessel. The location and orientation of each piece could be ascertained either from the locations of welds in the piece, or by matching fracture surfaces of adjacent pieces. A reference grid related to the welds was marked out on the pieces, and their boundaries were then plotted on a 1:12 scale model of the motor case made of

Lucite. A plane development of the cylindrical section of the model map is shown in figure 7. This map was obtained by tracing the fracture paths onto a piece of tracing paper wrapped around the model. The arrowheads on this map show the directions of propagation of the fracture along the various branches, as ascertained from chevron markings on the fracture surfaces. Figure 8 is a photograph showing the typical chevron markings on either side of one of the fracture origins discussed in the next section. The chevrons point back to the origin, opposite to the direction of fracture propagation. Similarly well-defined markings were found on most of the fracture surfaces and, taken together with collateral information, these were sufficient to define the complete course of the fracture without ambiguity.

Fracture Origin Location

From the fracture map (fig. 7), it is clear that the fracture pattern developed from an origin close to the W7/302 longitudinal weld and somewhat forward of the W8/3 aft Y-ring weld. Although they are not shown here, the fracture paths in the skirts and the domes were completely mapped, and it was established that they had developed from cracks running out of the cylindrical section. There were no independent origins in these parts of the motor case, although there were one or two fracture branches that had run from the cylinder into one of the heads and then continued on back into the cylinder.

Independent confirmation of the general location of the fracture origin was obtained by triangulation based on the recorded accelerometer signals. As discussed in appendix B, the origin of the stress wave detected at the time of failure was estimated to be located within a 20-inch-diameter circle centered at a point 8 inches from the W7/302 weld and 29 inches forward of the W8/3 weld. This location, shown as a dashed circle in figure 7(b), is in good agreement with the position of the source of the fracture paths.

Two distinct fracture origins were discovered in the expected region, both associated with areas of TIG weld repair on the inside surface of the W7/302 weld. One origin was oriented parallel to the weld centerline, and the other transverse to it. The positions of these origins and sketches of their contours are shown in the detail fracture map (fig. 7(b)). Because of the obvious difference in appearance to the naked eye, the longitudinal defect was termed the "clean" origin, and the transverse defect the "black" origin. Photographs of the mating surfaces of the clean origin are shown in figure 9. The boundary is quite distinct except for two damaged places on one of the mating surfaces that must have rubbed against another piece of metal, but the appearance of the origin surface differs only in texture and tone from that of the surrounding fracture: there is no suggestion of a deposit on the surface. On the other hand, the black origin was covered with a tightly adhering, black deposit, as shown in figures 8 and 10. This deposit was eventually identified as essentially an iron oxide. This difference between the two origins is probably connected with the fact that, whereas the boundary of the black origin extends to the outer surface of the vessel wall, the clean origin is completely submerged within the wall.

The inner and outer faces of the pieces containing the two origins were

ground and etched to reveal the positions of the fusion lines and heat-affected zones of the W7/302 weld. It was then found that each origin was located beneath a separate manual TIG weld that had been deposited on the inside of the vessel to replace part of the original subarc weld. These locations are indicated in figures 11 and 12. The clean origin (fig. 11) was located near one edge of what appeared to be a fusion line TIG repair weld, and the black origin (fig. 12) was located near one end of a TIG repair, which covered the whole width of the weld and heat-affected zones. These locations are discussed in greater detail later. The TIG weld areas were identified by the responsible welding engineer as simulated repairs to an originally sound subarc weld. The simulated repairs had been made as part of an investigation concerned with cracking that had been encountered in TIG repair welding of meridional dome welds. Experimental TIG repairs had been made at three places on the W7/302 weld, but a total of four nondestructive inspections by PT, UT, and RT at times varying from 1 day to 19 weeks after the repairs were made had revealed no indications of defects in the repaired regions. The more detailed examination of the two origins is discussed in the next section, following discussion of the sequence of fracturing.

There is no doubt that both origins contributed to the overall development of the fracture. Fracturing in the aft head developed from a crack that ran longitudinally from the clean origin and branched just before it reached the W8/3 Y-ring junction weld (see fig. 7(b)). Fracturing in much of the cylindrical section, and throughout the forward head, developed from cracks that ran circumferentially for short distances from the black origin and then branched into spiral and longitudinal paths, as shown in figure 7. It is most unlikely, however, that the fracture started simultaneously and independently at both origins. It is almost certain that the stress redistribution associated with propagation of cracks from one origin brought about secondary crack propagation from the other origin.

In fact, the local fracture pattern in figure 7(b) can only be explained satisfactorily if it is assumed that fracture started first at the clean origin with the initial, longitudinal crack running both aft toward the head and forward toward the position of the black origin. The intensity of the stress field around the black origin would have increased with the approach of the crack, so that secondary crack propagation would have been triggered at the black origin before the primary crack reached it. The subsequent intersection of the developing transverse crack by the primary crack would then have disturbed the stress field in a way that would account for the early branching of both ends of the transverse crack. Since the velocity of propagation of brittle fracture in steel can approach 5000 feet per second, it is likely that the interval between primary and secondary crack initiation would be of the order of a millisecond.

The alternative hypothesis, that fracture started first at the black origin, does not lead to a satisfactory explanation of the observed fracture pattern. The development of the transverse crack from the black origin, and of the branches stemming from it, would not have increased the intensity of the stress field around the clean origin; if anything the stress intensity at the clean origin would have decreased as the crack pattern developed from the black origin. There would have been no reason, therefore, for secondary crack

propagation to start at the clean origin. In this case the complete fracture pattern should have been significantly different from that observed, and the clean origin should not have been involved at all.

Independent support for the conclusion that the clean origin was the primary origin of the fracture is provided by a comparison of the distances between the position of the stress wave origin calculated from the accelerometer data and the positions of the two fracture origins. As shown in figure 7(b), the distance from the center of the 20-inch-diameter circle representing the stress wave origin to the clean origin is about 12 inches, while the distance to the black origin is about 32 inches. Statistically, the probability of a triangulation error of 12 inches is significantly higher than the probability of an error of 32 inches.

In the absence of the clean origin it is quite likely that the vessel would have fractured, starting at the black origin, at some pressure less than the intended hydrotest proof pressure. In any event, under no circumstances would either origin have been considered a tolerable defect if its presence and magnitude had been detected prior to the hydrotest.

The Consultants reports, which are presented in appendix C, are in general agreement with the foregoing analysis of the origination and development of the fracture.

An investigation was conducted on other factors that may have been related to the failure. This investigation, reported in appendix D, further substantiated the preceding findings.

Metallographic Examination of Fracture Origins

Detailed metallographic examination of the fracture origins and neighboring regions of motor case fragments was undertaken by the Applied Research Laboratory of the U. S. Steel Corporation, under the direction of Mr. George Pellissier. The findings summarized in this section are discussed in greater detail in appendix A.

The locations of both origins with respect to weld deposits were established accurately by sectioning and etching. These locations are most readily visualized by reference to the simplified isometric drawings (figs. 11 and 12). The clean origin is located just below the intersection of the TIG weld interface with the interface of the inside, second pass of the subarc weld, in the grain-coarsened region of the subarc weld heat-affected zone. The black origin (fig. 12) is transverse to the W7/302 weld and crosses the inside, second pass of that weld, extending into the heat-affected zones on both sides of the weld deposit. The nearly straight boundary lies just below the fusion interface of the TIG weld repair, close to one end of the repair. The enlarged end of the origin extends to the outside surface of the vessel at about the position of the fusion interface of the first pass of the subarc weld. This end of the origin is within the combined heat-affected zones of the TIG and subarc welds, but its extremity probably reaches the limit of the austenite reversion region.

By optical microscopic examination of fracture profiles in polished sections, and electron microscopic examination of fracture replicas, it was ascertained that the fracture topographies of the two origins were quite similar to one another, but different from adjacent fracture surfaces. The origin surfaces were predominantly intergranular, with relatively flat facets that corresponded either to prior austenitic grain boundaries, or to dendrite interfaces in the case of that part of the black origin located within the weld. The surrounding fracture surfaces were predominantly of the noncrystallographic, dimpled type, which is indicative of more ductile rupturing.

The association of each of the origins with a TIG repair weld, and the nature of the origin surfaces, suggests that their formation was a consequence of TIG repair welding. This suspicion is reinforced by the finding of three other flaws associated with TIG weld repair regions. A tension test specimen taken from the W7/101 weld after hydrotest failure was used to examine one of these flaws shown in figure 13. This flaw and two flaws that were found in the W6/3 TIG weld are discussed further in the section Reinspection of Weld Repair Areas After Hydrotest Failure. The detailed mechanism of formation of the flaws has not been established, but it appears that the defects were generated by stresses set up during TIG repair welding in regions exhibiting microstructural inhomogeneity and grain coarsening.

The black deposit on the transverse origin was examined by glancing-angle X-ray diffraction, electron diffraction, and electron-probe microanalysis. The diffraction patterns corresponded to a mixture of ferrous oxide (Fe_2O_3) and ferric oxide (Fe_3O_4). The analysis showed that the metallic constituent was predominantly iron with small amounts of nickel, molybdenum, cobalt, and titanium. This oxide must have formed at a high temperature. Comparison of the color with oxidized crack surfaces obtained by heating in air at high temperatures suggests a formation temperature at least as high as 800° F. It would appear that at least some of the oxidation must have occurred during the aging cycle at 835° F.

Polished sections and fractographic replicas were examined to determine the location of the fracture surface at a representative position between the primary and secondary origins. Near the surfaces of the vessel wall the fracture is interdendritic, through the subarc weld metal in which the dendrites are normal to the surfaces. Further within the wall the fracture is intergranular, through the grain-coarsened region just adjacent to the fusion interface of the subarc weld, conforming macroscopically to the fusion interface. The path taken by the fracture suggests that the grain-coarsened region has a low fracture toughness associated with a highly sensitized microstructure. This observation is consistent with the occurrence of the clean and black origins in similarly grain-coarsened regions.

From the metallographic evidence it may be surmized that the high heat input during subarc welding caused grain coarsening and thermal embrittlement in the regions of the base plate adjacent to the weld deposit. Such regions would be expected to be susceptible to cracking under thermal stresses such as those generated by subsequent repair welding. To establish the mechanism of formation of the fracture origins more conclusively would require the undertaking of a research program directed toward duplicating the phenomenon in the laboratory.

Fracture Calculations and Fracture Toughness

Fracture mechanics background. - Engineering calculations concerning fracture are conducted currently on the basis of the mathematical theory of linear elastic fracture mechanics, which deals with the stress field singularities associated with cracks in ideal elastic bodies (refs. 1 and 2). While it is recognized that this mathematical model represents a considerable oversimplification of the situation in a real engineering material, the calculations are nevertheless often useful, particularly when applied to materials of high yield strength subjected to relatively low stress levels as in the present investigation.

The distribution of stresses and displacements near the edge of an elastic crack is dominated by the influence of the stress-free surfaces of the crack. The crack stress field system can be resolved into three basic component systems, each referring to a particular set of displacement discontinuities associated with a principal mode of crack extension. For simplicity only the first or opening mode of crack extension needs to be considered here, namely, that in which the relative displacement of corresponding points on the mating crack surfaces occurs in a direction normal to those surfaces. The other two component modes involve forward or sidewise sliding of the crack surfaces over one another. In the opening mode, the stress components near the crack edge are all proportional to the scalar stress intensity factor K_I. The magnitude of K_I is proportional to the loading forces acting on the body containing the crack and also depends upon the configuration of the body, including the crack shape and size. The dimensions of K_I are those of stress multiplied by the square root of length. The evaluation of K_I for configurations that are of practical interest is a primary task of linear elastic fracture mechanics (ref. 3).

For engineering application of linear elastic fracture mechanics some criterion for fracture of a material must be assumed. The assumption is that a material will exhibit a characteristic plane strain fracture toughness K_{Ic} such that a crack in the material will become unstable if the value of K_I anywhere along the crack boundary reaches the K_{Ic} value of the material. In practice, K_{Ic} values are measured by conducting fracture tests on appropriately designed specimens that incorporate cracks and that have been subjected to a sufficiently accurate K_I stress analysis (ref. 4). In a failure analysis, the K_I value calculated from the fracture origin dimensions and the loads can be compared with K_{Ic} values obtained from tests of the material involved. It is important to appreciate, however, that only approximate agreement is to be expected because of the simplifications involved in the underlying assumptions. Furthermore, there may be other sources of error or uncertainty, as will be noted in discussing the subject failure.

Accurate methods have not yet been developed for calculation of stress intensities of cracks of irregular contour such as the two origins involved in the hydrotest failure of the SL-1 motor case. Estimates of the upper and lower bounds can be obtained, however, from the analysis of cracks of elliptical contour published by Irwin (ref. 5). Figure 14 is a convenient working plot of the relevant results from this reference, showing the dimensionless quantity

$K_I/\sigma\sqrt{a}$ against the ratio a/c, where K_I is the maximum value of the stress intensity factor around the elliptical boundary, σ is the nominal stress acting across the crack, and a and c are the minor and major semiaxes of the ellipse, respectively. The stress intensity is greatest at the position of least curvature of the boundary, that is, at each end of the minor axis. Where part of the boundary of a crack has negative (concave) curvature, as is the case with the clean origin, the stress intensity will be higher than at a position of convex curvature, but the magnitude of the difference is not accurately known.

Stress intensity factors. - The nominal stress across the clean origin was estimated to be approximately 100 000 psi at the failure pressure of 542 psi. This estimate allows for the static pressure head and for a supplementary bending stress due to deviation of the shell contour from the ideal cylinder. This bending stress supplement corresponds to the position of the inner boundary of the origin where K_I should have been greatest because of the negative curvature of the boundary. The stress values used in this fracture toughness analysis are in substantial agreement with the values quoted by the consultants (appendix C). The differences are small and the values used herein are best estimates. The estimate of nominal stress is probably accurate to within 5 percent.

The estimates of the upper and lower bounds of the stress intensity corresponding to this nominal stress are based on fitting ellipses to the clean origin as shown in figure 15. The lengths of the ellipses are equal to that of the origin. For the lower bound, the width of the ellipse is 0.10 inch, equal to the minimum width of the origin. For the upper bound, the width of the ellipse is 0.22 inch, equal to the distance from the convex boundary of the origin to the tangent spanning the opposite boundary. The estimated K_I bounds for the clean origin are then 39 000 and 57 000 psi$\sqrt{\text{in.}}$.

The nominal stress across the black origin is estimated to have been 46 000 psi at the failure pressure of 542 psi. This estimate allows for the static pressure head and the thrust on the fixed piston, but assumes the bending stress to be zero. The estimate of the lower bound of the K_I value for the black origin is based on an ellipse 1.6 inches long by 0.2 inch wide; these dimensions correspond to those of the black origin if the enlarged end is neglected. The estimated lower bound K_I value for the black origin is then 25 000 psi$\sqrt{\text{in.}}$, and this is probably a good estimate of the correct value for the narrow limb of the origin that crosses the subarc weld proper (fig. 12).

Estimation of the upper bound K_I value for the black origin is much more uncertain. The K_I value should be greatest at the sharp corner in the origin boundary (figs. 10 and 12), but advance of the crack front from this point would produce a smoother contour and, temporarily, a lower K_I value. Since there is no better basis for estimation, it will be assumed that the K_I value for this origin is unlikely to be greater than that based on an ellipse 1.6 inches long by 0.5 inch wide (this width being equal to the distance from the outer surface of the wall to the far boundary of the origin). The upper bound K_I value calculated on this basis is then 37 000 psi$\sqrt{\text{in.}}$. The fact that the black origin was open to the surface over a short distance will hardly

affect the K_I estimates because this distance amounts to less than 10 percent of the total length of the origin. This is a somewhat subtle point that is inferred from reference 5.

Residual stress effects. - The contributions of any residual stresses that may have existed in the origin regions have been neglected in the preceding K_I calculations. Experiments at the Newport News Shipbuilding and Dry Dock Company during the period when the motor case was under construction did reveal the existence of substantial residual stresses in the heat-affected zone of a subarc weld. A relaxation technique involving hole drilling was used. Substantial tensile stresses in the circumferential direction were measured in that part of the heat-affected zone just below the outside surface of the case. Compressive stresses occurred in the longitudinal direction. Unfortunately, there is no way of knowing the magnitudes and distributions of residual stresses in the regions of the clean and black origins at the time of the hydrotest. This uncertainty is aggravated by the somewhat contrary findings of the Boeing Company, who also conducted residual stress studies, as discussed in appendix C. Under the circumstances, the question of residual stresses can only be regarded as an additional factor of uncertainty of unknown magnitude affecting the accuracy of the K_I calculations.

Fracture toughness. - Measurements of K_{Ic} toughness were made at the NASA Lewis Research Center by using crack-notch bend specimens obtained from the W7/301 weld and adjacent plate material. This weld was made by the same welding procedure and joined the same two plates as the W7/302 weld where the failure originated. Unfortunately none of the K_{Ic} specimens were obtained from a region that had been repaired by TIG welding, and therefore the fracture toughness values were not properly representative of the material in the vicinity of the fracture origins. Because of a misunderstanding, the only part of the W7/301 weld that had been repaired by TIG welding was cut up in such a manner that it could not be used for fracture toughness specimens.

The types of four-point bend specimens used for the K_{Ic} tests are shown in figure 16. All the specimens had 90° notches that terminated in fatigue cracks. The crack notches in specimen types WT and HT were located so that the direction of crack propagation was from the inside to the outside of the original vessel wall. The crack notches in specimen types WL and HL were located so that the direction of crack propagation was along the weld. The cracks in types WT and WL were located in the center of the weld, and those in types HT and HL were located in the heat-affected zone to correspond approximately with the position of the clean origin. Base plate specimens, type BT, were also tested and were similar to types WT and HT.

Crack extension during the K_{Ic} tests was sensed by two independent methods. In one method a constant current is maintained through the specimen during the test, and the difference of electrical potential between two points located symmetrically on either side of the crack is detected, amplified, and used to drive one axis of an X-Y recorder. The other axis of the recorder is driven by the output of a load cell so that the resulting record is a plot of load as a function of a measure of the change in crack length. In the other method, acoustic vibrations emitted during crack extension are picked up by a

sensitive transducer attached to the specimen and recorded on magnetic tape together with a record of the load. Both methods are described in detail in reference 4. In most of the tests there was no ambiguity about the results because the specimens fractured completely at the maximum recorded loads without appreciable crack extension at lower loads. In the tests of three of the five HT specimens, however, small increments of abrupt crack extension did occur at loads well below the maximum. Nevertheless, the maximum loads were taken as corresponding to the K_{Ic} values in these cases as well as in the other cases because the increments of crack extension were isolated, that is, there was no further appreciable crack extension up to maximum load. It is considered that the explanation for the behavior of the three HT specimens is that the crack tips in these specimens were located in highly heterogeneous regions, low in toughness in the grain-coarsened part of the heat-affected zones, but higher in toughness in the finer grained part of the heat-affected zones slightly farther from the crack tips.

TABLE I. - FRACTURE TOUGHNESS VALUES FROM FOUR-POINT BEND SPECIMENS TAKEN FROM W7/301 WELD REGION

Specimen type[a]				
WT[b]	HT[c]	WL[d]	HL[e]	BT[f]
Fracture toughness, K_{Ic}, psi$\sqrt{\text{in.}}$				
45 000	77 700	38 800	54 400	83 100
55 400	77 500	38 900	50 400	81 000
50 300	75 400	40 500	53 000	83 000
43 400	84 500			69 800
51 900	75 000			81 000
Average K_{Ic}				
49 200	78 000	39 400	52 900	79 600

[a]See fig. 16.

[b]Weld centerline, through thickness crack propagation.

[c]HAZ, through thickness crack propagation.

[d]Weld centerline, longitudinal crack propagation.

[e]HAZ, longitudinal crack propagation.

[f]Base plate, through thickness crack propagation.

The results of the K_{Ic} tests are given in table I. The locations and directions of propagation of the cracks in the type HT specimens most nearly correspond to those of the clean origin. The average of the K_{Ic} values for these specimens is nearly as high as that for the base-plate specimens, and the lowest of the five values, 75 000 psi$\sqrt{\text{in.}}$, is considerably higher than the upper bound of the K_I estimated for the clean origin, which was

57 000 psi$\sqrt{\text{in.}}$. It is quite possible that the actual K_I level was greater than this upper bound if there were substantial residual tensile stresses at the clean origin, but is unlikely that the K_I level could have been as high as 75 000 psi$\sqrt{\text{in.}}$. On the other hand, it is quite reasonable to suppose that the K_{Ic} toughness of the material adjacent to the clean origin boundary could have been substantially lower than the values determined with the type HT specimens from the W7/301 weld. The very existence of the origin suggests the possibility of a locally embrittled region, not necessarily restricted to the actual origin. The effect of TIG weld repairs on the toughness of the underlying material is an unknown factor that would require a considerable program of welding and testing to clarify adequately.

An alternative possibility is that the K_{Ic} toughness of the material adjacent to the convex boundary of the clean origin may have been sufficiently low that propagation started first at this boundary rather than at the concave boundary. The material immediately adjacent to the convex boundary is subarc weld metal of low toughness (fig. 11). However, the bulk of the material between the convex boundary of the origin and the inside surface of the wall is TIG weld deposit, which is presumably of high toughness.

Taking into consideration the uncertainty regarding the actual K_I level at the clean origin at 542 psi pressure and also the uncertainty regarding the K_{Ic} toughness of the material adjacent to the clean origin indicates that the fracture mechanics analysis is not inconsistent with the conclusion from the evidence of the fracture pattern that the hydrotest failure started from this origin.

The K_{Ic} values listed in table I for the specimens of types WT, WL, and HL, in which the cracks propagated wholly or partly through the subarc weld material, are considerably lower than those for the heat-affected zone, type HT, and base plate, type BT, specimens. If these weld material K_{Ic} values are to be compared with the K_I value for the black origin, it must be remembered that only part of the narrow limb of the origin is located in the W7/302 weld deposit (fig. 12). As stated previously, the lower bound K_I value of 25 000 psi$\sqrt{\text{in.}}$ is probably a good estimate of the correct value for this part of the origin at 542 psi pressure. This K_I value is considerably lower than any of the K_{Ic} values reported in table I. On the other hand, the corresponding K_I value for the hydrotest proof pressure of 960 psi is 45 000 psi$\sqrt{\text{in.}}$, which is higher than the K_{Ic} values for the WL specimens in table I. There is, therefore, a distinct possibility that premature failure would have started at the black origin if the clean origin had not been present.

A transverse defect was also found in the W7/101 weld, as discussed in the section Reinspection of Weld Areas After Hydrotest Failure. A large, longitudinal tension specimen containing this defect was tested and failed at a gross stress of 115 000 psi. The defect is clearly defined in the fracture surface, shown in figure 13, and is 0.6 inch long by 0.12 inch wide. It is located in the heat-affected zone of the TIG repair weld, which was also in the center of the subarc weld deposit, and oriented transverse to the weld centerline. The K_{Ic} value calculated from this test result is 47 500 psi$\sqrt{\text{in.}}$, which is in good agreement with the values for the WT specimens listed in table I.

Reinspection of Weld Areas After Hydrotest Failure

Since the clean and black origins were undetected by nondestructive testing techniques prior to aging, the question arose as to whether the defects were caused by aging, and if they would have been detected if additional nondestructive testing had been conducted subsequent to aging. It was further reasoned that if these defects were caused by the aging cycle, additional defects, which would have been at subcritical size at the hydrotest failure pressure, may have been present in other welds in the motor case. As a result, the Failure Investigating Committee asked Newport News Shipbuilding and Dry Dock Company to reinspect all welds in the 260-SL-1 motor case by using the inspection procedures previously used (PT, RT, and UT) plus magnetic particle (MT). In addition the U. S. Naval Research Laboratory was asked to inspect independently some of the weld areas by using UT. About 85 percent of the nondestructive testing of welds was completed before contract termination on June 5, 1965.

It was determined during this investigation that magnetic particle testing was of questionable value in the examination of welds in the 18 percent nickel maraging steel alloy. Similar conclusions were drawn in research conducted by Excelco Developments, Inc. under NASA contract NASw - 687. All welds in this alloy exhibit narrow but significant bands of reverted metastable austenite in the parent material heat-affected zones, and in such zones created in the weld metal by the deposition of subsequent weld beads. Since such bands impose a change in magnetic permeability in a uniform magnetic field impressed across them through adjacent fully martensitic material, small magnetic leakage fields result. The austenitic areas are therefore clearly defined when magnetic particle powder is applied, and any small flaws in or near these zones will be masked. The problem proved to be even more acute when an attempt was made to apply the testing technique to weld areas that were repaired by the TIG process. In such cases, each repair weld bead was outlined by fine but distinct powder adherence lines parallel to the repair bead progression sequence. Reliable delineation of a tight surface crack (or one just beneath the surface) under such conditions was questionable.

During the postfailure inspection of welds, eleven defect areas were found that had not been evident, or not rejectable, by the applicable standards prior to hydrotest. Of these defect areas, seven were found by UT, two by PT, and two by RT. It is not certain how many of these defects may have been present or how big they were during prehydrotest inspection. It is possible that some of the defects may have enlarged during pressurization or at burst so that they were more easily detectable in the posthydrotest inspection.

Four of the seven defects found by UT could not be discerned by RT. Two of the remaining three defect areas had such faint RT indications that preknowledge of the presence of the defect was required to locate the indication. These two flaws were not rejectable based on the film indications. A defect area found on W7/101 weld was detected by both UT and RT and will be discussed in more detail subsequently.

The two defects determined by PT could not be detected by other NDT

methods. One of these defects was removed by a light sanding indicating that it was a probable surface scratch.

Two defect areas were determined by RT on the W6/3 TIG weld (aft skirt). One of the defect areas also proved to be on the prehydrotest film, but it was so faint that preknowledge of its existence was necessary to locate it on the film. In the other defect area, which was not detected by NDT until after hydrotest, two defects 1/4- to 3/8-inch long were found under a TIG repair. The defects under the TIG repair to this TIG weld were the only known instances of thermal-shock cracking of a TIG weld in the welding program of the 260-SL-1 motor case.

In addition to the abovementioned defects, three other defects were found by RT that had been missed by the film interpreter on the original films taken before hydrotest. In all cases the flaws showed very faintly on the original film.

The most serious defect found in the posthydrotest NDT investigation was in the W7/101 weld beneath a TIG weld repair. This defect area was investigated by personnel from both the Newport News Shipbuilding and Dry Dock Company and the U. S. Naval Research Laboratory. Conflicting indications by RT and UT were given on the size and location of the defect. It was indicated by RT that the defect was a transverse crack located and oriented relative to the subarc and TIG welds similar to the black origin found on weld W7/302, but somewhat smaller. The UT investigation did not pick up the defect as well as RT, but indicated that the defect was not of rejectable size, in contrast to the large apparent size indicated by RT. A section of the motor case containing the defect was shipped to the U. S. Naval Research Laboratory. Again, UT was used to locate the suspected defect. A tensile specimen was cut with the apparent position of the defect in the middle of a 4-inch-wide test section. Instead of the failure originating at the defect indicated by UT, the failure originated from a defect that was displaced from the center of the specimen and not indicated by UT inspection at the Naval Research Laboratory, as shown in figure 13. The failure origin defect was approximately 0.6 inch long and 0.12 inch wide and similar in appearance to the clean origin in weld W7/302. After the tensile test, the radiograph was again examined and it was determined that the fracture origin had, indeed, been indicated on the radiograph, but it was not indicated by UT. The defect that was giving the UT response has not been found. In the section Nondestructive Testing Sensitivity Evaluation it is shown that, for fatigue-cracked specimens, UT is much more sensitive than RT for finding surface cracks. On first thought, it would therefore seem strange that the defect in the W7/101 weld was not indicated by UT as readily as it was by RT. A brief description of the mechanics of defect detection by UT will help clarify the reason for surface cracks to be detected more easily than submerged cracks.

Cracks that are approximately normal to the surface are detected by UT by transmission of pulsed waves of acoustic energy into the plate at an oblique angle, as illustrated rather idealistically in figure 17. When the transmitted wave intersects a defect, the wave is reflected. If this reflected wave returns to the transducer, the reflected signal can be observed on an oscilloscope. Figures 17(a) and (b) show that defects near the surface readily re-

flect the energy waves back to the transmitter. It is possible, however, for reflected waves from submerged defects to miss the transducer as illustrated in figure 17(c) so that the defect may not be detected. Reflections generally scatter much more than illustrated in figure 17, but the use of single transducers may not permit detection of all submerged defects in relatively thick plate. It appears that the defect in the W7/101 weld may have been missed for this reason. In addition, very tight cracks may not be detectable in all cases by UT. It has been determined that when accurately machined gage blocks are held closely together, the signal obtained from UT that indicates the discontinuity between the blocks is quite low. Very tight cracks are not detectable by RT either. It therefore appears possible to have submerged cracks of a type similar to the clean origin that may not be detectable by presently available nondestructive testing techniques.

The lessons learned from both the original and reinspection of weld areas before and after the hydrotest failure are: (1) reinspection of welds by NDT is required after aging as indicated by the number of defects that were found - at least some of which were present at the time of inspection prior to aging, but were not detected at that time; (2) all applicable NDT inspection techniques must be utilized since no single one is infallible, as indicated by the very carefully inspected defect in the W7/101 weld where conflicting information was obtained by RT and UT; and (3) it appears possible to have submerged defects within welds that are not detectable by NDT methods now available.

Nondestructive Testing Sensitivity Evaluation

No indication of the existence of either the clean or the black origin had been obtained from the nondestructive inspection of the W7/302 weld region that followed the experimental TIG repair welding. The TIG repair regions had been inspected by radiography on the day after the repairs were made, by dye penetrant 1 week and 19 weeks later, and ultrasonically 16 weeks after making the repairs. The procedures followed were those described earlier in the section Nondestructive Testing. These inspections were conducted before the aging heat treatment of the part, and no further inspection was conducted after aging, which was approximately 20 weeks after the TIG repairs were made on the W7/302 weld. Under these circumstances it was considered important to ascertain the sensitivity of radiographic (RT) and ultrasonic (UT) procedures for detecting cracks (as distinguished from the usual penetrameter or calibration notch sensitivities). For this purpose, five small test plates were prepared from motor case plate stock at the NASA Lewis Research Center. One of these plates was a blank, and each of the others was provided with a surface fatigue crack. The five plates were circulated for either RT or UT or both by each of the following organizations:

(a) Newport News Shipbuilding and Dry Dock Company (RT and UT)

(b) Sun Shipbuilding and Dry Dock Company (RT and UT)

(c) U. S. Naval Ordnance Laboratory (RT only)

(d) U. S. Naval Research Laboratory (UT only)

(e) NASA Lewis Research Center (UT only)

The test plates were each about 12 inches long, 3 inches wide, and 0.7 inch thick, and were aged at 900° F for 3 hours before fatigue cracking. The surface fatigue cracks were generated from small crack-starter notches, located at the centers of the plate faces, by repeated cantilever bending so that the nominal maximum fiber stress was approximately one-half the yield strength. The size of each crack was controlled by observing the length at the plate surface with a microscope mounted on a micrometer slide. After completion of fatigue cracking, the faces of the plates were ground to remove any trace of the starter notches. It was still possible, however, to detect the crack traces visually under proper illumination. The cracks were readily detectable by liquid penetrant or magnetic particle methods, and the test plates were not intended to be used for evaluating these methods.

After the plates had been circulated to all five participants for inspection, they were aged in air at 900° F for 1 hour with the object of heat tinting the crack surfaces. They were then cooled with liquid nitrogen and broken in tension to reveal the cracks, which are shown in figure 18. The purpose of cooling with liquid nitrogen was simply to enhance the brittleness of the fracture so that the cracks would be readily distinguishable in the photographs. These cracks are perpendicular to the long axes of the plates, extending into the plate thickness from the center of one face.

The dimensions of crack C (fig. 18) are about the same as those in the standard part-through-crack specimens used for evaluating toughness of test modules representing motor case material throughout the course of fabrication. Based on penetrameter and calibration notch sensitivities, it was assumed that cracks of this size and larger would be detectable with a high degree of confidence by the inspection procedures. To provide some indication of the relative severities of the cracks in the test panels, the calculated fracture stresses for a K_{Ic} fracture toughness of 50 000 psi$\sqrt{\text{in.}}$ are 210 000 psi for B, 180 000 psi for C, 147 000 psi for D, and 105 000 psi for E. For other K_{Ic} values the fracture stresses would be proportionate.

The results of the cooperative inspection program did not justify the confidence that had been placed in the ability of RT and UT to detect cracks. None of the radiographs obtained by the three organizations that used this method showed a rejectable indication of any of the cracks. In two cases, faint indications of what appeared to be a crack were discernable in the correct location in plate E, but it is doubtful that these indications would have been noticed in the normal course of the radiographic inspection procedure. The report by Newport News stressed the point that, under no circumstances, could the indication that they obtained for plate E be construed as a rejectable radiographic indication.

The ultrasonic methods proved to be somewhat more successful in detecting the cracks. The two shipbuilding companies and the U. S. Naval Research Laboratory employed ultrasonic testing at a level of sensitivity equivalent to that

specified for the inspection of the motor case. This specified level of sensitivity was limited by the need to keep indications reflected from the weld centerline grain structure to a reasonably low level. As a matter of interest, the U. S. Naval Research Laboratory repeated their inspection of the test plates at a higher level of sensitivity, and the NASA Lewis Research Center also inspected the plates with experimental equipment of high sensitivity that was designed for research studies of fatigue crack growth. These high sensitivity methods employed 5-megacycle crystals. In both cases, all the cracks were detected by the high-sensitivity equipment, but it would be unwise to assume that this sensitivity could always be put to practical use in shop testing of weld regions.

The three participants that used ultrasonic inspection at the sensitivity level employed during motor case fabrication all detected crack E as a rejectable defect. Crack D was reported as rejectable by one participant, not rejectable by another, and not detected by the third. Cracks B and C were reported as not rejectable by one participant and not detected by the other two. Thus, the ultrasonic method at the specified sensitivity appears to be reliable for detecting cracks of size E and larger, but doubtful for cracks of smaller size. Since the clean and black fracture origins were both larger than crack E, the question of why these origins were not discovered by UT inspection is still not resolved. If the origins existed as definite discontinuities at the time the UT was conducted, the gaps between their mating surfaces must have been considerably less than the gaps between the surfaces of the fatigue cracks in the test plates. Since the clean origin was entirely subsurface and the black origin almost entirely so, the possibility cannot be dismissed that they were present in the form of very tight cracks at the time of the UT inspection.

The results of this nondestructive testing sensitivity evaluation program were somewhat confounded by the inspections of the defect in the W7/101 weld discussed in the section Reinspection of Weld Areas After Hydrotest Failure. This defect is shown in figure 13, near one edge of the fracture surface of the tension specimen taken longitudinally from the weld region. The defect is about 0.6 inch long and 0.12 inch wide - somewhat larger than the crack in test plate E. It is actually located near the centerline of the subarc weld, but that weld was close to the edge of the 4-inch-wide test section of the tension specimen. The defect is closer to the outer surface than to the inner surface of the weld, and there were two TIG weld repair areas on the outer surface that intersected at the position of the defect.

Of the radiographs taken of this region after the hydrotest failure, two taken with the source on the outer side of the weld showed the defect distinctly, but a third, taken from the other side of the weld, showed only a vague indication. Radiographs taken in August and September of 1964, prior to the hydrotest, showed no indication in this region. As mentioned earlier, the UT examinations conducted after the hydrotest did not give indications of rejectable size.

The fact that this defect was detected by RT after the hydrotest failure, but was not detected some months earlier by the same means, should be considered in relation to the fact that the somewhat smaller crack in test plate E could not be detected definitely by radiography, although it was unquestionably

present. The most reasonable explanation would seem to be that the sensitivity of radiography for detecting cracks depends very strongly on the gaps between the crack faces as well as crack orientation. Between prehydrotest and post-hydrotest inspection there must have been an increase in the size of the gap in the defect in the W7/101 weld sufficient to make it detectable.

The main conclusion to be drawn from this minimal, exploratory program of evaluation of nondestructive inspection sensitivity is that there is a serious and urgent need for a much more comprehensive evaluation program.

SUMMARY OF FINDINGS

The significant findings from the hydrotest failure of the Thiokol Chemical Corporation 260-inch-diameter motor case can be summarized as follows:

1. The failure originated from an undetected defect in a region of the heat-affected zone of the W7/302 longitudinal weld that had been covered by a manual TIG repair weld. The defect, which was submerged within the vessel wall and oriented longitudinally, was approximately 1.4-inches long and had a width of about 0.10 inch.

2. A second undetected defect associated with the W7/302 weld was involved as a secondary fracture origin. This defect was also located beneath a TIG repair weld. It was somewhat larger than the primary origin, but was oriented transversely so that the nominal stress acting across it was only about one-half that acting across the primary origin. In the absence of the primary origin, fracture might have originated from this secondary origin at a pressure closer to the intended proof pressure.

3. Three other undetected defects were discovered under manual TIG repair welds when the weld regions were reinspected by nondestructive test methods after the failure. One of these defects was transverse to the W7/101 subarc weld. A large tension specimen that was tested to determine the severity of this defect fractured at a gross stress of 115 000 psi. The other two defects of substantial size were submerged under a TIG weld repair to the W6/3 TIG weld.

4. The association of severe defects with four separate TIG weld repair regions strongly suggests that the formation of these defects was a consequence of the TIG repair welding over a grain-coarsened material structure resulting from the high thermal input of the welding processes used. The detailed mechanism of formation of the defects has not been established because an extensive research program would probably be required for this purpose.

5. The fracture toughness of the submerged arc welds in this 250 grade maraging steel motor case was inadequate to tolerate crack-like defects as large as those that actually occurred in the motor case. It had been believed previously that much smaller defects could be detected with high reliability by the nondestructive inspection procedures that were used. The fracture toughness would have been sufficient to tolerate defects of a size that had been considered to be detectable.

6. Because none of the critical defects had been discovered by nondestructive testing prior to the hydrotest, a limited investigation was undertaken to ascertain the sensitivity of radiographic and ultrasonic procedures in detecting cracks. The results of this study showed that the NDT methods as used in motor case inspection are much less sensitive and reliable than had been expected, and that there is more to be learned about nondestructive inspection for the detection of cracks. The criticality of the sensitivity of inspection depends, of course, on the toughness of the materials involved. In the present state-of-the-art, the materials and welding processes selected should provide the highest attainable toughness consistent with the requirements of the application. In general, the tougher materials will be among those that have the lower yield strengths consistent with the requirements of the application. The sensitivity of the nondestructive inspection procedures should be evaluated for any specific application in relation to the toughness of the materials used.

7. For new motor case projects it is recommended that the sensitivity of the selected nondestructive testing procedures be thoroughly evaluated to determine if defects of a critical size for the design loads and materials used can be detected with confidence.

8. There is a possibility that the defects that were not detected during the inspection of the motor case prior to aging might have been detected if the motor case had been reinspected just before hydrotest. The aging heat treatment may have caused the defects to "open up" and thus become more detectable. It is therefore recommended that pressure vessels that are to be hydrotested should be thoroughly inspected immediately prior to the hydrotest, regardless of any previous inspections that may have been performed.

9. There is no evidence that any external factors or inadvertent loads contributed to the failure. It was a straightforward example of the weakening of a structure by a severe flaw.

Lewis Research Center,
National Aeronautics and Space Administration,
Cleveland, Ohio, October 19, 1965.

APPENDIX A

METALLOGRAPHIC EXAMINATION OF FRACTURE ORIGIN SITES

by A. J. Baker, A. J Birkle, P. S. Trozzo, and R. P. Wei,
of the Applied Research Laboratory, U. S. Steel Corporation

Figure 19 shows the pieces that were cut from the fragments of the SL-1 rocket motor case for examination at the U. S. Steel Applied Research Laboratory. The cuts were made along the W8/3 and W9/23 circumferential welds, and parallel to the W7/302 longitudinal weld at a distance of about 18 inches on either side. The individual fragments are identified in this report by the numbers shown in figure 19.

Immediately after the fracture fragments were received, the fracture surfaces around the two defects and on fragments 2 and 5 were photographed. Faxfilm replicas of the defect areas were prepared for fractographic examination. Pieces containing the two defects were then cut (sawed dry) from the fragments and prepared for metallographic examination and for X-ray diffraction and electron-microprobe analyses. Prior to cutting, plastic casts of one of the fracture surfaces in each defect region were made by using silicone rubber molds.

Since the surfaces of the two defects were damaged to varying degrees, it was necessary to section mating portions of each defect. A region halfway between the two defects (fig. 19) was taken to be representative of fracture along the longitudinal weldment and was selected for metallographic examination to determine the location of the fracture path.

Clean Defect

Figure 20 shows photomacrographs of the inner surface of the motor case, the fracture surfaces, and several transverse sections in the clean defect region. The circled numeral denotes the nondestructive test (NDT) station number scribed on the motor case. Figure 20(a) shows the presence of a multipass TIG weld repair over the fusion line of the subarc weld. The TIG weld deposit was predominantly in fragment 2.

The transverse sectional views in figure 20 shows that the clean defect (the upper and lower boundaries of which are denoted by the black marks in the section B-B views) was located in the grain-coarsened region of the subarc weld heat-affected zone (HAZ) just below the dark etching band of the TIG repair weld. The forward terminus of the clean defect corresponded approximately with one end of the TIG repair weld (fig. 20(a)). Its aft terminus conformed to the dark etching bands of both the subarc and TIG weld (fig. 20(a), section A-A).

Previous investigations (ref. 6) have shown that the dark etching zones are regions of maximum austenite reversion that exhibit high fracture toughness at a somewhat reduced strength level. The dark etching bands correspond to regions that have experienced a maximum temperature in the range of 1200° to

1300° F during the welding cycle. Regions between the dark etching bands and the fusion line have experienced temperatures ranging from approximately 1300° to 2700° F, and thus these regions were re-austenitized and grain-coarsened to varying degrees. Regions outside the dark etching bands, having reached maximum temperatures less than 1200° F, were aged to different extents.

Figure 21 shows fracture profiles in the clean defect region. Figure 21(a) shows a fracture profile from near the center of the clean defect proper and is representative of the portion of the defect that has a crystalline appearance. The grain-coarsened structure is evident. Fracture within the area of the defect proper was predominantly intergranular, that is, along the grain boundaries of the coarsened grains. Regions below the clean defect exhibited transgranular cracking with "ductile" tearing typical of maraging steels (ref. 7, fig. 21(b)). A secondary crack perpendicular to the main fracture surface also appears in figure 21(b).

Fractographic results confirmed the light microscopy observations. Figure 22(a) shows predominantly grain-boundary fracture in the region of the clean defect. Away from the clean defect, the fracture appears to be interdendritic through the subarc weld metal (fig. 22(b)) and shows a more ductile, "dimpled" type failure in the finer grained re-austenitized region of the HAZ of the base plate (fig. 22(c)).

Extraction fractographs over the clean defect were made in an attempt to ascertain the possible presence of embrittling constituents. However, because of the long exposure to atmosphere (approximately 1 month had elapsed before the fragments were received for laboratory investigation), the fracture surfaces were too badly contaminated to yield definitive results.

Replication electron micrographs (figs. 23 and 24) taken in the region of the clean defect show microstructures typical of subarc weldments. Figure 23 shows representative microstructure in the grain-coarsened zone lying directly behind the clean defect. Figure 24 shows the microstructure in a region adjacent to the subarc weld fusion zone; it contains a significant amount of reverted austenite, mainly at grain boundaries. The prior austenite boundaries - and to some extent, the martensite plate boundaries - show an enhanced etching characteristic, which suggests that the grain-coarsened HAZ of the base plate experienced some embrittlement (ref. 6) as a result of the thermal cycles that occurred during welding and weld repair. Additional investigations would be necessary to confirm this observation.

These metallographic observations indicate that the clean defect occurred in the grain-coarsened region of the base plate in the subarc weld HAZ, and was located directly under a region of TIG repair welding; one edge of the defect coincided with the dark etching band of the TIG weld. Fracture in the defect area was mainly intergranular. Without further research on specimens representing all stages of the thermal history of the weldment, it is only possible to speculate on the process of formation of the clean defect. During subarc welding, a coarse-grained, brittle zone was created adjacent to the weld-metal deposit. The embrittlement reaction would be akin to the embrittlement of maraging steels produced by heating to 2200° F, cooling, and holding at 1400° F (ref. 8) except for the higher temperatures encountered and the much shorter

time at temperature. Intergranular cracking of this grain-coarsened region was probably produced by the thermal and/or transformation stresses associated with the TIG repair welding. The proximity of the forward end of the clean defect to the front edge of the TIG repair weld tends to support this hypothesis. However, the possibility that the flaw originated during the aging process cannot be ruled out. For reasons not understood, the aft end of the defect deviated into the tougher reverted zone and was thus arrested.

Black Defect

Figure 25 shows a photomacrograph of the inner surface of the motor case in the region containing the black defect. The main line of the subarc weld can be seen, with the general features of a TIG repair superimposed on it. The apparent surface cracking along the left side of the main fracture was caused by the macroetching procedure. The black defect lies transverse to the subarc weld, on the face B-B, at the point where the main fracture intersects that section. The general features of the defect are shown in section B-B given in figure 26. A polished cross section A-A provides a comparison between the black-defect fracture surface and the underlying macrostructure (fig. 26). This cross section was taken outside the region of the repair and consequently shows only the features of the subarc weld. Section C-C in figure 26 provides a better representation of the structure in the black-defect region, although the penetration of the TIG repair is greater in this section than in the plane of the black defect proper.

The black defect consists of a region covered with a black film, with fracture lines radiating from it. The defect has an L-shape, and at one point extends to the outer surface of the motor case through a region of the base plate adjacent to the dark etching band of the subarc weld HAZ. The blackened region extends from one side of the subarc weld completely across the weld metal to the base metal on the other side. The markings of the columnar solidification pattern of the subarc weld metal are clearly visible in the black-defect area of the fracture surface. Various sections transverse to the black defect and parallel to the main fracture path are shown in figure 27. The transverse sections (D-D to G-G) show that the entire length of the black defect (the boundaries of which are indicated by the black marks) is located immediately below the dark etching band of the TIG repair. The crack in section G-G can also be seen in the surface macrograph (fig. 25) and was probably generated during the case failure. The parallel sections H-H and I-I show that no flaw similar to the black defect exists at the aft end of the TIG repairs.

Figure 28 shows fracture profiles through the black-defect surface. The black layer between the steel and the nickel plate in figure 28(a) is a plastic mounting compound that seeped under the loose nickel coating during metallographic mounting. Figures 28(a) and (b), which were taken from section E-E in figure 27, show the profile of the grain-coarsened base plate in the region of the subarc weld HAZ. Figures 28(c) and (d), which were taken from section D-D in figure 27, show a region of base plate outside the subarc weld HAZ.

The fracture path in the black defect itself appears to be intergranular, and there is evidence of grain-boundary cracking perpendicular to the main

Fracture. The grain structure visible is that of the prior austenite. Outside the black-defect area, the fracture path has a more ductile, transgranular appearance.

Fractographs of the black-defect surface taken in the various locations, identified as areas 1, 2, 3, 4, and 5 in figure 26, are shown in figure 29. Areas 1 to 3 are located within the black defect itself, and the fractographs (figs. 29(a) to (c)) show a generally flat, intergranular appearance. Various fine-scale surface features are visible in figures 29(a) to (c), but the presence of the black surface film prevents any detailed interpretation. Area 4 (fig. 29(d)), which lies in the subarc weld metal but outside the black defect, exhibits a somewhat more ductile appearance. Area 5 (fig. 29(e)), in a region of the fracture in the base plate outside the black defect, shows a distinctly dimpled contour indicative of ductile fracture.

TABLE II. - ANALYSIS OF FILM ON BLACK ORIGIN

(a) X-ray diffraction analysis

Lattice spacing, d, Å			Relative sensitivity, I/I_o
Fe_2O_3	Fe_3O_4	Sample	
3.67	----	3.67	VVW
----	2.96	2.96	VW
2.69	----	2.69	M
2.51	2.52	2.52	M
2.20	----	2.20	W
----	2.09	2.02	VS
----	----	1.86	VW
1.84	----	1.83	VVW
----	----	1.77	W
1.69	1.71	1.68	W
1.60	1.61	1.59	VW

(b) Electron-probe analysis

Extraction	Metallic elements present, percent					
	Iron	Nickel	Molybdenum	Cobalt	Titanium	Manganese
Wet[a]	87	9	3	0.5	0.5	-
Dry[b]	87	8	2	1	---	2

[a]Average of 4 readings.

[b]Average of 2 readings.

The HAZ of the base plate was examined at high magnification by replica microscopy; figure 30 shows typical areas near the black defect. The prior austenite boundaries - and to some extent, the martensite plate boundaries - show an enhanced etching characteristic and some evidence of second-phase particles, possibly austenite and/or TiC (ref. 6). These observations support the conclusion that the HAZ of the base plate experienced some embrittlement as a result of the thermal cycles that occurred during welding and weld repair.

The black film on the surface of the black defect was examined by X-ray and electron-diffraction techniques. The X-ray diffraction d-spacings and relative intensities, obtained by a glancing-angle technique on a bulk sample, are given in table II(a). The pattern was that of a mixture of Fe_2O_3 and Fe_3O_4. Electron-diffraction analysis of particles of the surface film, dry-stripped on replicas, confirmed the X-ray diffraction result. An electron-microprobe analysis (ref. 9) of the dry-stripped oxide (table II(b)) revealed the presence of all the metallic elements to be expected in an oxide formed on maraging steel (iron, nickel, molybdenum, cobalt, and titanium). However, because iron predominated, some preferential oxidation of iron is indicated.

The black defect thus consisted of an oxidized flaw running predominantly across the subarc weld metal and the grain-coarsened region of the subarc weld HAZ, below a TIG repair. The highly oxidized state of the surface indicates that the flaw was exposed to the atmosphere at an elevated temperature. It is unlikely that the oxidation resulted from the heat of the TIG repair welding alone because a considerable portion of the black defect was located outside the HAZ regions of these welds, as shown in figure 27 (section D-D). Because of the presence of an opening to the plate surface, some oxidation of the defect surface certainly took place during aging at 835° F.

The mechanism by which the flaw was generated cannot be definitely established. The point of origin cannot be ascertained, but the widest area, and also the point at which penetration to the surface occurred, is in the region of the subarc weld dark etching HAZ. Since the defect follows a line produced by the HAZ of the TIG repair, it appears that the flaw was generated by stresses set up during TIG repair in a region in which severe microstructural inhomogeneity and grain coarsening occurred. However, the possibility that the flaw originated during the aging process cannot be ruled out. Further investigation of specimens from all stages of the thermal history of the weldment would be necessary to clarify this matter.

Fracture Path Between Primary and Secondary Origins

Figure 31 shows the appearance of the fracture along weld W7/302, approximately midway between the two defects, and a macrograph of a cross section through the fracture. (The circled numeral again denotes the NDT station number scribed on the motor case.) The fracture path is unusual in that it was not macroscopically flat in the midthickness region. The fracture appears to be interdendritic through the subarc weld metal near the two surfaces of the weld, where the dendrites were oriented nearly normal to the weld surface. In the midthickness region, the fracture tended to follow the triangular-shaped fusion interface. At some places, the fracture path followed the fusion inter-

face on one side while traversing the weld metal (interdendritically) on the other side.

Fracture profiles (fig. 32) show a typical path followed by the main fracture through the midthickness region of the weldment (fig. 32(a)) and near the weld surface (fig. 32(b)). It is interesting to note that the fracture in the midthickness region occurred entirely in the grain-coarsened zone, just outside the subarc weld metal. The unusual path taken by the fracture suggests that this region possessed perhaps the lowest fracture toughness in comparison with other regions of the weldment, and consisted of an embrittled microstructure.

Summary

The results of this investigation showed that a multipass TIG repair weld is associated with each of the two defects. One edge of each defect is closely associated with the dark etching band of the HAZ produced by the TIG repair weld. The primary clean origin lies in the grain-coarsened region of the base plate in the subarc weld HAZ. The secondary black origin traverses the subarc weld metal, the grain-coarsened HAZ of the subarc weld, and extends some distance into the base plate. Fracture paths in the defects themselves are primarily intergranular, along prior austenite grain boundaries or along dendritic interfaces in the subarc weld metal. Fracture adjacent to the defects exhibits a more ductile appearance, characteristic of maraging steels. The film of black material associated with the black defect consists of iron oxide (both Fe_2O_3 and Fe_3O_4) with small amounts of oxides of other metallic elements (nickel, molybdenum, cobalt, and titanium). It appears that the defects were generated by stresses set up during TIG repair in a region exhibiting severe microstructural inhomogeneity and grain coarsening.

The fracture path between the primary and secondary origins tends to be interdendritic through the subarc weld metal near the two surfaces of the plate, where the dendrites were oriented nearly normal to the plate surface. In the midthickness region, the fracture path conforms generally to the fusion interface, and lies entirely in the grain-coarsened zone just outside the subarc weld metal. The fracture was intergranular. The unusual path taken by the fracture suggests that the grain-coarsened region possesses the lowest fracture toughness with a highly sensitized microstructure. This observation is consistent with the production of the two defects described previously in just this region of the weldment.

These results suggest that the high heat input during submerged arc welding creates grain coarsening and thermal embrittlement over an extensive region of the base-plate adjacent to the weld-metal deposit. This region is susceptible to cracking under stresses, such as those that are generated by subsequent high-temperature cycles associated with repair welding.

APPENDIX B

STRESS-WAVE DETECTION SYSTEM

When a crack or flaw suddenly propagates in a motor case or other stressed structure it triggers stress waves that radiate outward from the initiation source. Two primary types of stress waves are generated: (1) a dilational wave causing particles in the motor case wall to move in a direction parallel to the wave propagation direction, and (2) a shear wave causing particles in the case wall to move in a direction normal to the wave propagation direction. The dilational wave is difficult to detect with instrumentation, but the shear wave can be detected by placing small accelerometers on the case wall that measure accelerations normal to the surface of the wall. By knowing the wave velocity and measuring the arrival times of the stress wave by means of accelerometers placed on the case it is possible to determine the origin of the stress wave by triangulation.

The dilational wave has a velocity of approximately 200 000 inches per second, and the shear wave velocity is approximately 118 000 inches per second for maraging steel. The actual shear wave velocity is determined on the motor case by impacting the case and measuring the time for the impact pulse to propagate between adjacent accelerometers that have a known separation distance.

During this investigation, 24 accelerometers were located on the motor case as shown in figure 3. During the hydrotest the output from the accelerometers was continuously recorded by multichannel tape recorders. One of the accelerometers (number 12) was also connected to a cathode ray tube oscilloscope in the control room to provide a visual display of stress-wave occurrences during the hydrotest. Another accelerometer (number 19) was connected to an audio amplifier and a loudspeaker in the control room to provide an audible display of stress-wave occurrences.

In the final reduction of the accelerometer data to determine the stress wave origins, it was necessary to provide time expansion for the recorded data. This time expansion was obtained by reducing the tape recorder playback speed by a factor of 100, relative to the recording speed, and recording the data on an oscillographic recorder with a speed of 160 inches per second to obtain an effective oscillographic recording speed of 16 000 inches per second.

The accuracy by which the stress origin can be pinpointed is determined primarily by the frequency response of the instrumentation and the accuracy in determining the wave propagation velocity. The frequency response during these tests was 10 kilocycles, resulting in a time resolution of approximately 100 microseconds. With all factors considered, and based on past experience, the "circle of confusion" for determining the location of the stress origin was approximately 20 inches in diameter.

The stress wave detection system used during the hydrotest is under development by the Aerojet-General Corporation, Sacramento, Under NASA contract NAS7-310. The stress-wave detection tests and reduction of data from the hydrotest were conducted by Aerojet-General personnel.

The locations of stress wave origins are indicated approximately in figure 3. More accurate location of the stress wave origins, along with the acceleration amplitudes recorded, is given in table III.

TABLE III. - STRESS-WAVE ORIGINS

Pressure, psig	Acceleration amplitude, g's	Stress-wave origin (See fig. 7 for weld locations)
242	7	17 in. left of weld W7/102 and 4 in. forward of weld W6/1
267	3	On weld W9/23 and 44 in. right of weld W7/301
379	1	8 in. aft of weld W8/1 and 54 in. left of weld W7/102
432	7	9 in. aft of weld W9/12 and 9 in. left of weld W7/202
495	0.5	35 in. forward of weld W8/3 and 10 in. left of weld W7/302
518	0.4	On weld W8/1 and 111 in. left of weld W7/101
518.5	0.2	48 in. forward of weld W8/3 and 18 in. left of weld W7/302
542 (Failure)	---	29 in. forward of weld W8/3 and 8 in. right of weld W7/302

APPENDIX C

SUMMARY OF CONSULTANTS REPORTS

The summaries provided herein contain the general content of the reports by the Consultants, but they are not direct transcripts of the reports submitted to the Failure Investigating Committee. The reports have been edited, but the interpretations of their findings have been preserved. The reports are opinions that were expressed by the Consultants in the early phases of the failure investigation. In some cases these opinions differ from those of the Failure Investigating Committee.

Ward D. Abbott, Excelco Developments, Incorporated. - A written report on the motor case failure was not presented by Mr. Abbott. In an informal discussion he expressed the following opinions:

(1) The amount of damage that occurred to the motor case at failure was surprising. Hydrotests that have been conducted on smaller (120 in. diam) tanks at higher pressures have resulted in more strain energy being present, but the fracture of these tanks was less severe. The severe damage to the 260-inch-diameter motor case and the appearance of the fracture surfaces indicate that the material in this case had been degraded to a much lower fracture toughness. The many small fragments resulting from the failure are also an indication that the fracture toughness of the 260-inch-diameter case was not typical of what to expect from 18 percent nickel maraging steel.

(2) The submerged arc welding process heats the surrounding materials to the point that material properties are degraded to a greater extent than with multipass TIG welding. The massive heat-affected zones clearly indicate poorer mechanical properties. This condition is probably further irritated by having to use preheat with the subarc welding process.

(3) Based on experience at Excelco with TIG welding, it is unlikely that residual stresses in welds and heat-affected zones contribute to crack growth. However, when welding with the subarc method, considerable delayed cracking has been experienced that would indicate that residual stresses may be a contributing factor with this type of welding method.

(4) Although limited past experience has not shown aging of maraging steel to increase defect size, nondestructive testing should be conducted after aging as well as before aging. At present there is not enough experience in the use of 18 percent nickel maraging steels to eliminate any of the nondestructive testing cycles.

(5) The techniques of nondestructive testing have been improved during the development of large, solid rocket cases. Principally, this improvement has been in the field of ultrasonics. All methods should be used in combination to detect and identify defects. Briefly it is felt that the individual methods contribute as follows:

(a) Dye penetrant: Single best method for detecting surface defects that are generally the most dangerous

(b) Magnetic particle: Good for surface and immediate subsurface except in areas where heat-affected zone (austenitic layer) may mask a defect; the method would generally be used for information only to help identify a known defect

(c) X-ray: Properly interpreted X-ray films can be dependable for all defects except tight cracks not parallel to the exposure angle; after such a defect has been found (probably by ultrasonics) X-ray techniques can be used to verify and define

(d) Ultrasonic: The technique of the operator is of utmost importance; the shear-wave technique is particularly good for finding defects in welds; longitudinal wave is particularly good for finding laminar defects parallel to the surface; identification of a defect with ultrasonics is very poor; however, once detected by ultrasonics, the defect can be identified readily with X-ray

Thomas H. Burns, Thiokol Chemical Corporation. - After careful study of available fracture faces and the included chevron pattern existent in the same, two possible origins of failure are designated:

(1) The light banana-shaped longitudinal internal defect

(2) The dark heat-tinted transverse crack

Both these defects were contained in the W7/302 weld of the aft cylinder.

Metallurgical observation of the fracture faces existent bring forth the following comments:

(1) The fracture progressed forward from the bright origin in essentially a ductile manner.

(2) The fracture pattern was not affected or altered by weld areas, slicing across them and continuing in the parent metal plate.

(3) Some flat fracture was existent in both parent metal and weld, but there was little evidence of brittleness. Idealizing the transverse crack shape, a K_{Ic} value has been calculated as 39 000 to 47 000 psi$\sqrt{\text{in.}}$ The longitudinal defect has been calculated at 43 900 to 54 800 psi$\sqrt{\text{in.}}$ Either of these values are considerably lower than the K_{Ic} values previously determined for subarc weld. This then raises the question of

(a) The reliance of which may be placed in fracture toughness determinations made on panels containing symmetrical cracks

(b) The accuracy of assessing fracture toughness values from nonsymmetric crack front in a burst vessel

(c) The variation of K_{Ic} values across the weld, fusion line and HAZ, and the effect on K_{Ic} in areas beneath repairs

It should be remembered that the K_{Ic} values for submerged arc-welded panels have been adequately established at 58 000 to 62 000 psi$\sqrt{in.}$, BUT that virtually all fracture toughness tests have been conducted with the fatigue crack located in the center of the weld bead surface. It is of further significance to note that the K_{Ic} of the TIG repair deposit has been determined at 70 000 to 75 000 psi$\sqrt{in.}$. This then leaves unanswered the reason for the seemingly low K_{Ic} value of the two defective areas lying immediately below TIG repairs.

A cursory look has been taken at some of the requirements necessary to produce the type of shear failure exhibited by 91 of the 92 bolts contained in the aft lifting ring. Extrapolation of these loads from requisite formulas predicts the need for a force of 1 million pounds. The acceleration of the lifting ring required to produce this force is estimated at 71 g's.

A brief analysis was made of the crack extension force resultant from release of strain energy contained in the case at failure. If this energy was restricted to none other than crack extension, sufficient force was available to run a crack 241 billion inches long. Therefore, it is entirely conceivable that enough energy was available at the time of failure to produce the catastrophic failure mode exhibited by this case.

In summation of the preceding points, it can be concluded that

(1) Either the longitudinal light defect or the black transverse crack may be reasonably assumed to be the locus of the primary origin of failure.

(2) No importance has been attached to other locations of a secondary origin of failure.

(3) Considerable significance should be attached to the K_{Ic} values extrapolated for the defective areas when compared with either the subarc weld deposits centerline or the TIG repair deposits.

(4) The fracture faces were considered normal for maraging steel with such a failure mode existent.

(5) Assessment should be made of the extremely high g loads necessary to shear the bolts in the aft lifting ring.

(6) It is reasonable to expect the catastrophic failure mode exhibited by this case with the release of the stored energy available.

Charles F. Tiffany, The Boeing Company. - The actual inspection of the failed motor case was conducted by Joseph N. Masters of the Boeing Company. He prepared the consultant's report for the failure committee in collaboration with Mr. Tiffany. They reported the following findings:

(1) Fracture patterns and markings clearly pointed to the aft shell W7/302 weld as the general area of failure origin, and thus little time was spent outside this area. One general comment is noted, however, only minute and intermittent splits, as opposed to general and gross delamination, were observed in the base metal fractures, and chevron markings were therefore quite distinct. Shear lips occupied possibly less than 10 percent of the faces of the cylindrical shell base metal.

(2) The fracture paths through the aft shell were as shown in figure 7. The arrows depict fracture propagation directions. Two crack-like appearing indications were found as detailed in figure 7(b). The black origin intersected the outside surface at one local area and was a uniform black color, apparently tinted from the aging cycle. The clean origin was totally embedded and was only slightly different in color and texture from the surrounding material.

(3) A short length of the fracture surface near the clean origin, exhibiting a generally square face, displayed signs of fracture markings emanating from the midpoint of the crack and traveling both fore and aft. Good clear indications of fracture direction between the two origins were not present, except for those just noted adjacent to the clean origin.

(4) Independent of these observations, stress intensity values K_I can be calculated for both defects, based on membrane stresses supplemented by possible secondary stresses such as are discussed in Air Force contract AF 33(615)-1623 progress reports:

(a) X-ray diffraction measurements of residual surface stresses were made by Boeing at several locations on the maraged center shell subassembly. With few exceptions the readings indicated a compressive stress generally in the range of 50 000 psi. Measurements made on flat-welded panels gave similar results. By taking measurements on successively deeper layers of the flat panels exposed by electropolishing, it was apparent that the compressively stressed layer did not extend much deeper than 10 to 15 mils, and that within the measuring accuracy of ±10 000 psi, significant tensile stresses were not observed. It was considered, therefore, that residual stresses would not have significant effects on any but extremely shallow surface defects, and in that case the effect would generally be beneficial.

(b) Considerable effort in AF 33(615)-1623 has been devoted to the problems of design deviations (e.g., weld sink-in and mismatch). Fair confidence is placed on the Boeing Company analyses of girth-weld deviations because of inherent stiffness of the compound curvatures involved. It has been felt that these analyses of gradual deviations of longitudinal weldments were conservative and if nonlinear deflections could be accounted for, actual effects might be considerably less important than calculated. However, based on contour and strain gage data obtained on the 260-inch-diameter motor case, possibly some better insight might be obtained. One longitudinal and one tangential strain gage were located on the outside surface of the W7/302 weld, 10 inches forward of W8/3 (Y-ring weld). Reduced data at 500-psi hydrotest pressure showed stresses of

45 200 and 77 300 psi, respectively, and based on the final pressure of 540 psi, the stresses would become 48 800 and 83 500 psi. The Boeing Company analysis of Y-ring discontinuity stresses shows that, at this same location, the total fiber stresses (at 540 psi) without weldment deviations are:

Outer surface:

S_1 = 96 800 psi

S_2 = 55 550 psi

Inner surface:

S_1 = 91 800 psi

S_2 = 38 950 psi

where S_1 = hoop stress

S_2 = longitudinal stress

If it is temporarily assumed that the discrepancy between calculated and strain gage measured stresses is a result of weld-contour deviations, a deviation-induced bending stress of 96 800 minus 83 500 psi, or about 13 000 psi, exists inside the surface in tension. Contour readings obtained show an outward deviation (cusp) at all places along the W7/302 weld; this deviation averages about 0.06 inch (at the weld centerline) outward when measured at the neutral axis. The 13 000-psi bending stress assumed for a 0.06 inch cusp is about 30 percent of the values that can be calculated through the use of linear elastic solutions, but it compares favorably with a value of 16 000 psi computed from an approximate nonlinear approach. At the clean origin (36 in. forward of the W8/3 Y-ring weld), the Y-ring discontinuity has been sufficiently washed out to be neglected. Therefore, maximum hoop fiber stress at the clean origin can be assumed to be the membrane stress (95 000 psi) plus or minus the bending stress (13 000 psi) for the cusp. Using this assumed stress, and the clean origin flaw dimensions gives the maximum applied stress intensity $K_{I,max}$ of 55 000 psi$\sqrt{in.}$. The irregular shape of the black origin precludes firm stress intensity expressions; however, some estimates are provided. The maximum stress (51 500 psi) is obtained from the longitudinal membrane stress (47 500 psi) and the longitudinal bending stress (4000 psi). At this stress, K_I values with varied simplified flaw shapes are shown as follows:

TABLE IV. - FLAW SHAPES

Shape	Location	K_I, psi $\sqrt{in.}$
0.19×1.3 ellipse	Internal	27 500
0.50 diameter penny	Internal	29 500
0.50 radius semicircle	Surface	48 000

From table IV it is difficult to imagine that the actual applied K_I at the black origin could be much greater than 30 000 to 40 000 psi$\sqrt{\text{in.}}$

(5) The Boeing Company tests of subarc weld test plates supplied by Newport News Shipbuilding and Dry Dock Company indicate K_{Ic} values from surface flaw specimens of approximately 55 000 psi$\sqrt{\text{in.}}$ at yield strengths of 215 000 to 220 000 psi.

(6) Conclusions

(a) Two possible failure origins were observed near the W7/302 weld. The primary failure cause was a crack-like defect parallel to the weld at the clean origin. Failure occurred when the applied stress intensity reached a critical value of about 55 000 psi$\sqrt{\text{in.}}$

(b) Stresses caused by contour deviations were present, but had less than a 10-percent effect on failure pressure. Residual stresses are not considered to be a significant factor in the failure.

(c) Had failure initiated at the black origin, the straight-line fracture parallel to W7/302 is unexplained; the fact that the straight-line fracture lined up with the clean origin would also be unexplained; the markings just forward of the clean origin would have to be neglected; and the critical K_I value for transverse directions of subarc weldments would have to be less than 40 000 psi$\sqrt{\text{in.}}$

Max L. Williams, Jr., California Institute of Technology. - Based on personal inspection of the propellant case failure and study of related aspects of fracture mechanics:

(1) It appears reasonable to conclude that the primary fracture occurred at the so-called clean origin, with the secondary fracture at the black origin being triggered by the primary unloading wave.

(2) Evaluation of the stress intensity at the primary fracture yields a value of approximately 45 000 psi$\sqrt{\text{in.}}$ based on the final shape of the fracture surface. It is not evident a priori, however, that a preexisting (open) internal flaw was present before the final loading cycle.

(3) The predicted stress analysis for the rocket case is consistent with the strain-gage measurements recorded during the test.

It is recommended that

(1) The final fracture surface of the clean origin be carefully examined to determine, if possible, whether there was an (open) preexisting flaw.

(2) Mechanical and physical properties be determined in the vicinity of both clean and black origins.

(3) Castings be made of the fracture surface of both origins, so that the

three-dimensional geometries may be preserved for possible later discussion and analysis.

(4) Consideration be given to a closer theoretical assessment of the stresses in the fracture vicinities, based on the actual final fracture-surface configurations. Recent advances in analytical procedures suggest this is practicable, although not necessarily simple or rapidly obtained. Because of the large difference between the estimated stress intensity at failure (K_I = 45 000 psi$\sqrt{\text{in.}}$) and the critical value (K_{Ic} = 60 000 psi$\sqrt{\text{in.}}$), one would like to verify that the apparent discrepancy is <u>not</u> a result of the approximations in the analysis. If this point were established, one would then be in position to conclude that special circumstances such as residual stress or metallurgical deviations were present.

APPENDIX D

INVESTIGATIONS OF FACTORS SUSPECTED TO BE RELATED TO FAILURE

In order to be certain that all factors which may have contributed to the failure of the motor case were given adequate consideration, an investigation was conducted by the Thiokol Chemical Corporation to evaluate all conditions that could have possibly had an influence on the failure. This investigation included interviews with all personnel associated with the hydrotest and those that were nearby or witnessed the failure. In addition, analyses and inspections were made subsequent to the failure to determine the possible significance of factors that may have been related to the failure. The investigation covered the following factors:

(1) Investigation of the strain energy present in the case at the time of failure to determine if it could account for the extensive fracture damage that occurred.

(2) Review of the case design stresses and the stresses measured by strain gages during hydrotest to determine if they were consistent.

(3) Determination if a possible structural failure in the hydrotest tower or binding between the test piston and test nozzle could have put a load on the motor case that would have contributed to failure.

(4) Investigation of the possibility that gas generation or an explosion could have initiated failure.

A brief discussion of the interviews and the investigation of each of the preceding factors follows:

Interviews. - Forty-two people were interviewed to determine what they observed at the time of the failure and to determine if they knew of any factors that may have influenced the failure. The reports from most people were quite similar. There were no warnings or indications that failure was imminent either in any of the gage readings or audible noises. The people that were reading pressure and strain gages stated that they were all reading in a uniform manner up to the instant of failure.

Prior to pressurization, water was bled from the top of the motor case through the top piston to ensure that there were no trapped gases within the case. The man who was on the top of the motor case observing the bleeding was certain that all air was vented from the case.

Prior to the hydrotest a chain fall fell and hit the case. Examination by several people indicated that the damage was limited to abraded paint and was of no significance relative to hydrotest failure.

Strain energy in motor case. - A calculation of the total strain energy in the case at the failure pressure showed it to be of the order of 5×10^6 foot-pounds, which was amply sufficient to account for the extensive destruction

that occurred at failure. It was therefore concluded that this extensive damage was not the result of some unusual and undiscovered phenomenon.

Stress analysis. - After hydrotest, an investigation was conducted to re-examine the case design and evaluate the strains recorded during test. From this analysis it was determined that in the locations where strains were measured there were no indications of excessive stresses above those calculated from the original design. At locations where out-of-contour occurred, the measured strains were slightly less than one-half that calculated from the "worst condition" assumptions. The worst condition assumed that the out-of-contour portion of the case took the shape of a cusp. In the actual case, the deviations from true contour were much less severe. It was concluded from this investigation that there was no apparent evidence that a design deficiency existed.

Hydrotest tower effects. - Some holddown bolts on the tower were found to be loose after hydrotest, leading to the suspicion that some overloads had been applied to the tower. It was speculated that the overload could have possibly resulted from excessive binding of the piston, producing an eccentric load on the motor case, or that binding with a sudden release could have produced dynamic loads. Investigation subsequent to hydrotest showed the motor case to be so much stiffer than the hydrotest tower that loads imposed by the tower would be small. In addition there was no concrete evidence of piston binding. A review of extensometer readings on piston movement and comparison with calculated movements indicated no abnormal movements of the case or piston.

Gas generation or explosion. - Consideration was given to gas generation within the motor case by water electrolysis either by battery action or from a potential generated by electric-arc weld repairs to a bleed line on the motor case. Consideration was also given to the possibility of an explosion occurring in the space between the motor case and the tower enclosure as a result of propane leakage from some gas cylinders located at the site with the rubber hoses terminating inside the enclosure. After a thorough analysis of the possibilities of gas generation and explosions, it was concluded that neither was likely, and they were not significant considerations in the failure.

Conclusions. - All areas pertinent, or which could be suspect, to the cause of premature failure of the 260-SL-1 rocket motor case have been observed and evaluated. The general appearance of the extensive fracture and damage resulting from hydroburst can be supported from the standpoint of stored strain energy available at the time of burst. It can be confirmed that the case design was sufficient in detail to establish the fact that design stresses were not excessive and were not a contributing factor in this failure.

Rational fracture analysis appears to support the theory that the origin of failure was in the area of the bright flaw and that this flaw was of sufficient size to initiate rapid propagation even at the low average stress levels demonstrated by strain-gage measurements. There does not appear to be any reasonable basis for the suspicion that unusual phenomena of an external causative nature may have contributed to the premature failure.

REFERENCES

1. Irwin, G. R.: Fracture. Vol VI of Encycl. Phys., S.Flugge, ed., Springer-Verlag (Berlin), 1958, pp. 551-590.

2. Anon.: Fracture Toughness Testing and Its Applications. STP No. 381, ASTM, 1965.

3. Paris, Paul C.; and Sih, George C.: Stress Analysis of Cracks. Fracture Toughness Testing and Its Applications. STP No. 381, ASTM, 1965, pp. 30-33.

4. Srawley, John E.; and Brown, William F., Jr.: Fracture Toughness Testing. NASA TN D-2599, 1965. (See also Fracture Toughness Testing and Its Applications. STP No. 381, ASTM, 1965, pp. 133-196.)

5. Irwin, G. R.: Crack-Extension Force for a Part-Through Crack in a Plate. J. Appl. Mech. (Trans. ASME), ser. E, vol. 29, no. 4, Dec. 1962, pp. 651-654.

6. Birkle, A. J.; Reisdorf, B. G.; and Salmon-Cox, P. H.: An Investigation of the Mechanical Properties and Microstructures of 18 Ni (250) Maraging Steel Weldments. Tech. Rept. AFML-TR-65-364. Air Force Materials Research and Technology Division. Air Force Systems Command, Wright-Patterson Air Force Base, Mar. 1965.

7. Pellissier, G. E.: The Physical Metallurgy and Properties of Maraging Steels. Rept. No. DMIC 210, Battelle Memorial Inst., 1964, pp. 173-188.

8. Birkle, A. J.; Dabkowski, D. S.; Paulina, J. P.; and Porter, L. F.: A Metallographic Investigation of the Factors Affecting the Notch Toughness of Maraging Steels. Trans. ASM, vol. 58, no. 3, Sept. 1965, pp. 285-301.

9. Reisdorf, B. F.; and Baker, A. J.: The Kinetics and Mechanisms of the Strengthening of Maraging Steels. Rept. No. AFML-TR-64-390, United States Steel Corp., Jan. 1965.

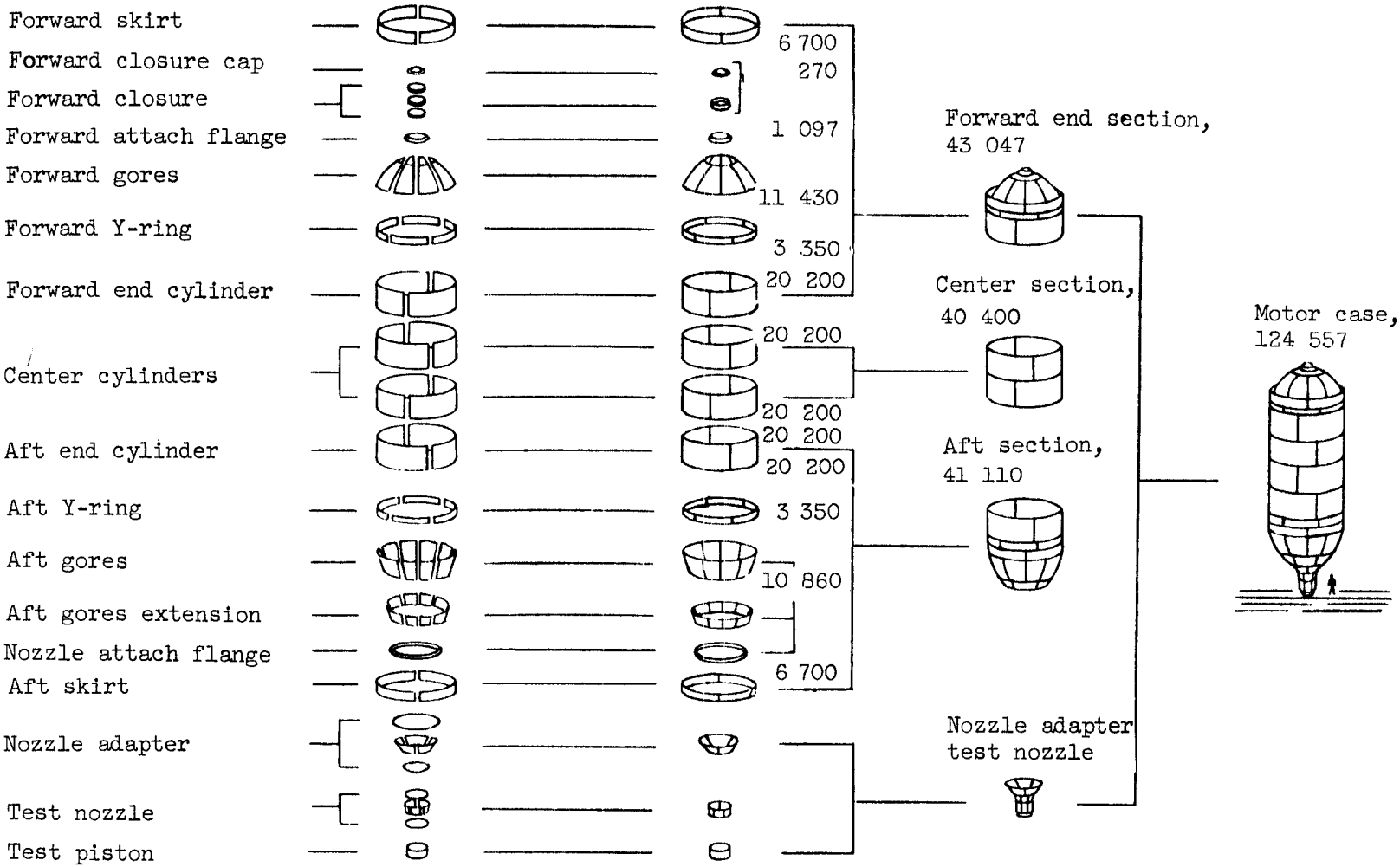

Figure 1. - Fabrication sequence for 260-inch-diameter solid-fuel rocket motor case. (All values are weight in pounds.

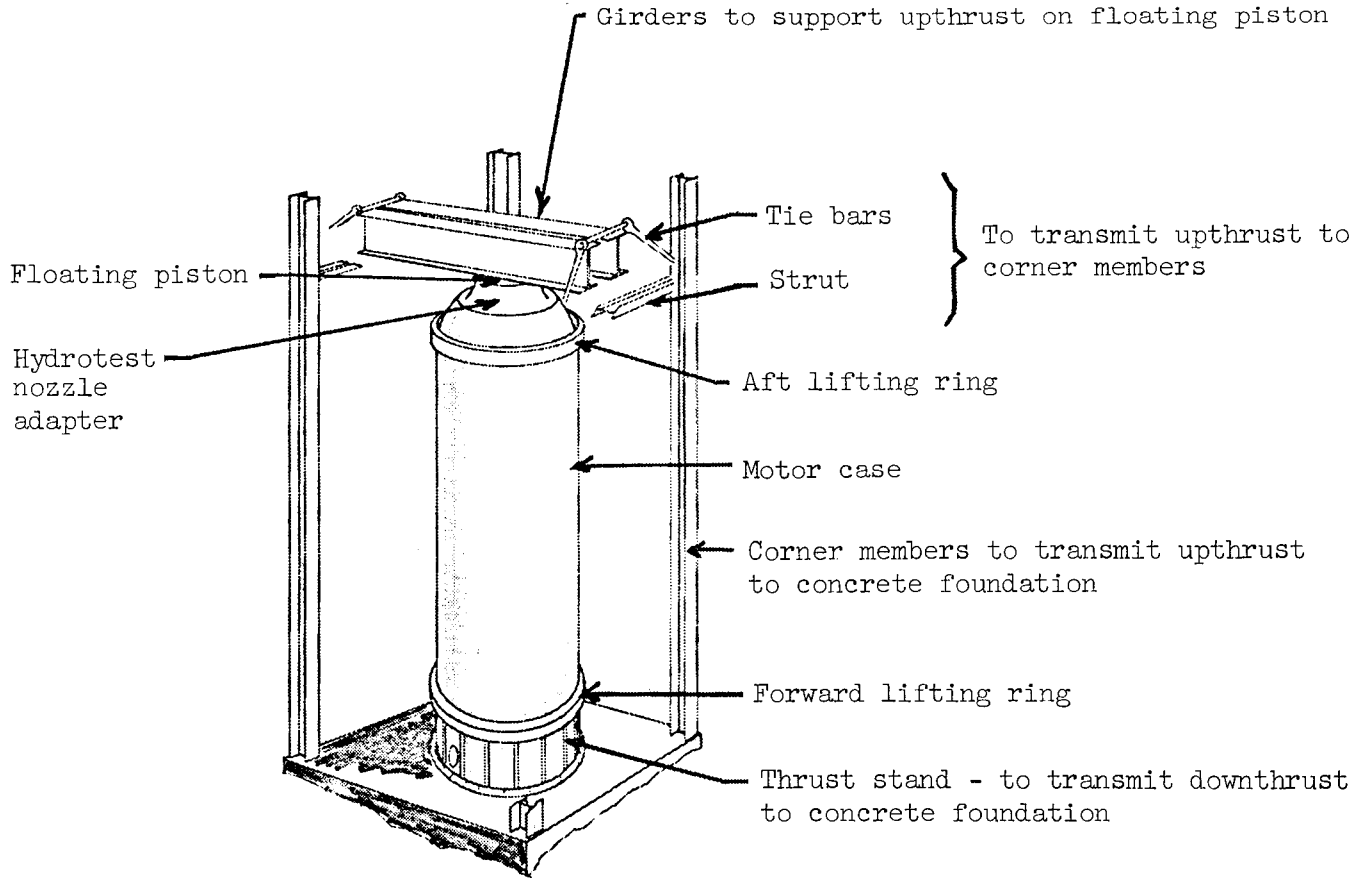

Figure 2. - Motor case installation in hydrotest tower.

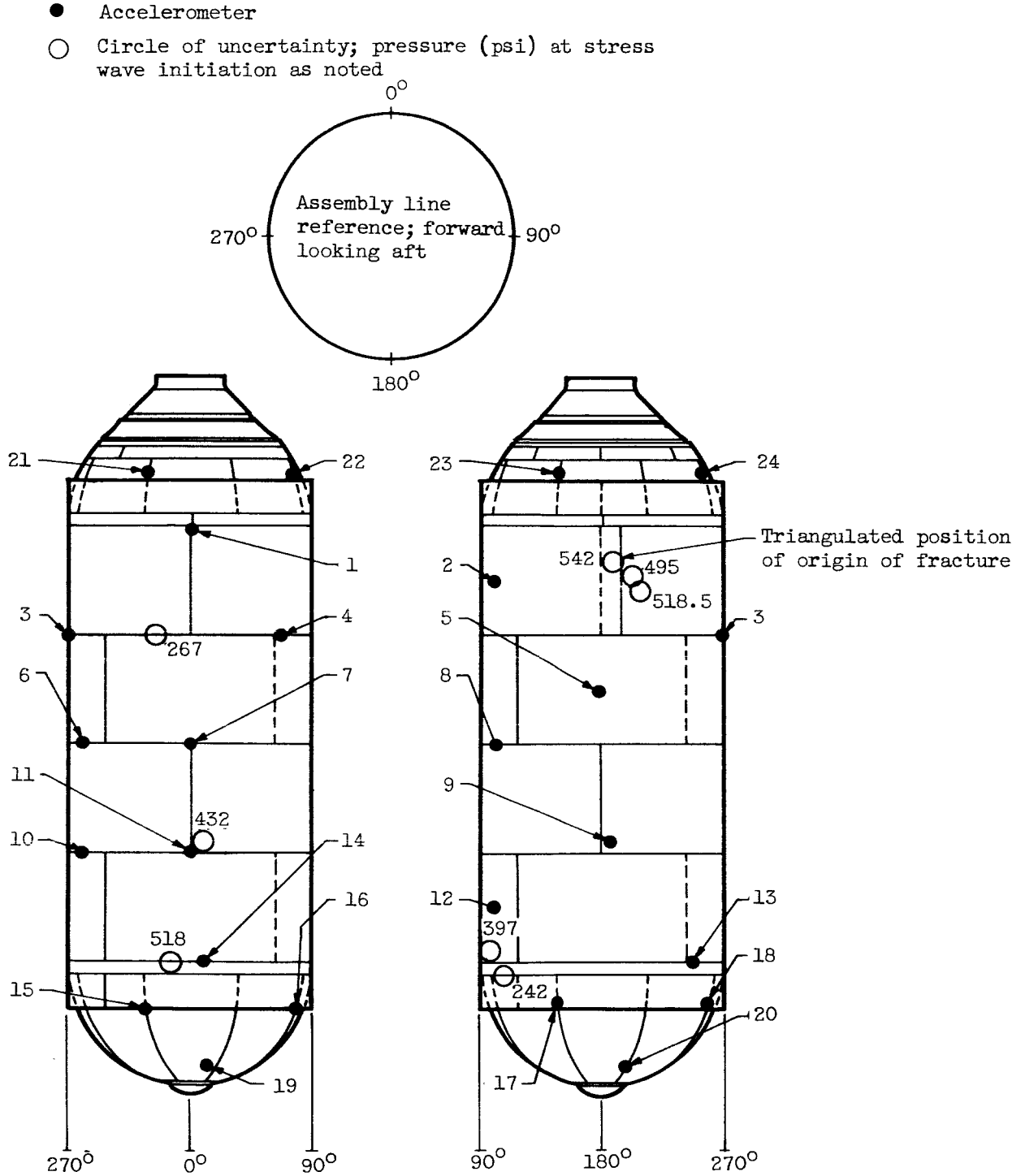

Figure 3. - Locations of accelerometers and stress wave origins on 260-inch-diameter SL-1 motor case.

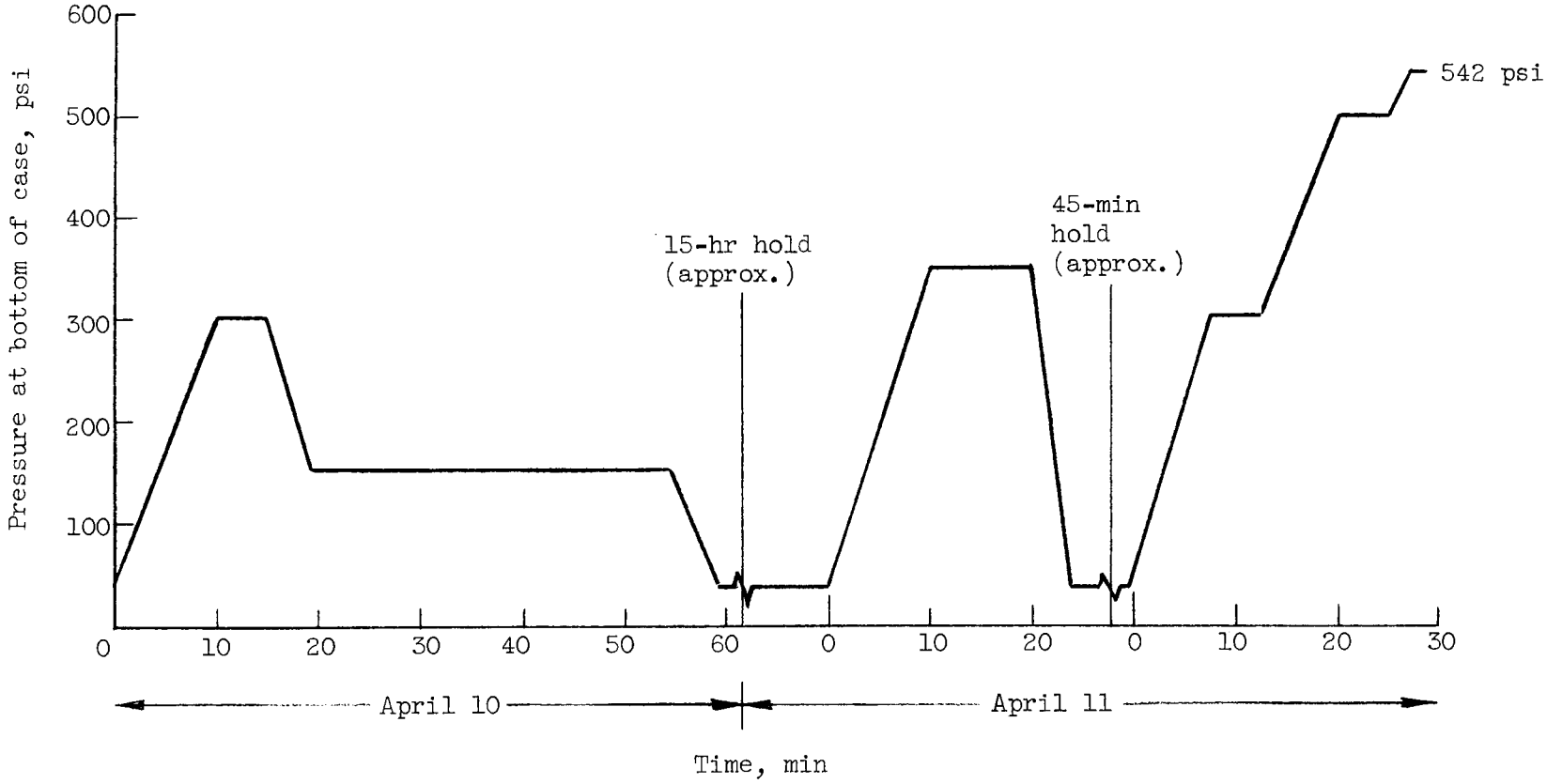

Figure 4. - Pressure-time history during hydrotest.

Figure 5. - Portion of failed motor case as it was being removed from hydrotest tower.

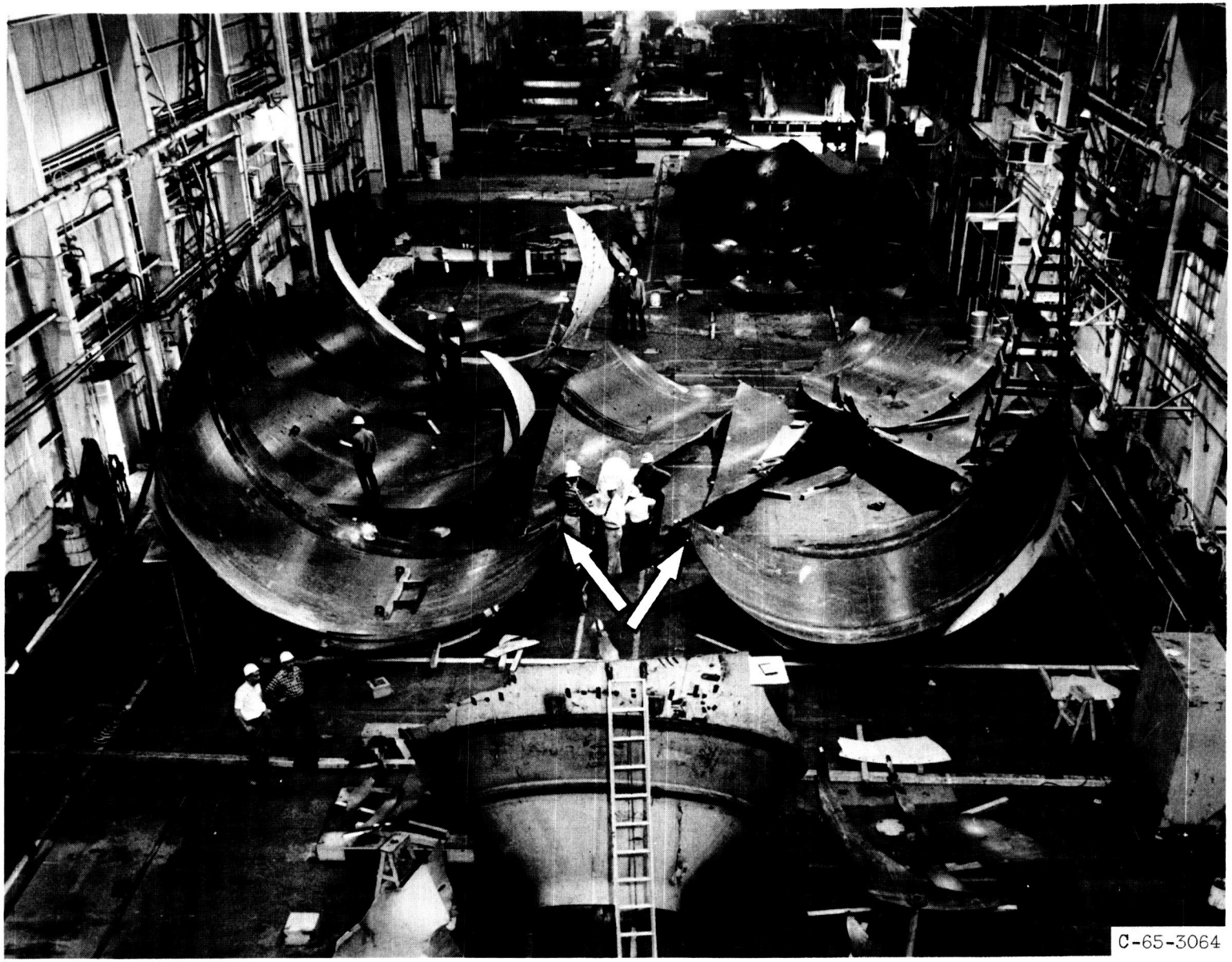

Figure 6. - Failed motor case with pieces laid out in approximately the proper relation to each other. View is looking forward with aft head in foreground. Origin of fracture indicated by arrows.

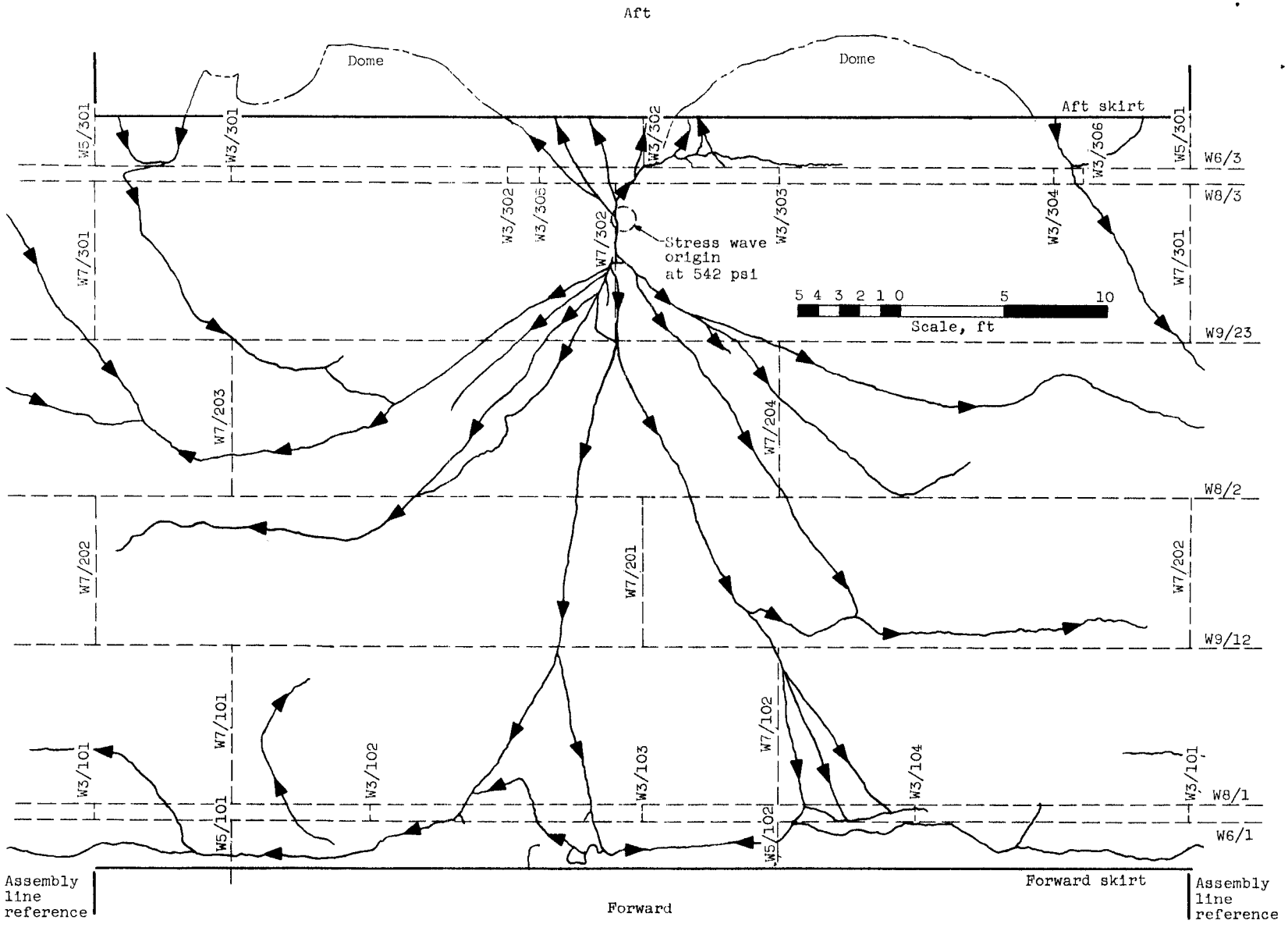

(a) Cylinder and skirts.

Figure 7. - Map of fracture paths as viewed when looking at inside surface developed onto plane obtained by unrolling cylinder. Arrowheads indicate directions of fracture propagation.

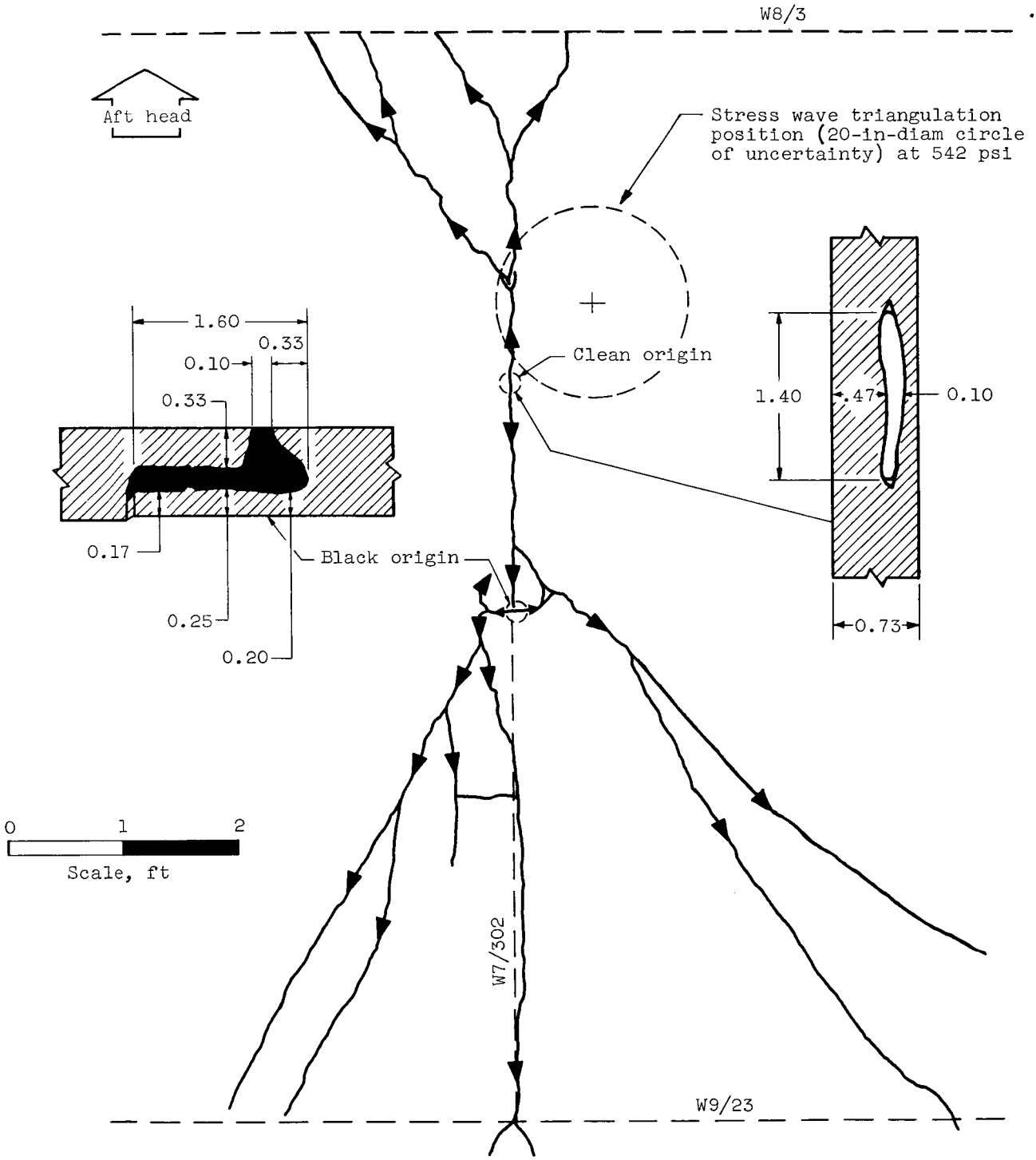

(b) Detail in immediate vicinity of primary and secondary origins. Inset sketches show shapes and dimensions of the two origins.

Figure 7. - Concluded.

Figure 8. - Typical chevron markings on fracture surface showing directions of fracture propagation away from black origin.

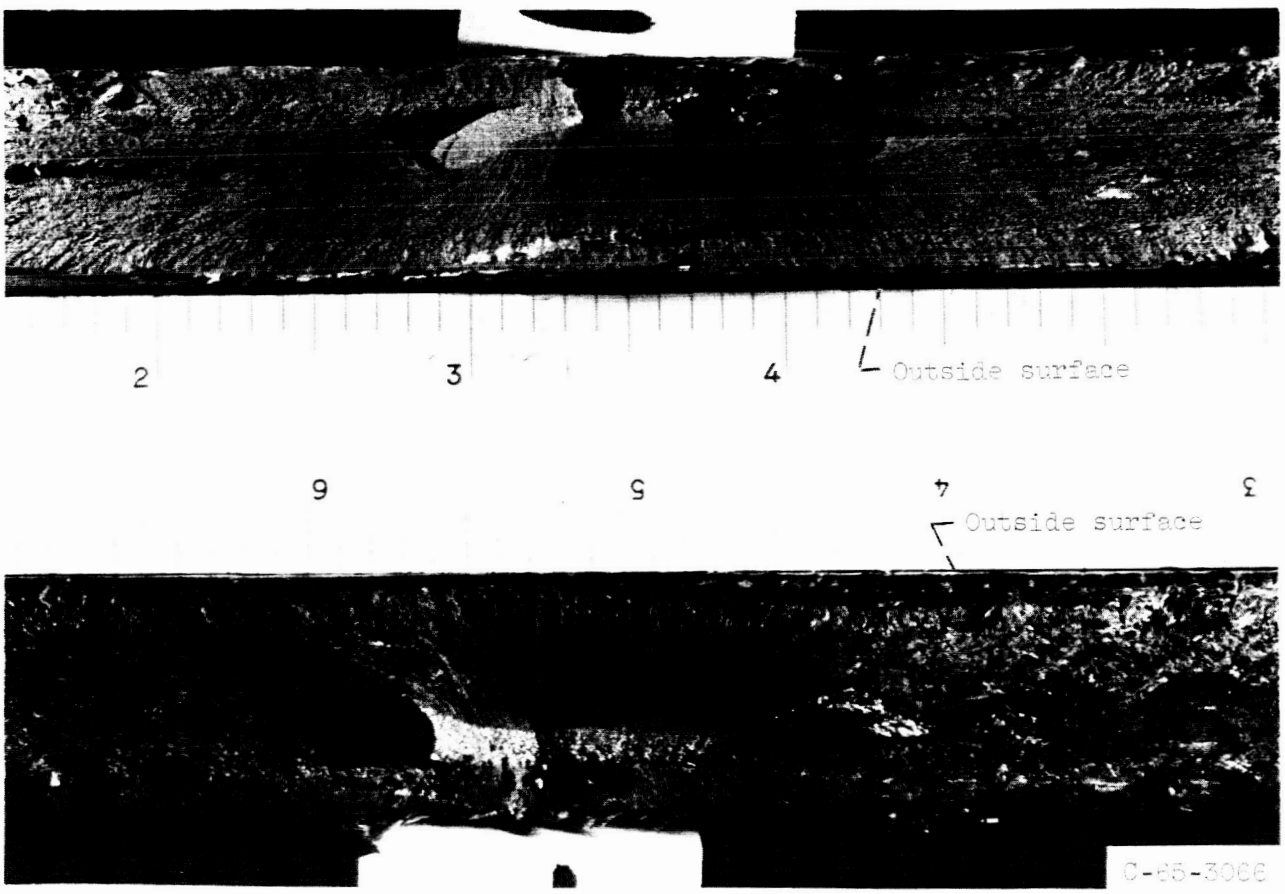

Figure 9. - Mating surfaces of clean origin on W7/302 weld.

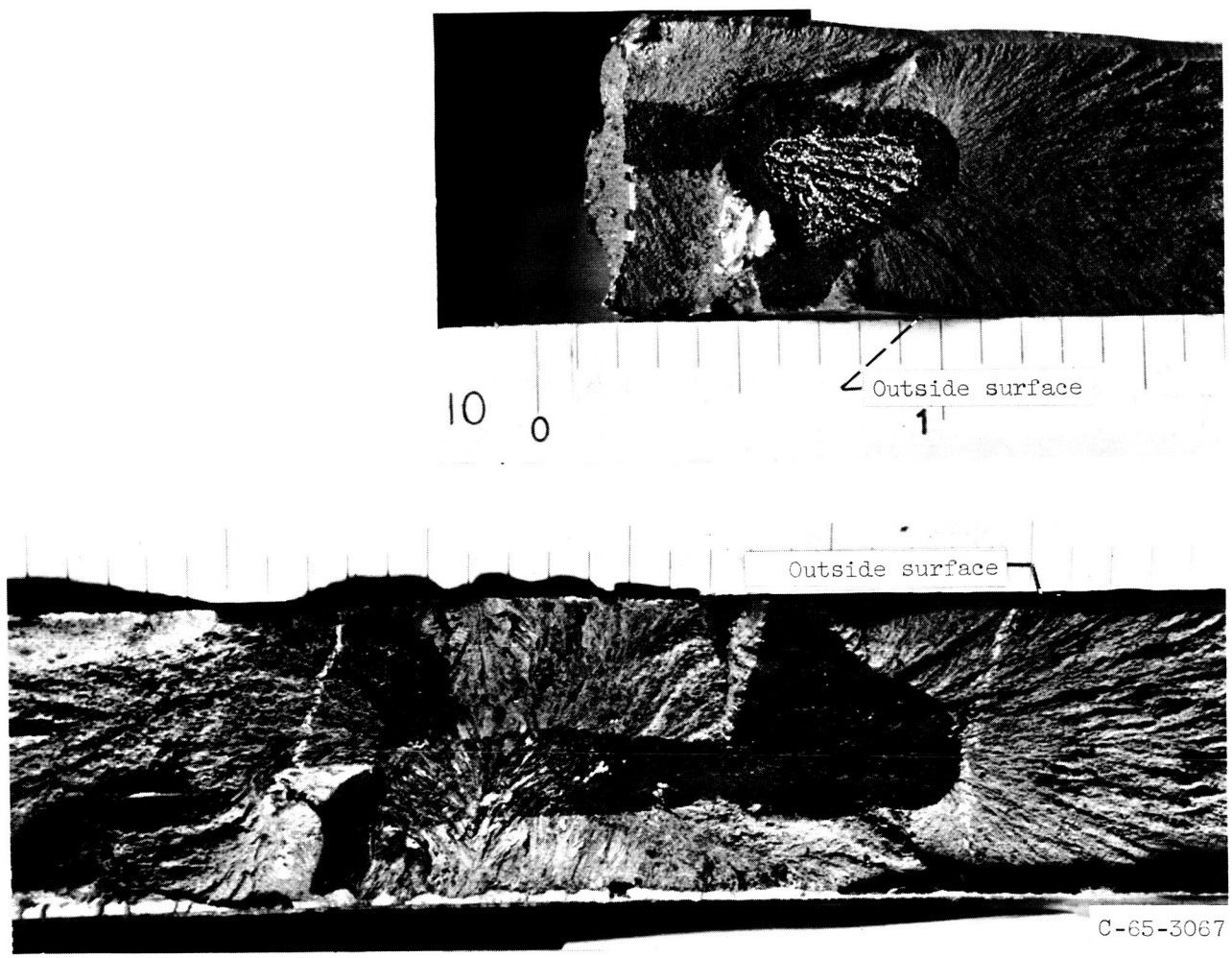

Figure 10. - Mating surfaces of black origin on W7/302 weld. (Part of black material has been removed from one surface for analysis.)

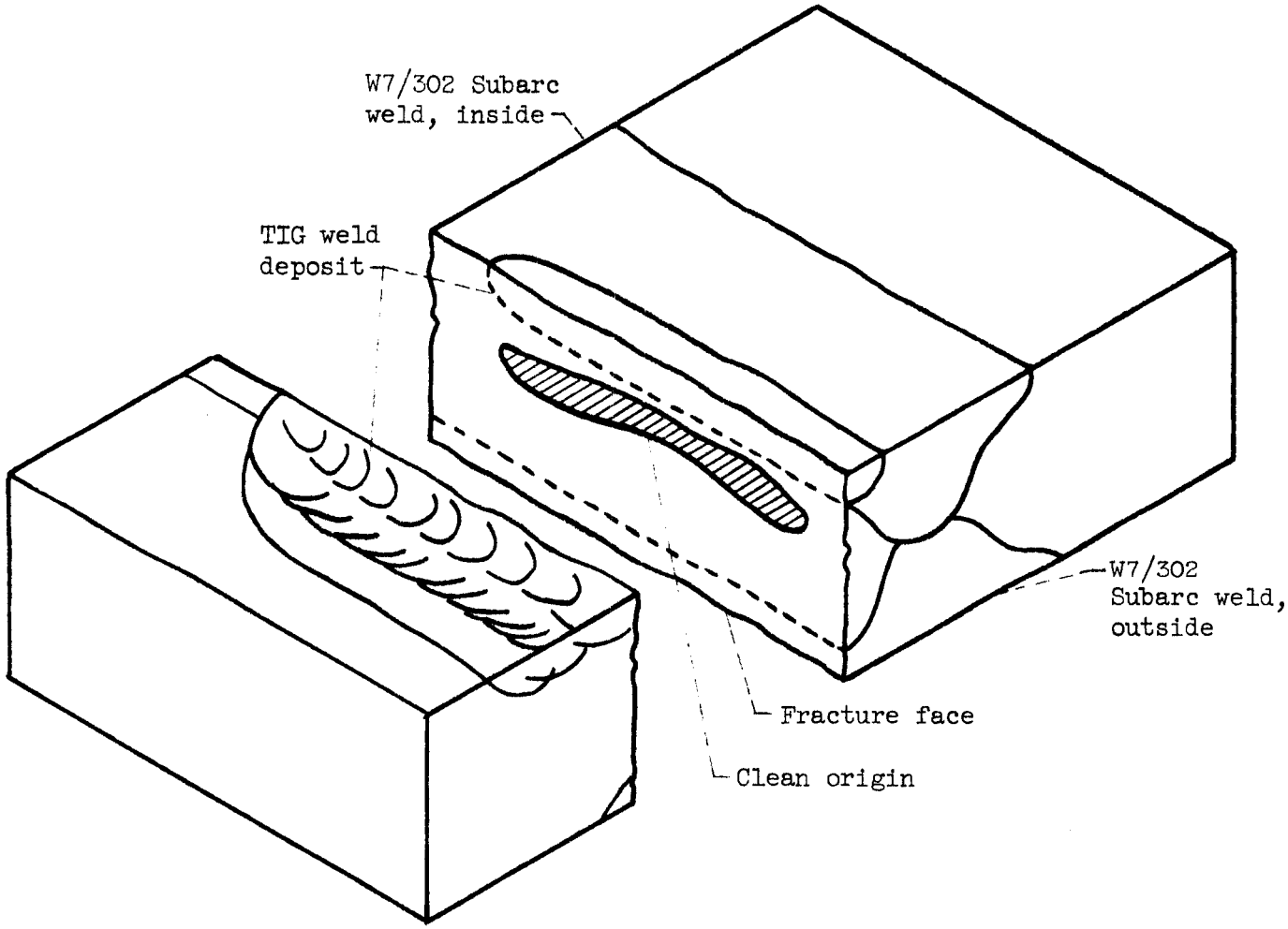

Figure 11. - Isometric drawing showing relation of clean origin to weld deposits.

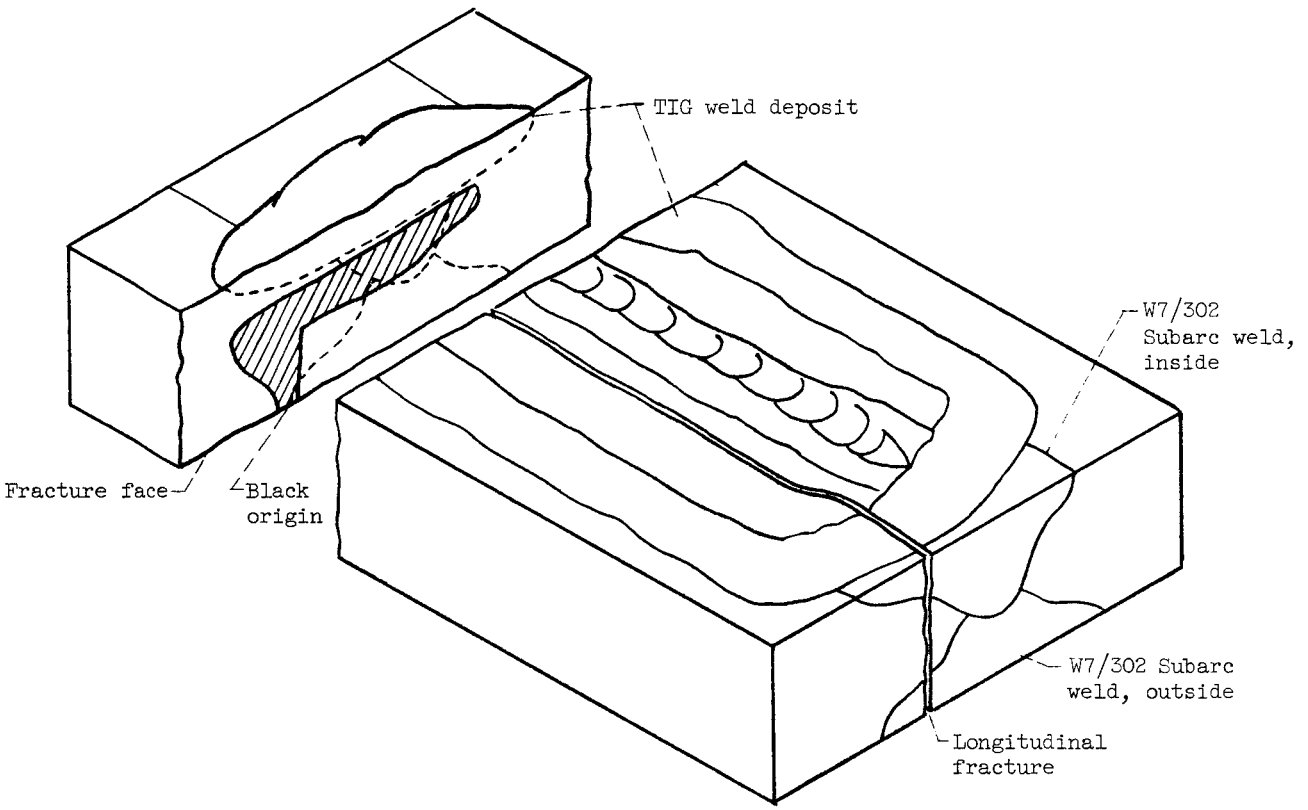

Figure 12. - Isometric drawing showing relation of black origin to weld deposits.

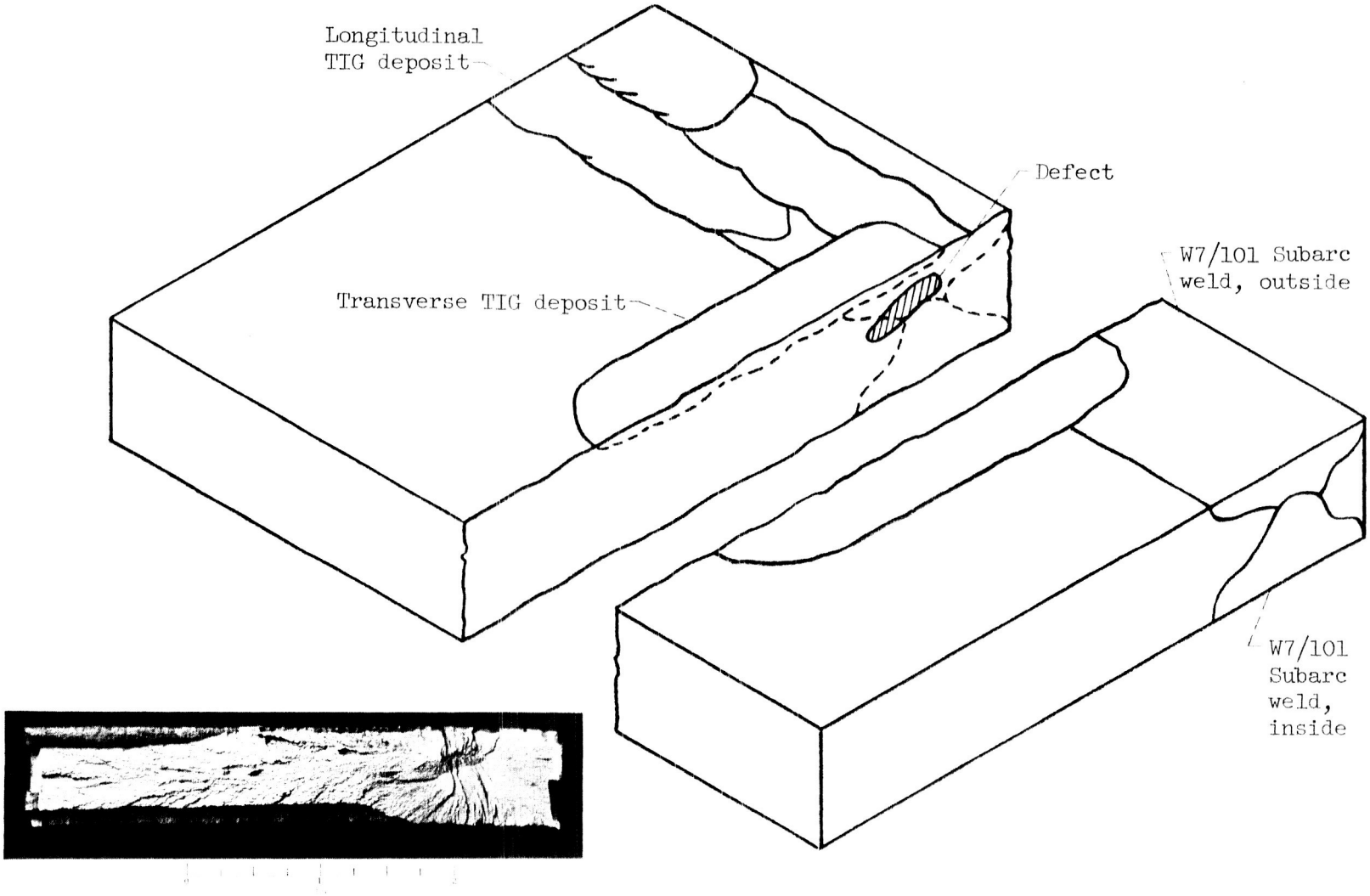

Figure 13. - Isometric drawing and photograph of fracture surface of longitudinal tension specimen from W7/101 weld region showing defect related to weld deposits.

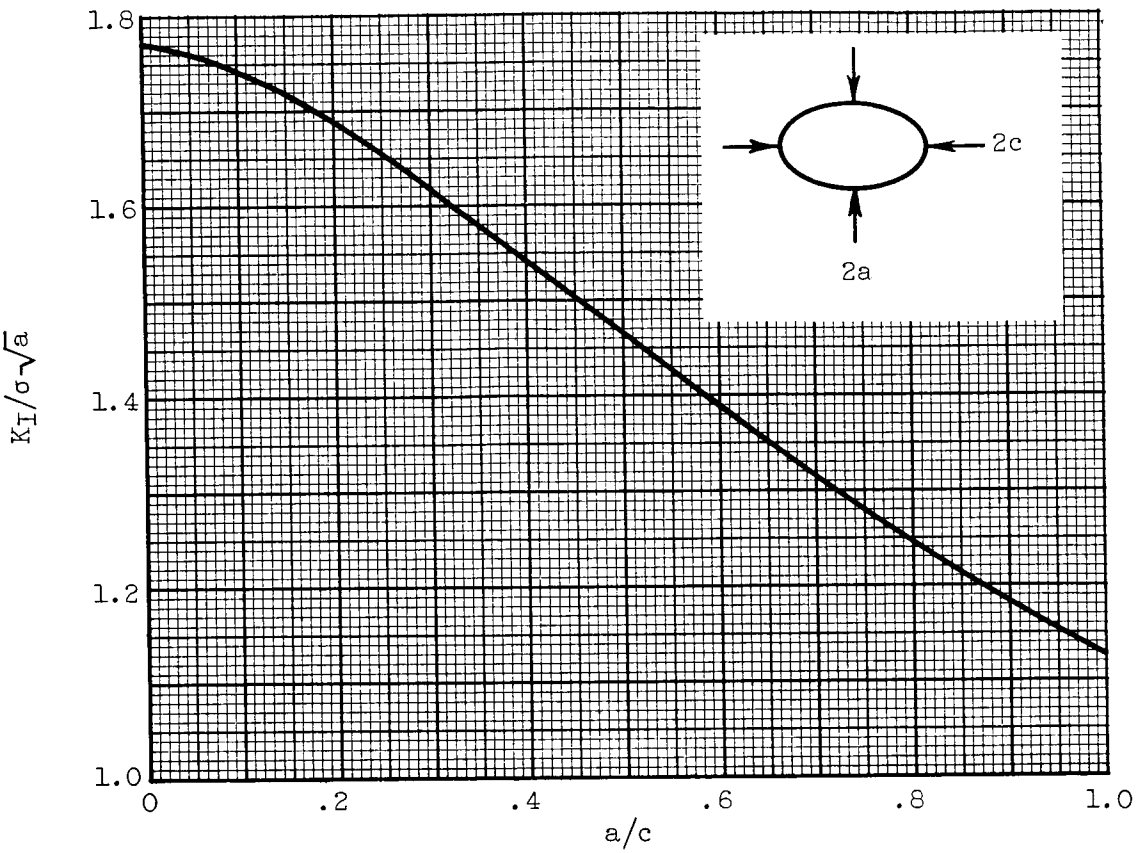

Figure 14. - Plot for calculation of K_I for submerged elliptical crack where σ is nominal stress acting across crack.

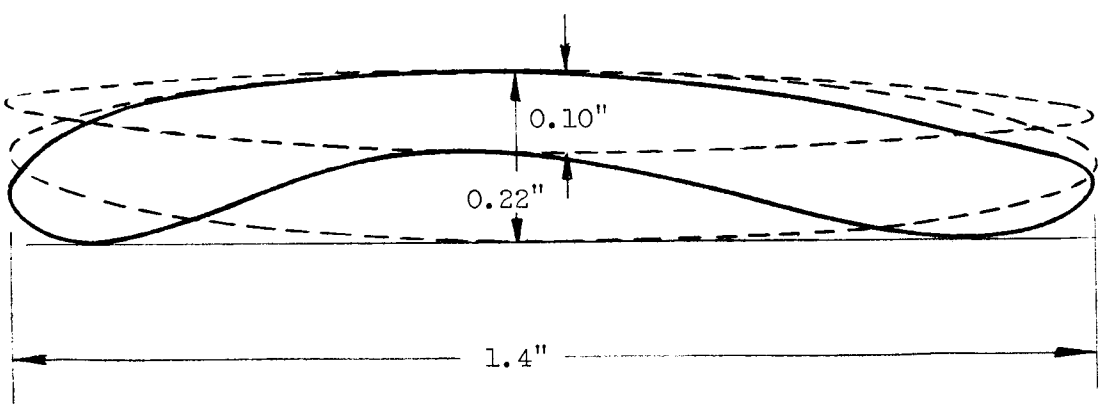

Figure 15. - Ellipses used to calculate upper and lower bounds of K_I for clean origin.

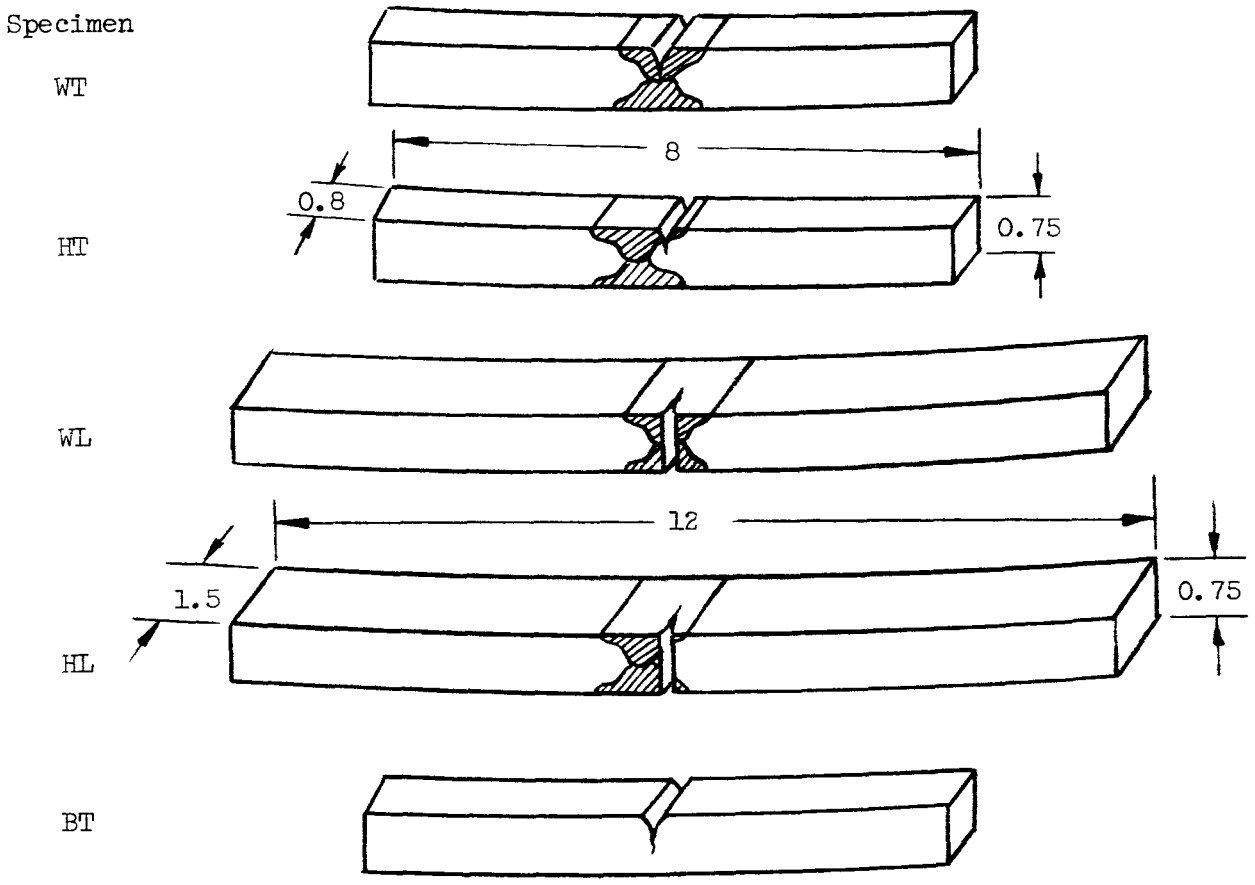

Figure 16. - Types of specimens used for K_{Ic} bend tests. Widths and thicknesses shown are nominal.

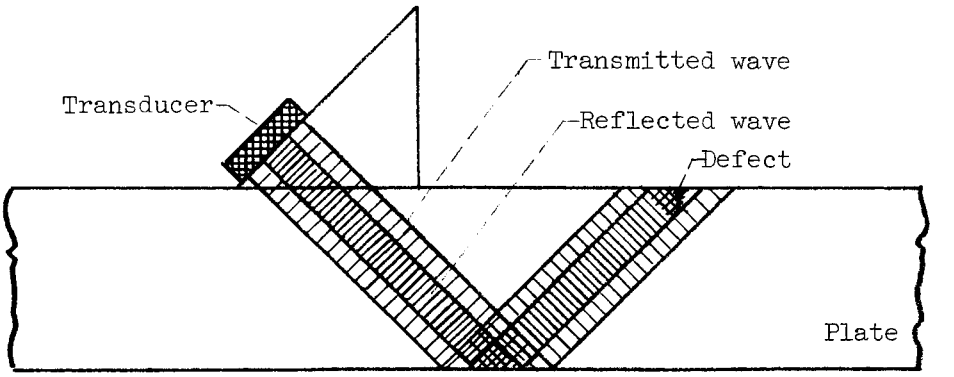

(a) Defect on same surface as transducer.

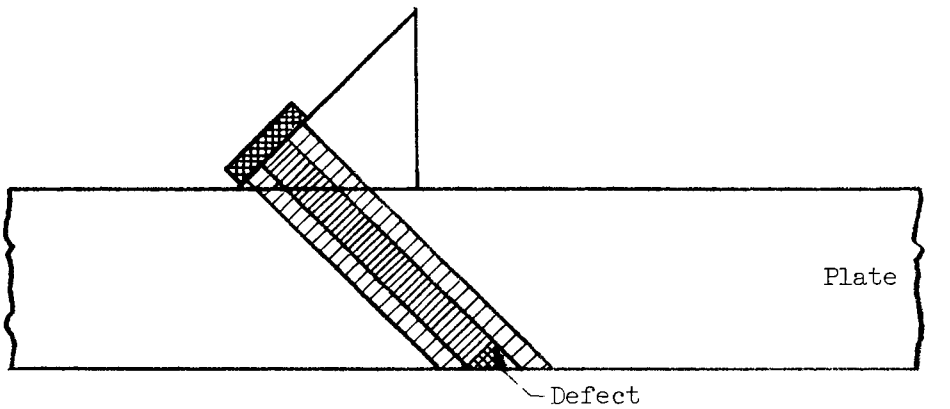

(b) Defect on surface opposite to transducer.

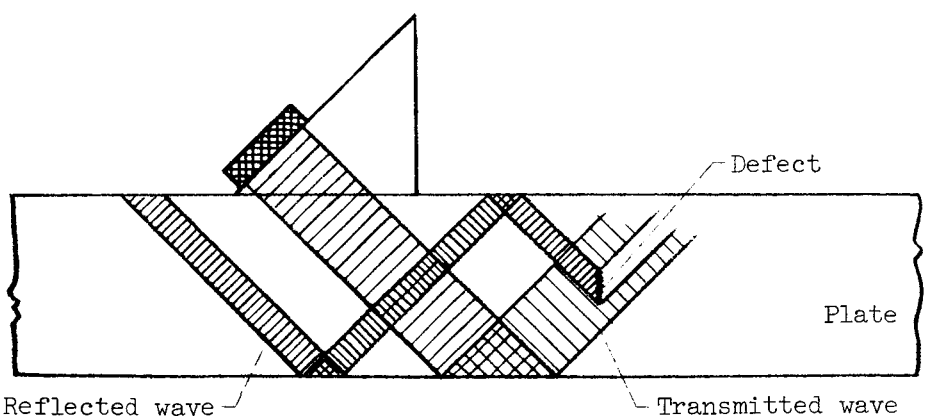

(c) Defect submerged within plate.

Figure 17. - Effect of defect location on detectability by ultrasonic techniques.

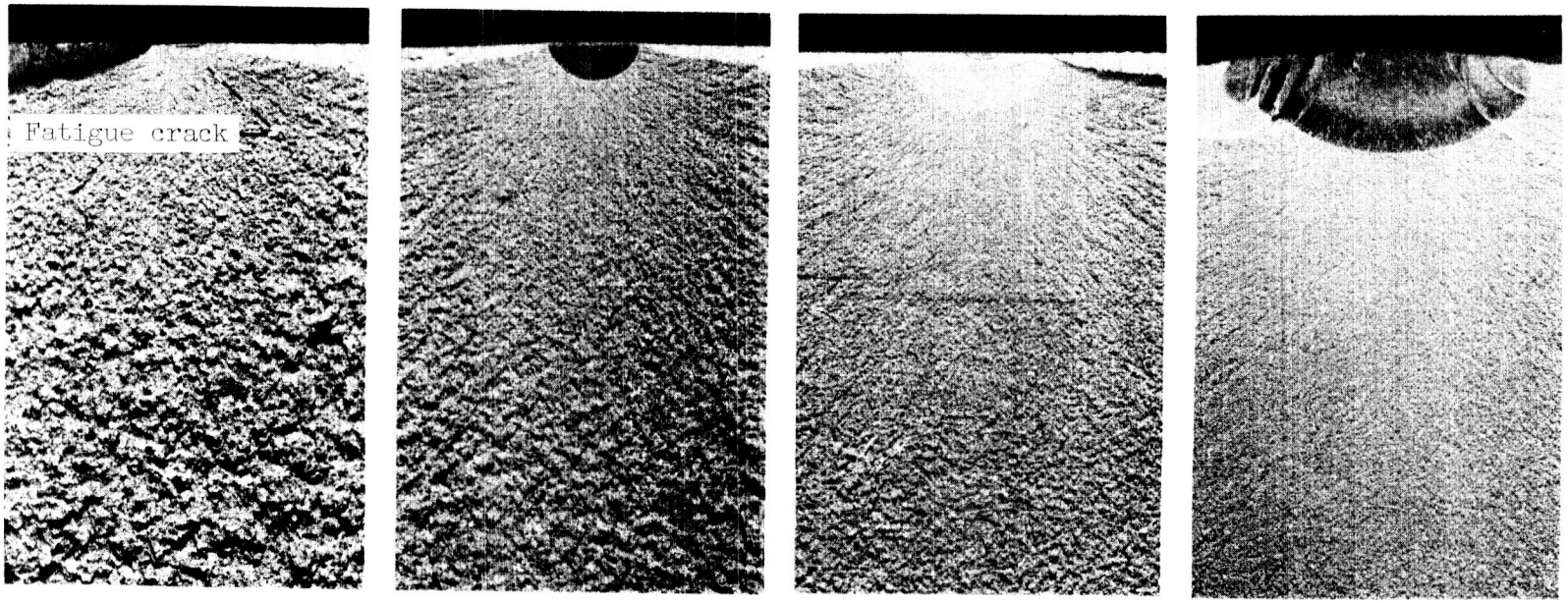

Specimen:	B	C	D	E
Fatigue crack depth, in.:	0.030	0.041	0.063	0.106
Fatigue crack surface length, in.:	0.075	0.100	0.155	0.309
Thickness, in.:	0.743	0.747	0.713	0.737

C-65-1147

Figure 18. - Fatigue cracks in test plates for nondestructive inspection evaluation program. ×5. (Specimen A had no fatigue cracks.)

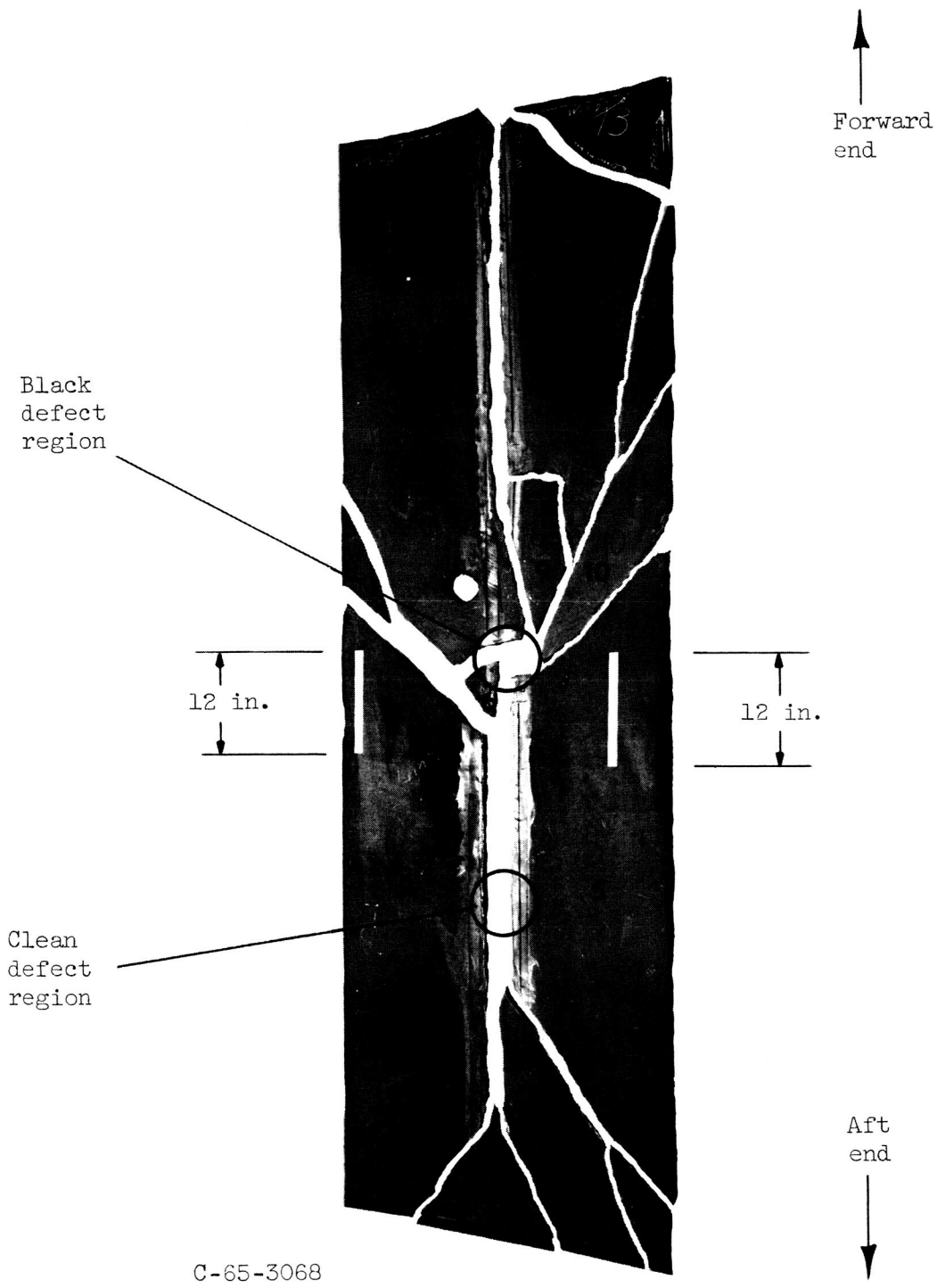

Figure 19. - Plan view of fracture paths (inside surface of motor case shown).

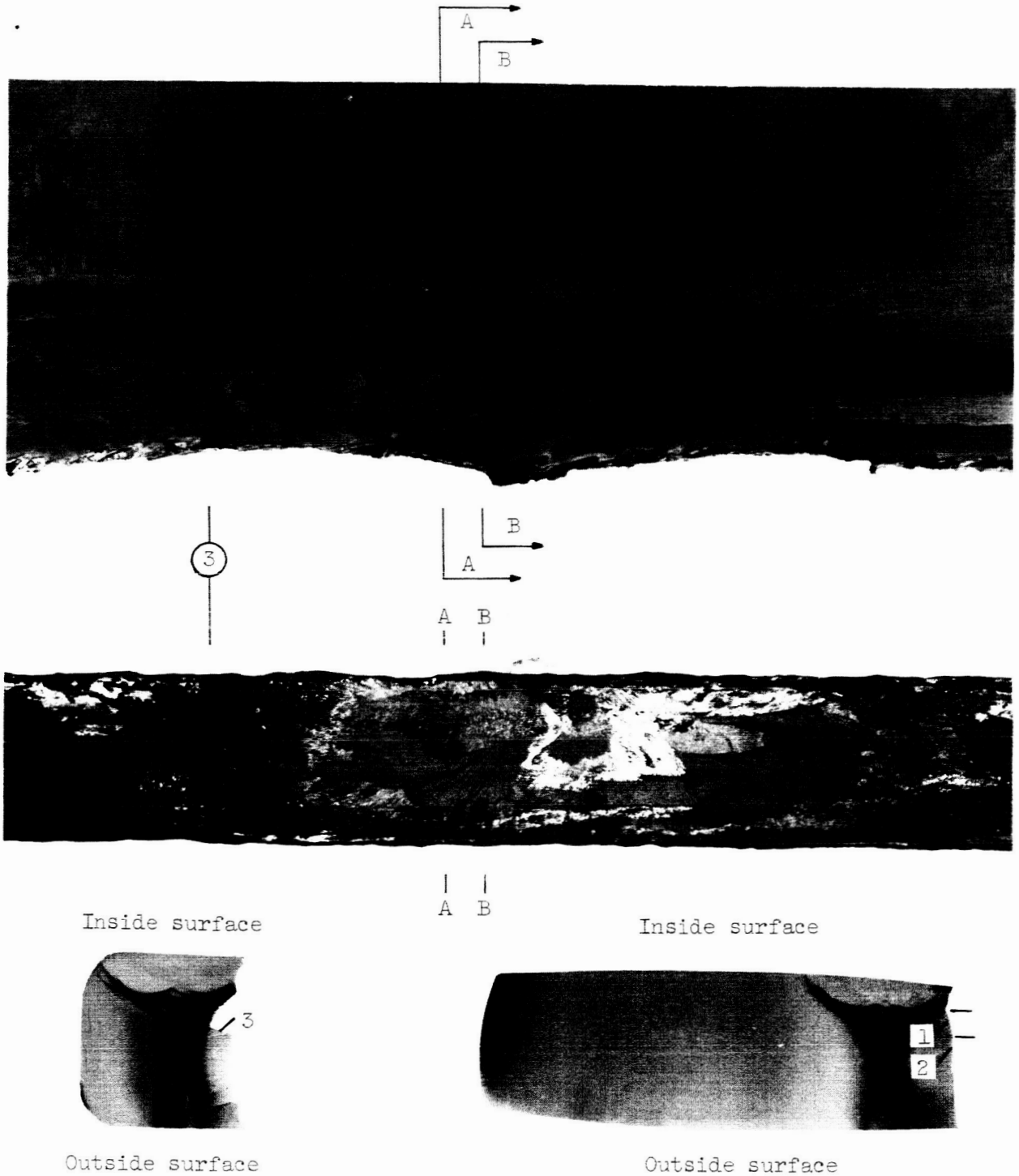

(a) Fragment 2.

Figure 20. - Photomacrographs of clean defect region. ×1.5.

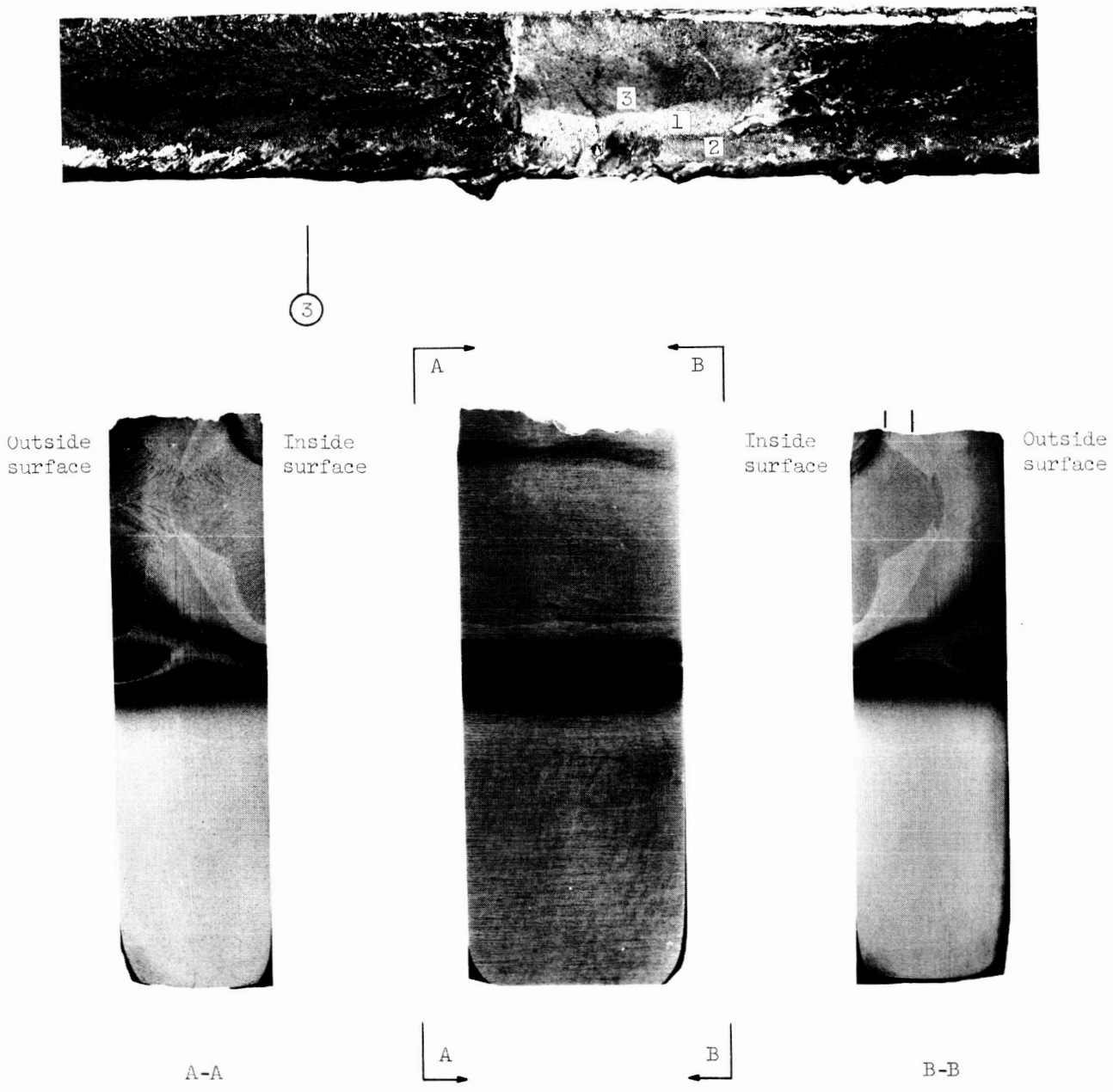

(b) Fragment 5. (Reduced 11 percent in printing.)

Figure 20. - Concluded.

(a) Area 1.

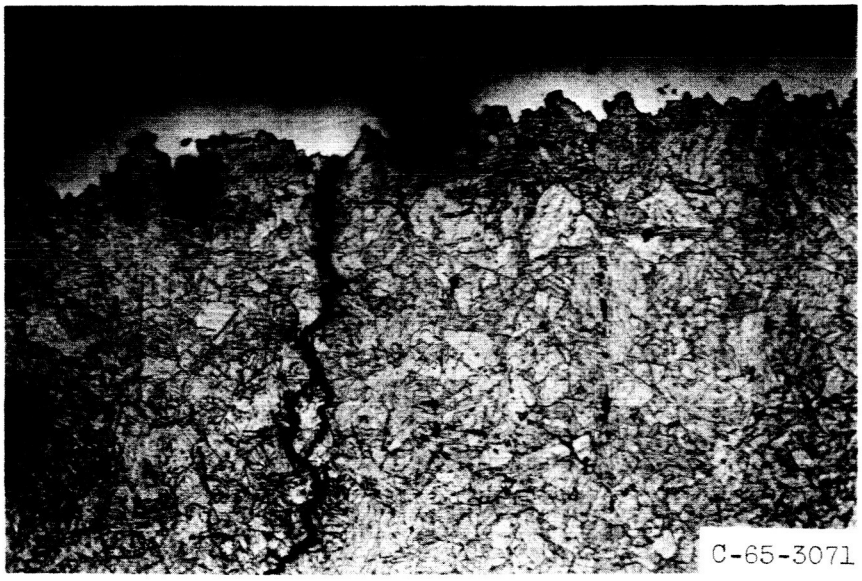

(b) Area 2.

Figure 21. - Fracture profiles of clean defect region (section B-B of fig. 20(a)). Nital etchant. ×200.

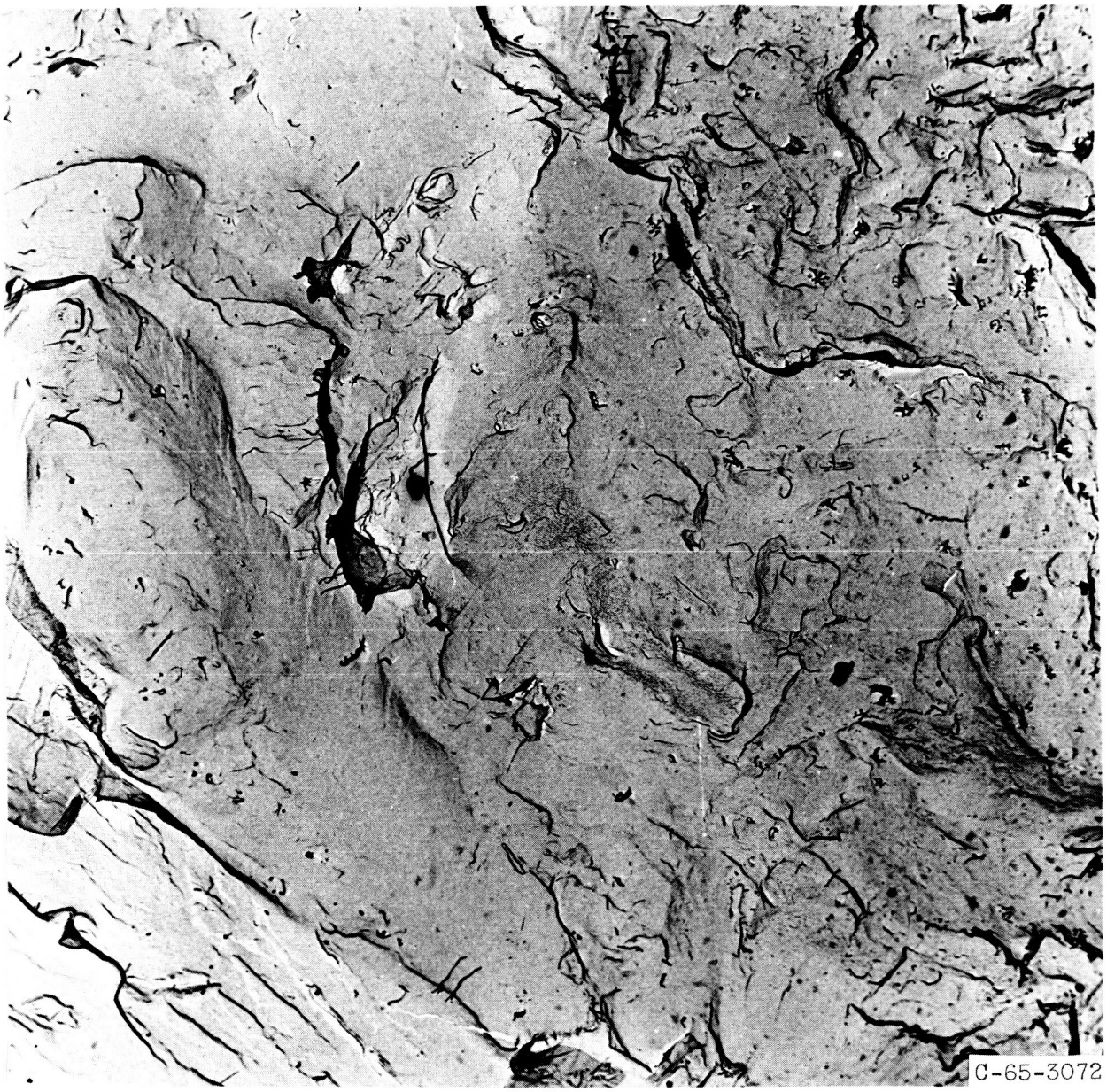

(a) Area 1 of figure 20 (b).

Figure 22. - Fractograph of clean defect. ×5000.

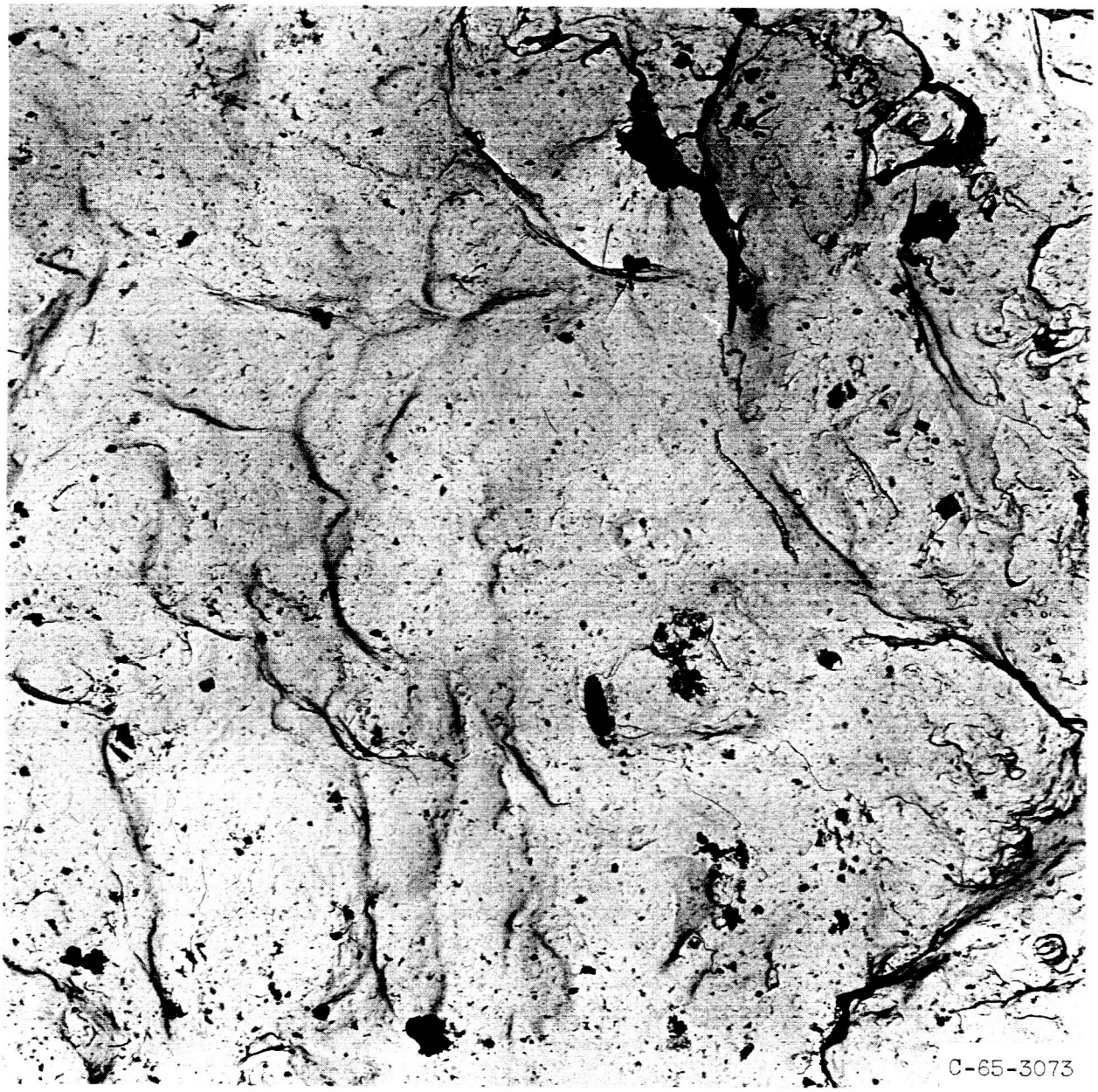

(b) Weld metal - area 2 of figure 20 (b).

Figure 22. - Continued.

(c) Base plate - area 3 of figure 20(b).

Figure 22. - Concluded.

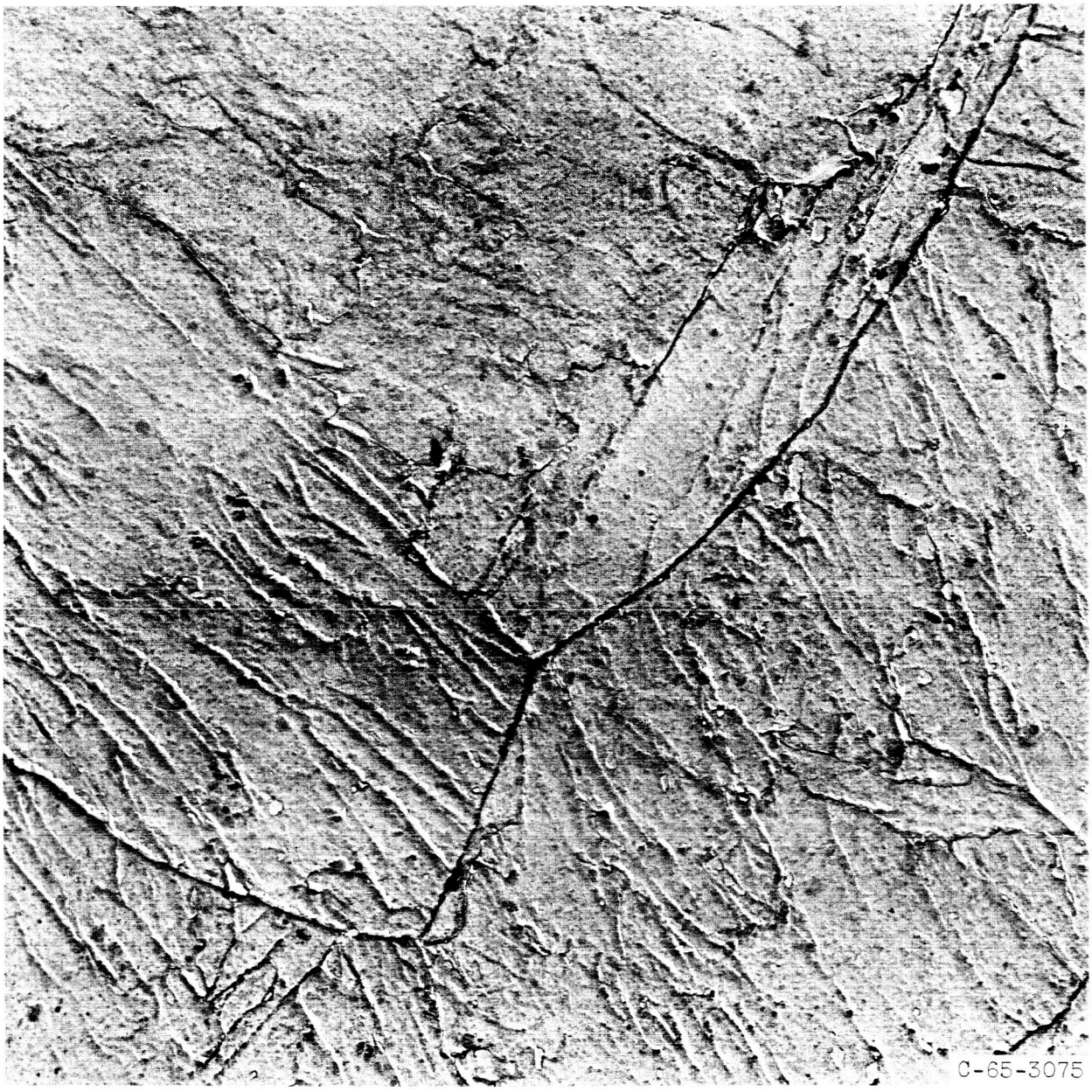

Figure 23. - Replication electron micrograph of area near clean defect. ×12 000.

Figure 24. - Replication electron micrograph of region of base plate near subarc weld fusion zone in clean defect region. ×10 000.

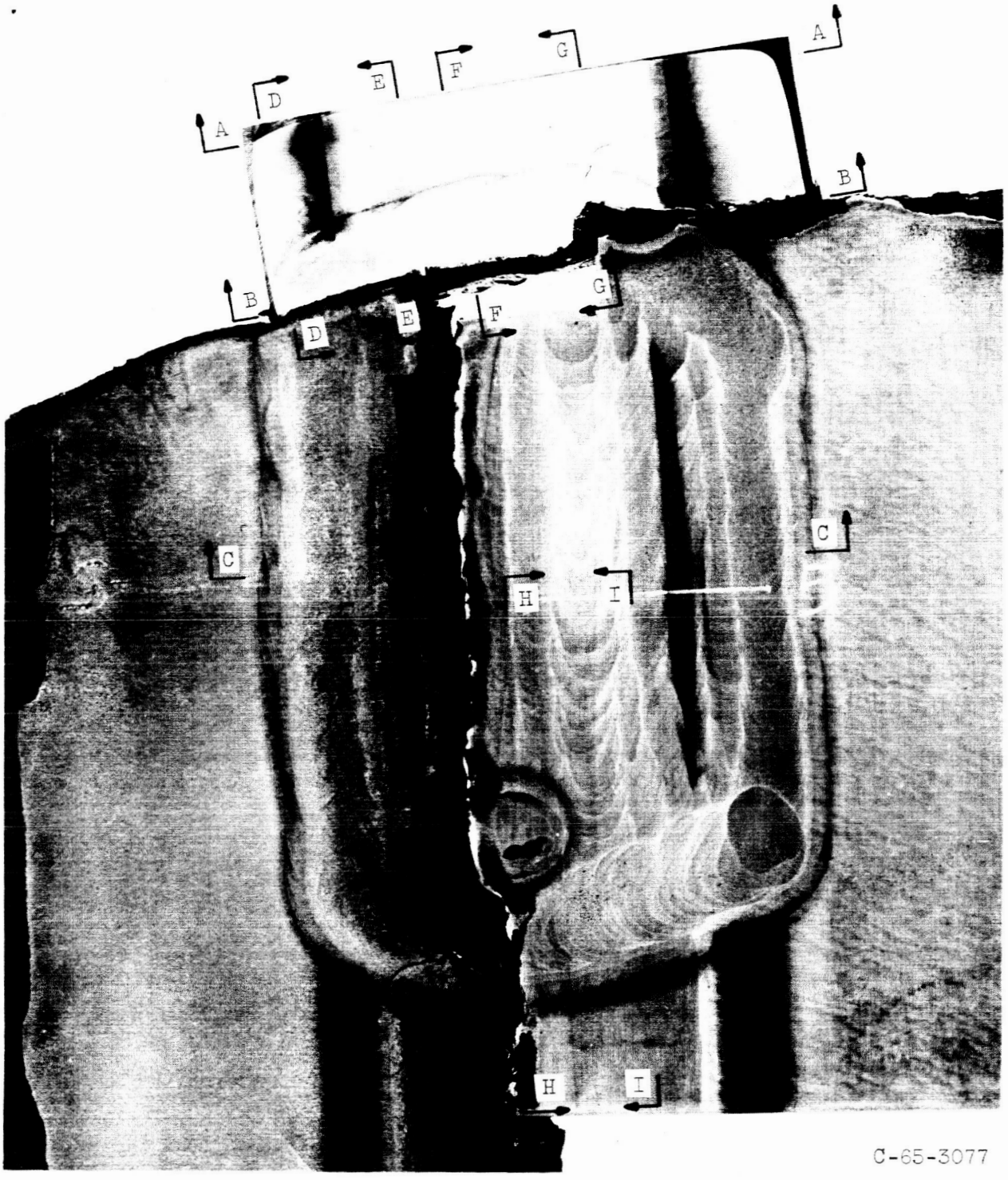

Figure 25. - Composite view of black defect region. Fragments 5, 6, and 8. ×1.5.

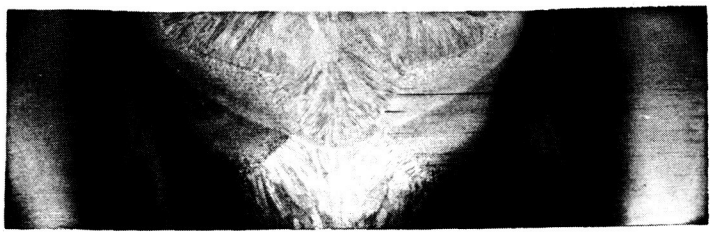

Inside surface

Outside surface

A-A

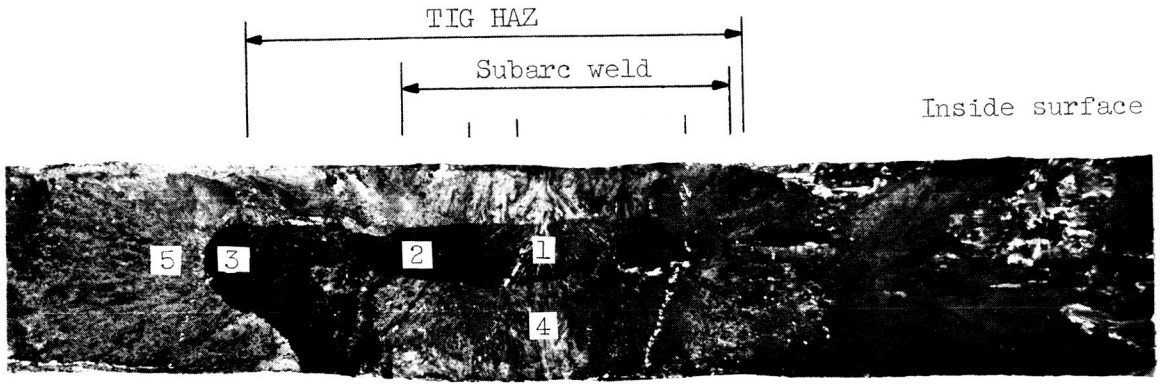

B-B

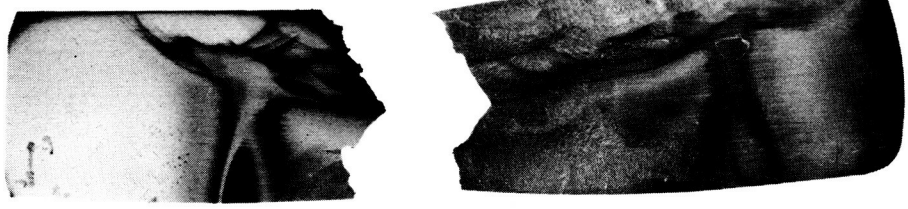

C-C

C-65-3078

Figure 26. - Photomacrographs of black defect region (see fig. 25). ×1.5.

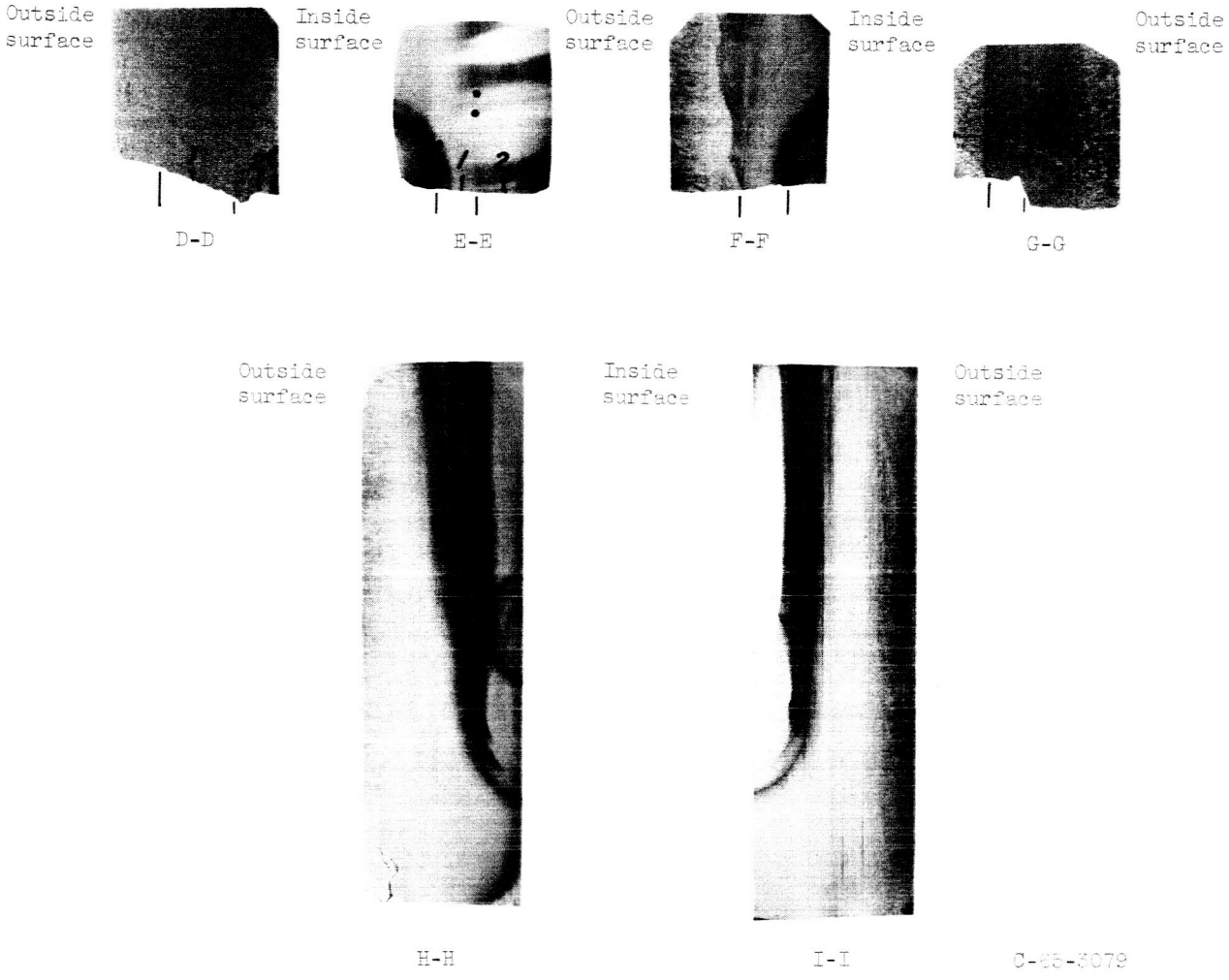

Figure 27. - Cross-sectional views through black defect region (see fig. 25). ×1.5. (Reduced 17 percent in printing.)

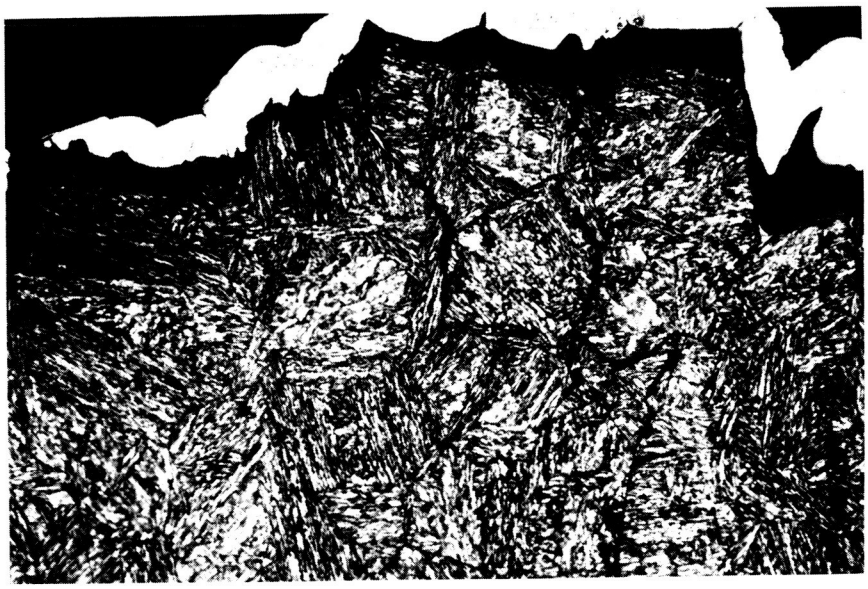

(a) Black defect (from area 1, section E-E, fig. 27).

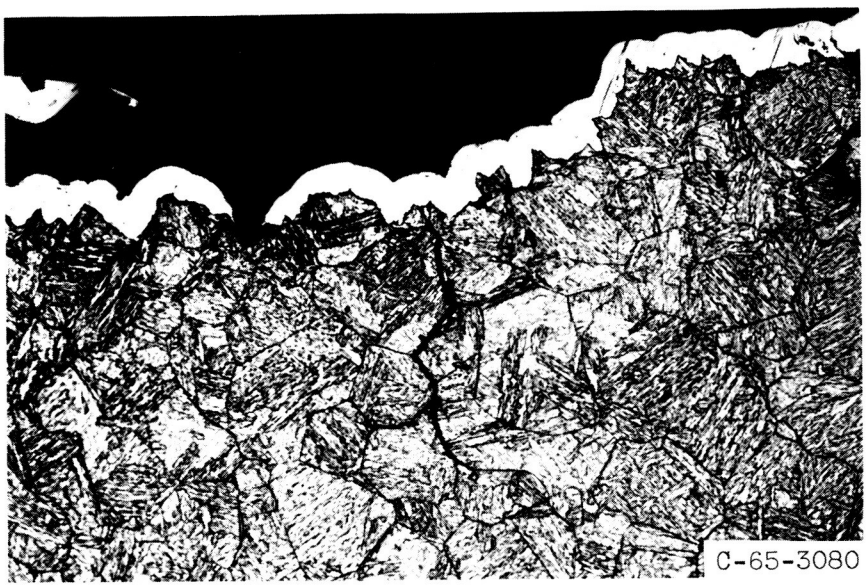

(b) Away from black defect (base plate, from area 2, section E-E, fig. 27).

Figure 28. - Fracture profiles of black defect region. Nital etchant. ×200.

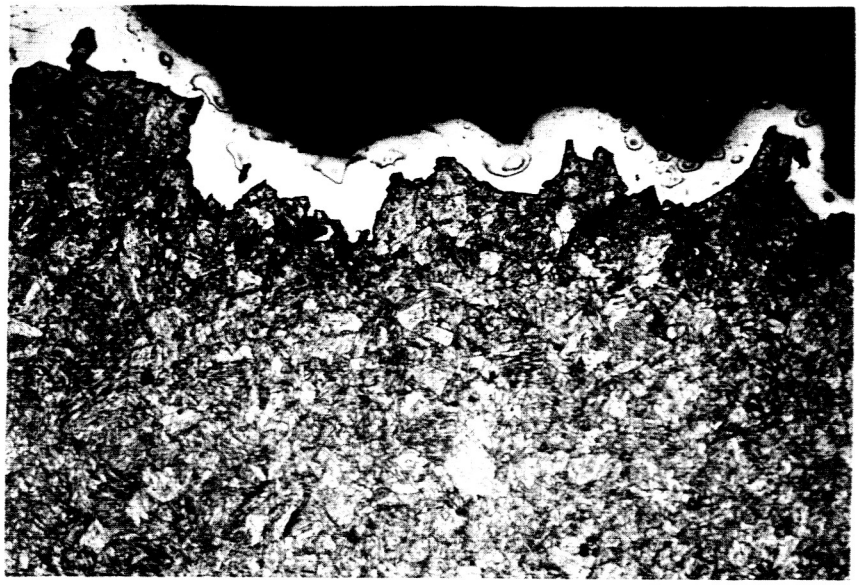

(c) From area 1 (section D-D, fig. 27).

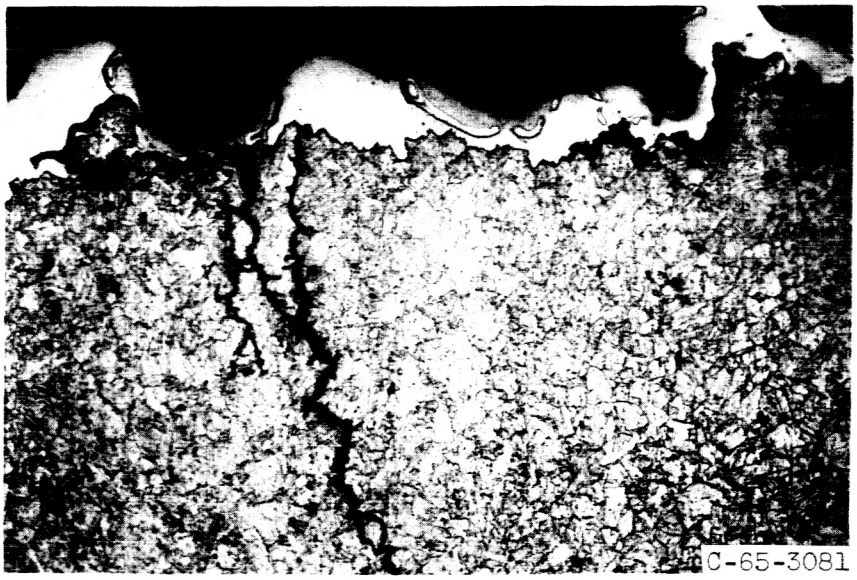

(d) From area 2 (section D-D, fig. 27).

Figure 28. - Concluded.

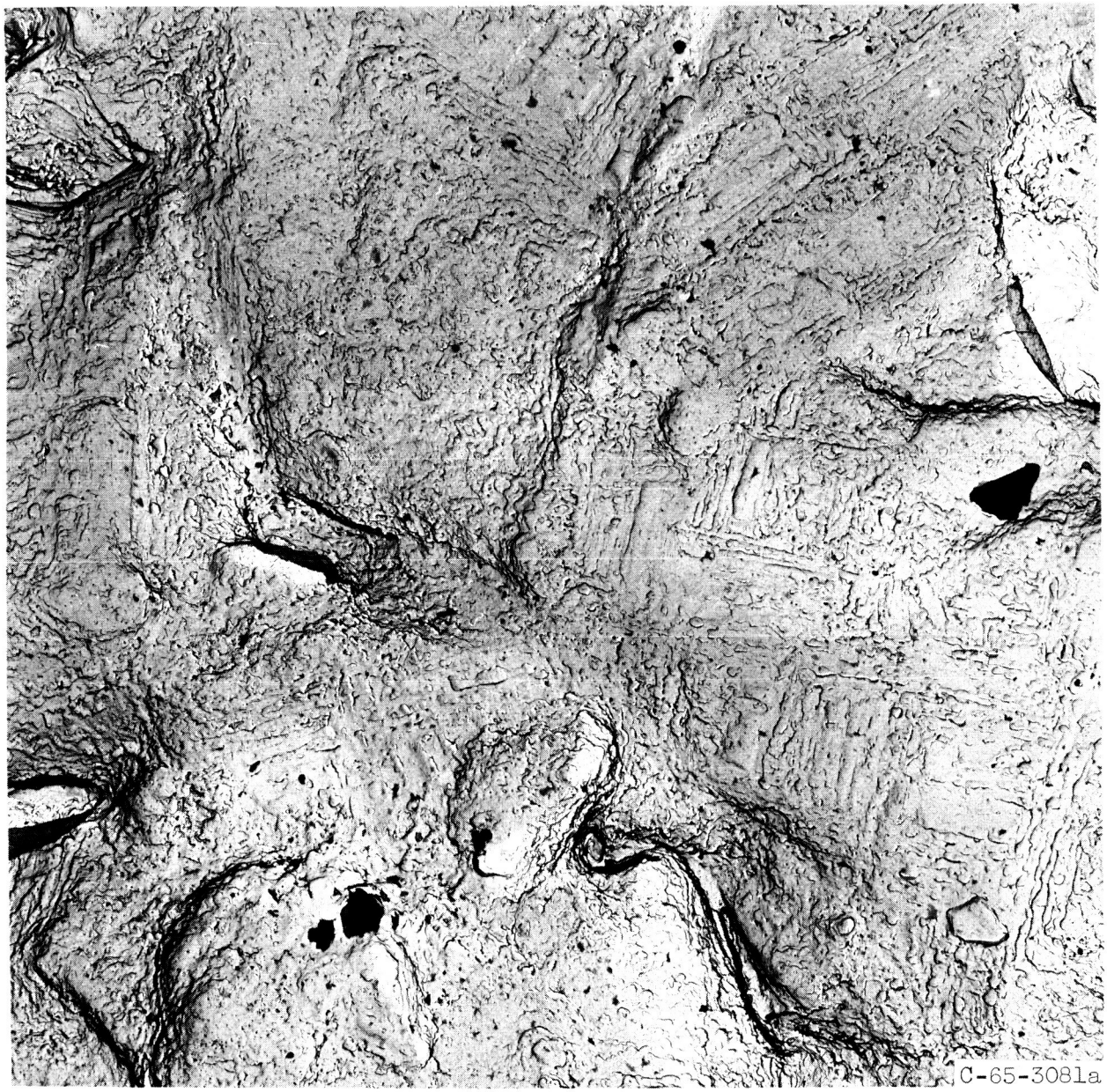

(a) Area 1 of figure 26.

Figure 29. - Fractograph of black defect. ×5000.

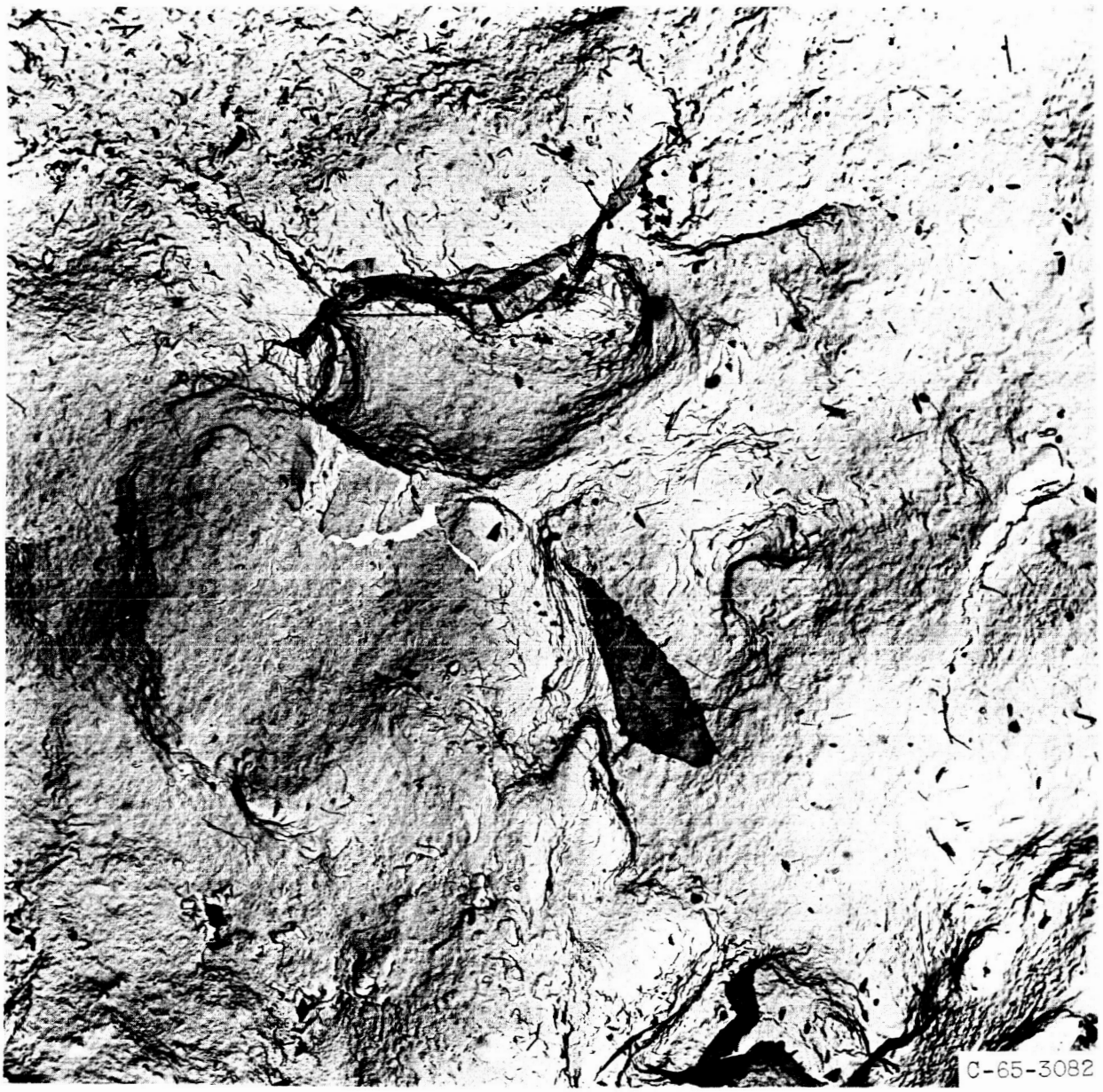

(b) Area 2 of figure 26.

Figure 29. - Continued.

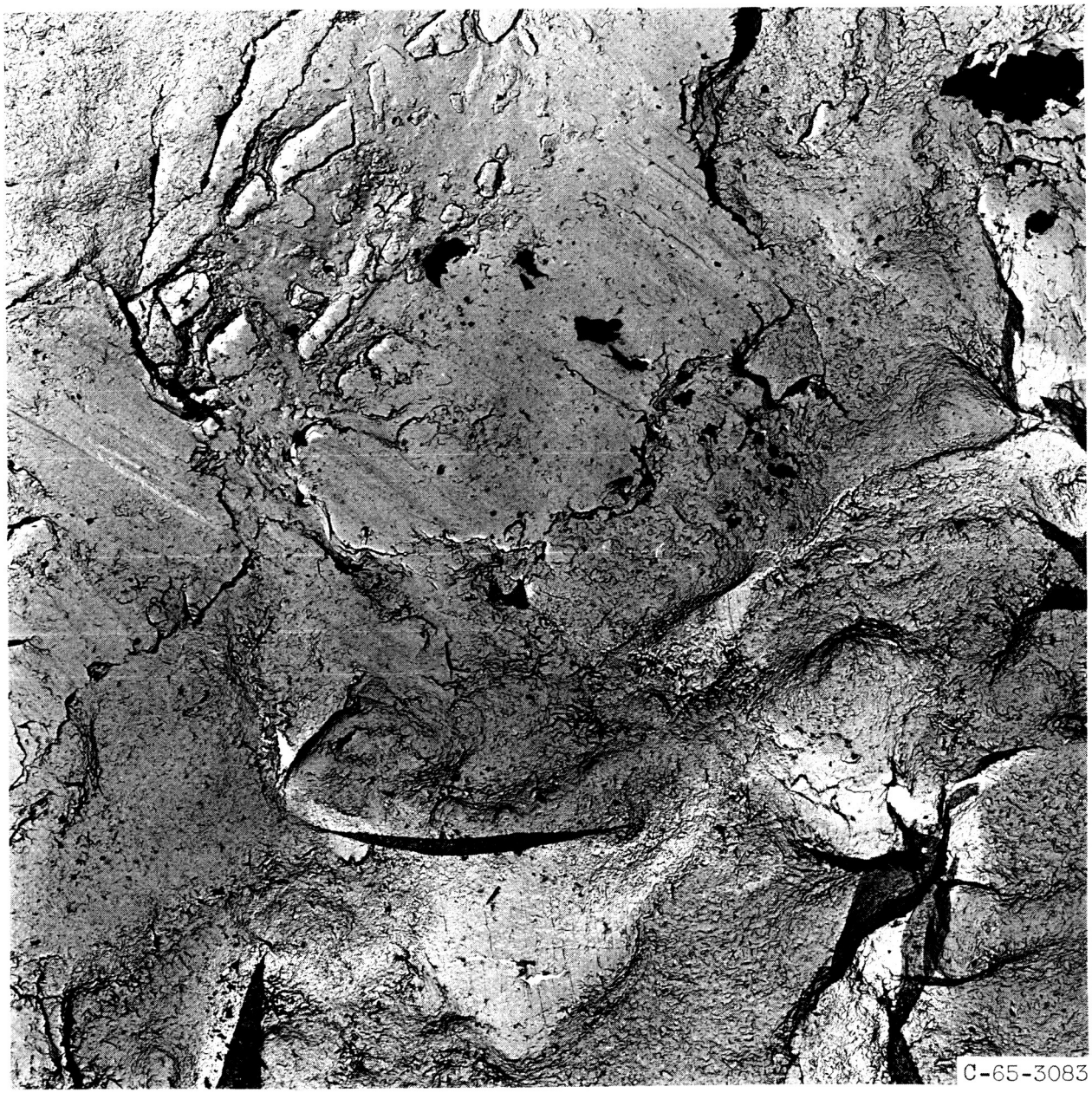

(c) Area 3 of figure 26.

Figure 29. - Continued.

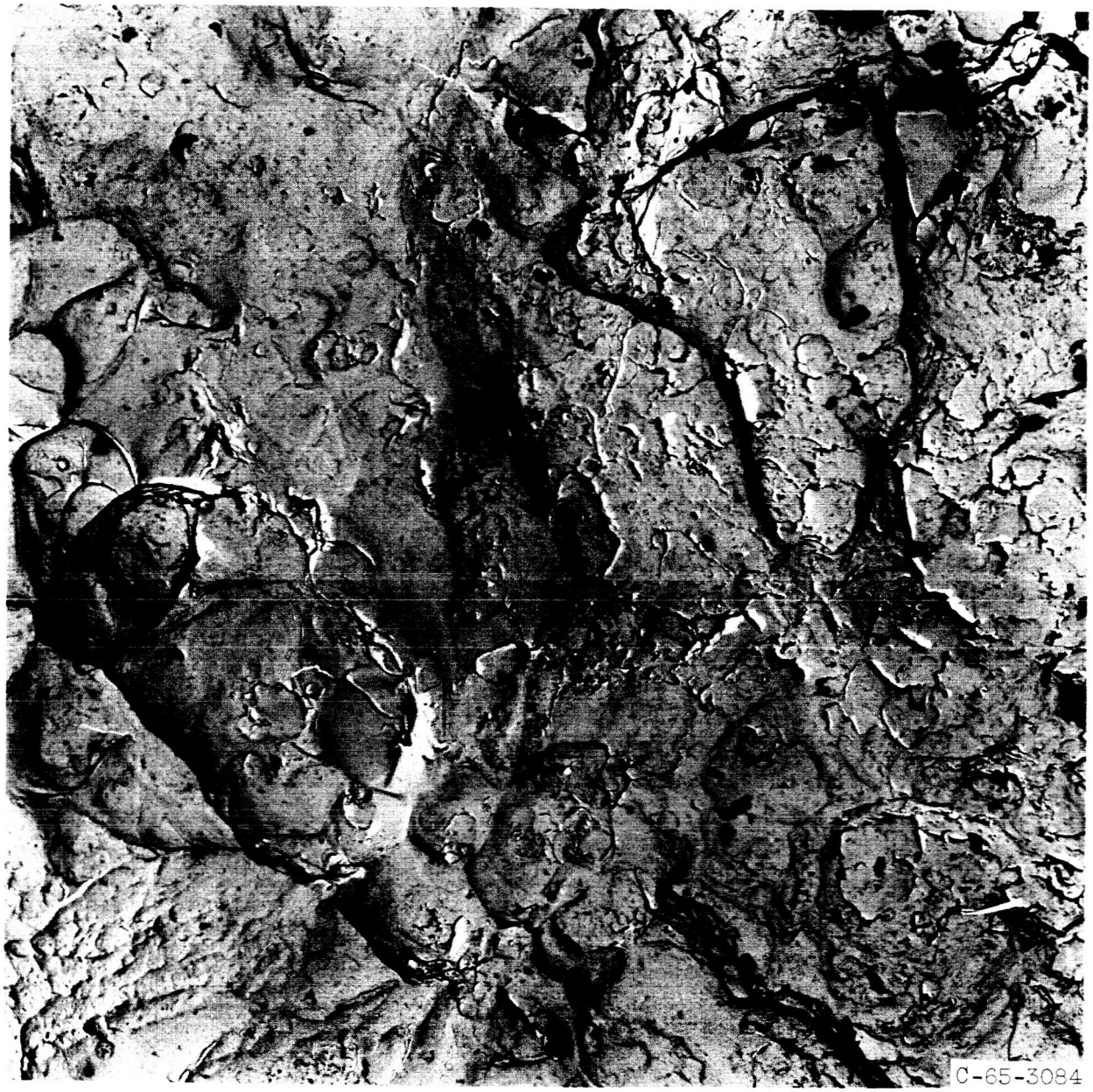

(d) Subarc weld - area 4 of figure 26.

Figure 29. - Continued.

(e) Base plate - area 5 of figure 26.

Figure 29. - Concluded.

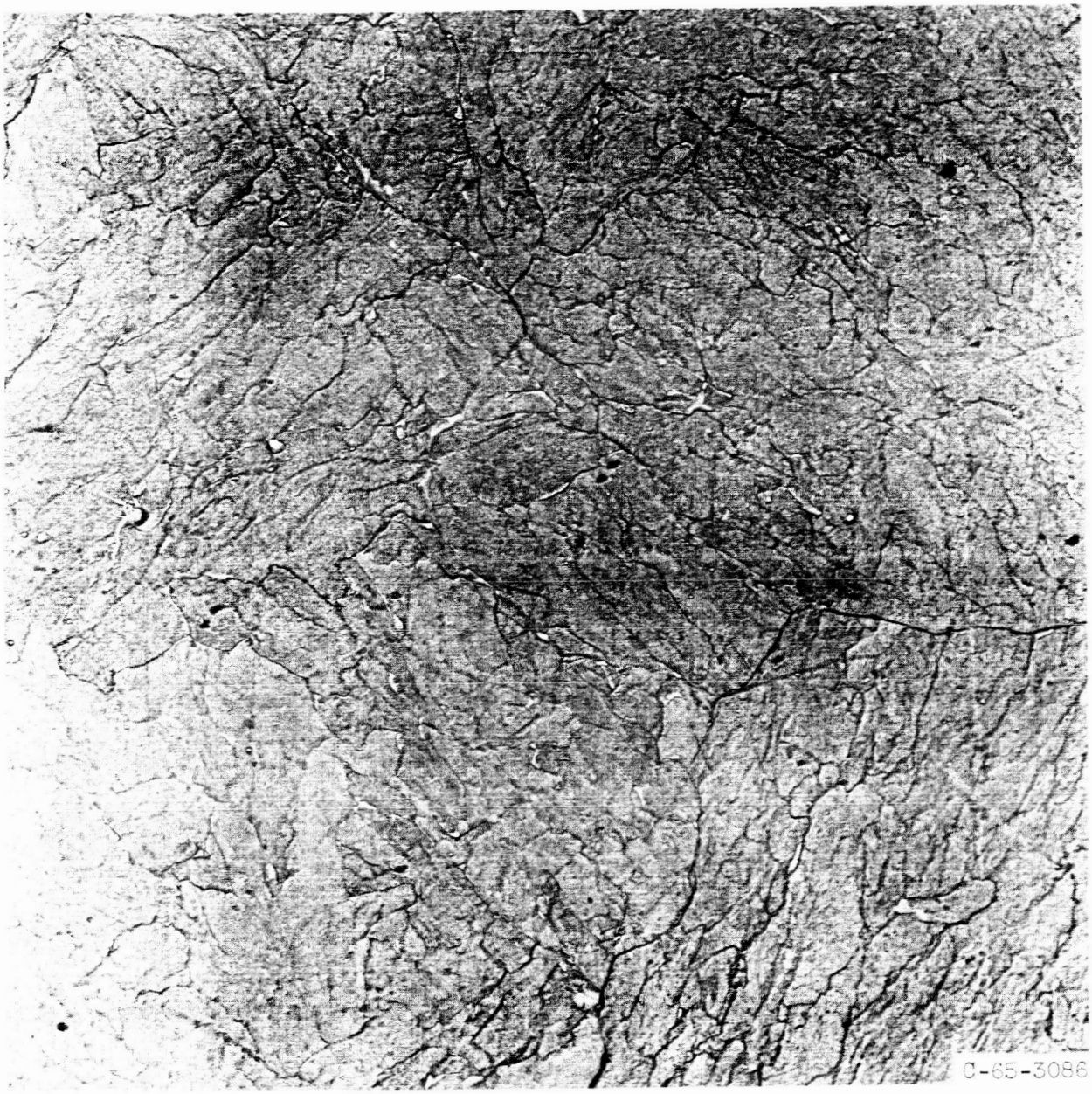

Figure 30. - Replication electron micrograph of area near black defect (HAZ of base plate). ×10 000.

Inside surface

Outside surface

Inside surface

Outside surface

C-65-3087

Figure 31. - Photomacrographs of fracture path along weld W7/302 between clean and black defects. ×1.5.

(a) Area 1 of figure 31.

(b) Area 2 of figure 31.

Figure 32. - Fracture profiles of fracture along weld W7/302. ×200.